FINAL
SENSITIVITY REPORT
GAMMA RADIATION DETECTION SYSTEMS
FOR FIELD GAMMA SCANNING
AREA IV RADIOLOGICAL STUDY
SANTA SUSANA FIELD LABORATORY
VENTURA COUNTY, CA

Prepared for:

U.S. Environmental Protection Agency Region 9
75 Hawthorne Street
San Francisco, CA 94105

Prepared by:

HydroGeoLogic, Inc.
5800 Woolsey Canyon Road
Building 204
Canoga Park, CA 91304

July 27, 2012

This page was intentionally left blank.

ABSTRACT

The U. S. Environmental Protection Agency's Santa Susana Field Laboratory Area IV Radiological Study includes surface gamma scanning of accessible areas within Area IV and the NBZ, determination of gamma radiation anomalies at surface or near surface locations, and borehole gamma logging in support of soil sampling for radioactive constituents. Gamma scanning and the determination of gamma radiation anomalies provided strong evidence for the selection of targeted soil sample locations. The gamma scanning detection systems were designed, built, assembled, and field tested as a part of the study. These are unique, state-of-the-art detection systems that have not previously been characterized for gamma detection sensitivity. This report describes the field testing efforts under taken to provide a robust characterization of the detection systems. Additionally, scanning and borehole detectors were tested off site to assess their responses to known concentrations of radiological contaminants.

Characterization of the gamma scanning detection systems included quantification and evaluation of data to determine a field of view, operating height, and maximum scanning velocity, each of which influences detection sensitivity in the field. Tests designed to establish a field of view included assembling the detection system response data from an array of source–detector positions. The maximum efficiency was determined by placing a cesium-137 source directly under the center of each system at the operation height (the closest distance overall between the source and the detection system). Data evaluations were then based on comparison of efficiency at a specific location to the maximum efficiency. The quantifications of field of view were ultimately tied to detection efficiencies. Detection system heights were selected mainly for practical field considerations, and not based on empirical data; however, empirical data was collected to support height decisions by comparing static count rates over several heights. Velocity tests were designed to evaluate the decrease in count rate with increasing velocity so that a balance between sensitivity degradation and surface coverage was quantified. Gamma attenuation in soil was calculated using National Institute of Standards and Technology gamma attenuation coefficients. Finally, as a practical matter in the field, soil moisture was measured to ensure that the gamma data collected was representative of the areas surveyed and was not significantly attenuated by soil moisture.

Subsurface tests evaluated the efficacy of borehole gamma logging to support soil sampling for radioactive constituents. This testing determined the approximate depths in soil at which gamma radiation sources could be detected. Gamma scanning detection system subsurface test results and borehole detector responses to a calibration borehole were acceptable, indicating that borehole gamma logging and gamma scanning were effective in determining optimal depths for collecting subsurface soils.

The data from field of view, height, and velocity tests were combined with the gamma transmission through soil to estimate overall scanning detection sensitivities for minimum detectable concentrations of cesium-137 and cobalt-60 for each detection system using a variety of contaminant distributions. Based on the field tests, operating parameters for each surface scanning detection systems were established as shown in the following table.

Operating Parameters for Each Surface Detection System

Detection System	Field of View Width (inches)	Transect Width (inches)	Operating Height (inches)	Maximum Velocity (ft/s)
Enhanced Radiation Ground Scanner II	86	72	15	2
Mule Mounted Gamma Scanner	104	90	35	3
Track Mounted Gamma Scanner	56	48	15	2
Single Track Mounted Gamma Scanner	36	30	15	2
Wheel Mounted Gamma Scanner	28	24	12	2
Hand Held Gamma Scanner I and II	48	24	18	1

Notes:
ft/s – feet per second

TABLE OF CONTENTS

LIST OF TABLES

This page was intentionally left blank.

LIST OF FIGURES

LIST OF FIGURES (CONTINUED)

LIST OF FIGURES (CONTINUED)

This page was intentionally left blank.

LIST OF ACRONYMS AND ABBREVIATIONS

ANSI	American National Standards Institute
ArcGIS	Arc Geographic Information System software
bgs	below ground surface
Bq	Becquerel (1 disintegration per second)
cm^3	cubic centimeters
Co	cobalt
cpm	counts per minute
cps	counts per second
Cs	cesium
DOE	Department of Energy
ERGS	Enhanced Radiation Ground Scanner
°F	degrees Fahrenheit
FOV	field of view
FRA	field reference area
ft/s	feet per second
g/cm^3	grams per cubic centimeter
GPS	global positioning system
GRAY	gamma radiation anomalies
HGL	HydroGeoLogic, Inc.
HHGS	Hand Held Gamma Scanner
HPGe	high purity germanium
in^2	square inch
in^3	cubic inch
ISGS	In Situ Gamma Scanner
K	potassium
keV	kilo electron volt
μCi	microCuries
MDA	minimum detectable activity
MDC	minimum detectable concentration
MeV	mega electron volt
MMGS	Mule Mounted Gamma Scanner

LIST OF ACRONYMS AND ABBREVIATIONS (CONTINUED)

NaI	sodium iodide
NIST	National Institute of Standards and Technology
pCi	picocuries
pCi/g	picocuries per gram
PVC	polyvinyl chloride
R^2	coefficient of determination
Ra	radium
RE	relative efficiency
ROI	region of interest
RPD	relative percent difference
SD	standard deviation
SSFL	Santa Susana Field Laboratory
STGS	Single Detector Track Mounted Gamma Scanner
Th	thorium
TMGS	Dual Detector Track Mounted Gamma Scanner
TPC	The Palladino Company, Inc.
USEPA	U. S. Environmental Protection Agency
U	uranium
WMGS	Wheel Mounted Gamma Scanner

FINAL
SENSITIVITY REPORT
GAMMA RADIATION DETECTION SYSTEMS
FOR FIELD GAMMA SCANNING
AREA IV RADIOLOGICAL STUDY
SANTA SUSANA FIELD LABORATORY
VENTURA COUNTY, CA

1.0 INTRODUCTION

1.1 PURPOSE OF THE SENSITIVITY REPORT

This report is written to establish operating parameters for surface gamma detection systems used in the Santa Susana Field Laboratory (SSFL) Area IV Radiological Study and to estimate or quantify field detection sensitivities in accordance with the Final Gamma Radiation Scanning Sampling and Analysis Plan prepared by HydroGeoLogic, Inc. (HGL) and The Palladino Company, Inc. (TPC) (HGL and TPC, 2010). This Sensitivity Report is written for a technical audience with some prior knowledge of radiation detection and field gamma detection operations. The term sensitivity is synonymous with detectability, meaning the ability of a detection system to detect gamma radiation that may be present in the environment.

The principal operational objective of the Area IV Radiological Study is to select the detection system with the greatest sensitivity for the field conditions encountered during gamma scanning and therefore to gain the greatest gamma detection sensitivity possible in the field. However, because of accessibility, safety and other considerations, it is not always possible to use the largest and most sensitive system. Thus the suitability of a detection system to survey a particular area is ultimately a field decision. An objective of the Radiological Study of the SSFL is to scan as much of the ground surface as possible to determine the presence of gamma radiation anomalies (GRAY) in surface soil and, to a limited degree, in subsurface soil, within the boundaries of Area IV and the Northern Buffer Zone of the SSFL. The objective of this field survey is to map the locations of GRAYs, which will be evaluated and will factor into selection of targeted soil samples for radiochemical analyses.

The general process for evaluating field scanning data to support soil sampling is:

- Data from ground gamma scanning systems are merged and normalized to form a map of each study Subarea
- Anomalies are determined based on subarea data evaluation
- Potential GRAYs are further investigated by performing a static count using the scanning systems and some are investigated using in situ gamma detection
- Based on gamma data as well as other lines of evidence such as historical site assessments, geophysical anomalies, and historical sample results, a gamma borehole

log is completed to locate depths with the highest relative levels of gamma activity to identify the depths of soil sample collection

Gamma anomalies are mapped surface areas of the locations of elevated gamma measurements. The gamma measurement may be elevated either due to the total gamma spectrum (i.e., total counts per second [cps] in the spectrum) or to an elevated region of interest (ROI) of a specific gamma-emitting radionuclide. Because of interactions of the many gamma emitting radionuclides present in soil, extensive calculations involving the sensitivities of many radionuclides are outside the scope of this document. For this reason, the sensitivities reported are for cesium (Cs)-137 and cobalt (Co)-60, which are common gamma emitting radionuclides that may be encountered in the study.

Figure 1 is a photograph showing some of the terrain in the Radiological Study area. This photograph shows that it is a flat, sloped, steeply sloped, and rocky terrain. The various gamma detection systems are described in detail in Section 2.0. The gamma detection systems differ by the number and arrangement of detectors and their overall size and mobility. Due to the highly varied terrain, one type of gamma detection system is not sufficient to obtain complete surface coverage.

Figure 1
Partial View of Santa Susana Field Laboratory Area IV

An objective of the field gamma scanning effort is to scan all accessible areas for GRAYs. The SSFL Area IV terrain is quite varied and includes flat, sloped, steep sloped and rocky surfaces. Different detection systems are suited to scan different types of terrain.

1.2 FIELD METHODS USED TO DETECT GAMMA RADIATION

Gamma ray spectrometry has been used successfully for decades to delineate the environmental distribution of gamma emitting radionuclides (International Atomic Energy Agency, 2003). Various detection systems and survey techniques have evolved and continue to be developed particularly for field applications (Interstate Technology and Regulatory Council, 2006; Aage et al., 2006). The large sodium iodide (NaI) detectors described in this report have been used to perform gamma spectroscopy surveys for various purposes. They are used in aerial surveys to map geographical features across large areas for mineral exploration, such as locating potential sites for uranium (U) extraction. Sodium iodide detectors mounted on ground-based vehicles are used to find missing radioactive sources, to locate sites requiring radiological cleanup, or to rapidly respond to a radiological event.

Field methods for the detection of gamma radiation range from stationary detection to mobile detection depending on the purpose of the survey. Gamma detectors characterize gamma emitting radioactive materials present due to both natural background radiation contributed by soils, rocks, and minerals, etc., and from anthropogenic sources. Gamma spectrometry is primarily based on two types of detectors: scintillation detectors and solid state detectors. Scintillation detectors are constructed of various materials such as NaI, cesium iodide or specialty plastic materials. Solid state detectors include intrinsic germanium crystals. Scintillation detectors can operate at ambient temperature and thus are better suited for field work. Germanium gamma detectors require cooling to very low temperatures to operate, using either liquid nitrogen or mechanical cooling. Sodium iodide crystals are available in much larger detector volumes than an equivalent germanium crystal detector and the overall detection efficiency is strongly dependent on detector size. However, germanium detectors have much better gamma energy resolution than do most scintillation detectors. For these reasons, gamma scanning systems designed for field use are typically fabricated using NaI scintillation detectors and high-resolution germanium detectors are used to augment or to uniquely identify gamma emitting radionuclides.

Several factors contribute to gamma detection sensitivity (U.S. Nuclear Regulatory Commission, 1998, Multi-Agency Radiation Survey Assessment of Materials and Equipment, 2009). These are:

- the efficiency and resolution of the detection system,
- radiation background,
- radioactive source to detector distance,
- the operational scanning parameters, such as field of view (FOV) and velocity,
- intrinsic emission characteristics of individual radionuclides, such as gamma energy, branching intensity, and the number and strength of gamma peaks, and
- contaminant spatial distribution and the gamma transmission through the medium.

Mounted beneath mobile platforms, large NaI detectors (4-inch by 4-inch by 16-inch) offer the most sensitive and reliable method available to perform radiological surveys of relatively large areas of land to identify the presence of GRAYs at the surface and in near-surface soils. These

same detection systems can operate in both scanning (mobile) and static (stationary) modes. The static mode is used for verifying or confirming potential GRAYs, and for conducting quality control tests. The smaller 3-inch by 3-inch hand-held NaI detector offers better access and maneuverability in rugged terrain but lacks the gamma spectroscopy capabilities and sensitivity of the larger NaI detectors.

1.3 SCOPE AND ORGANIZATION OF THIS REPORT

Several gamma detection systems were used or tested for use in the SSFL Area IV Radiological Study to perform scanning or static measurements.

- The Enhanced Radiation Ground Scanner (ERGS) II, an all terrain vehicle with a large NaI detector array.
- The Mule Mounted Gamma Scanner (MMGS), with two large NaI detectors mounted to an outrigger saddle which is placed on a mule (*Equus mulus*).
- The Dual Detector Track Mounted Gamma Scanner (TMGS), with two large NaI detectors mounted to a self-propelled gas-powered platform that has two parallel tracks to scan both small areas and potentially steep terrain.
- The Single Detector Track Mounted Gamma Scanner (STGS), with one large NaI detector mounted to a self-propelled gas-powered platform that has two parallel tracks to scans both small areas and potentially steep terrain.
- The Wheel Mounted Gamma Scanner (WMGS), a hand propelled three wheeled cart with a single large NaI detector.
- The Hand Held Gamma Scanner (HHGS) I, a Ludlum model 44-20 NaI detector mounted on a harness worn by the field surveyor to scan areas not accessible by more sensitive detection systems.
- The HHGS II, a Ludlum model 44-20 NaI detector hand carried by the field surveyor to scan areas not accessible by more sensitive detection systems. This detection system is similar to the HHGS I with the exception that the detector is not attached to a support harness. Henceforth, this report will not differentiate between the HHGS I and II as the sensitivity specifications are identical.
- Other portable survey instrumentation including the relatively small NaI detectors used in gamma borehole surveys to profile gamma activity with depth in a borehole using static counts at specific depth intervals.
- In Situ Gamma Spectrometer (ISGS) consisting of a high purity germanium (HPGe) detector (designed for field deployment) used to perform static measurements for investigation of PGRAYs.

This report calculates the sensitivities of the ERGS II, MMGS, TMGS, STGS, WMGS, and HHGS gamma detection systems, most of which are large NaI detection systems that are configurations of the same detector and differ by their arrangement and methods of propulsion. These systems are described in detail in Section 2.0. The tests conducted to establish operating parameters (FOV, height, and scanning velocity) are described herein. Much of the report is

devoted to test methods, data analyses and interpretations, particularly for evaluation of the FOV and velocity.

Tests conducted onsite and at other locations are described in separate sections. Onsite tests consisted of measuring the ability of each system to detect known quantities of radioactive sources at specific depths in soil, as well as brief studies of the effects of soil moisture and barometric pressure on gamma count rate data. In general, sensitivity is strongly dependent on physical factors such as the source to detector distance, background levels of radiation, soil attenuation, and shielding by solid materials; thus, gamma detection of surface contamination is much easier than subsurface contamination. In comparison to these conditions which strongly affect detection, soil moisture and barometric pressure account for relatively small fluctuations in sensitivity. This is due in large part to minimizing the effects of soil moisture by adherence to the project requirement of a maximum soil moisture limit of 15 percent.

In general, uncertainty is not covered in this document. There are several sources of uncertainty, that fall into two basic categories: (1) detection system parameters such as measurement uncertainty (over which there is an element of control), and (2) contaminant source type, activity, distribution, etc. uncertainties (which are not controlled). Many calculations and estimations presented in this document include considerations for the first category of uncertainties, but do not account for the uncertainties associated with uncontrolled conditions.

Assembling the data from several different detection systems to form a map showing merged gamma count rate data requires data normalization. This is fully addressed in the Normalization Report, Gamma Radiation Detection Systems (HGL, 2011), but is not discussed in this sensitivity report.

This page was intentionally left blank.

2.0 MATERIALS AND METHODS

2.1 OVERVIEW OF SENSITIVITY TESTS

Sensitivity tests were designed to establish the FOV, operating height, and operating velocity for each ground scanning detection system. Together the test data provide an estimation of the approximate amount of radioactivity that may be detected in the field with a specific detector configuration. Separate comparisons of observed and expected count rate data from subsurface sensitivity measurements provide an approximation of the amount of gamma radiation which may be detected at a particular soil depth. The borehole detectors and in situ gamma detectors are not designed for ground surface scanning; therefore, the aforementioned parameters do not apply. However, calibration to a specific static height or a specific diameter borehole does. Estimated minimum detectable activity (MDA) and minimum detectable concentrations (MDC) is discussed in Section 3.7.

The tests were conducted in a controlled laboratory setting in the high bay work area of the project field office located in the SSFL, Building 204. Three types of tests were performed:

1. The first test was a radial matrix efficiency test designed to establish the FOV for each configuration. A source was placed at various positions relative to the detection system, gamma data was collected, and then the data from many positions was assembled into a matrix or field of detector response data. Using the data from various source positions, the detection system efficiencies were integrated and evaluated to establish a FOV. The extent of the FOV was calculated relative to the integrated source efficiencies directly under the active detector surface areas. This test also evaluated indirectly any problems with the detector mount and unintended shielding effects.
2. The second test was a detection system height test performed to compare discrete detector scanning heights. Selecting an operating height requires consideration of the maneuverability and stability of the scanning system in the field, the detection efficiency, FOV, and other factors.
3. The third test was a velocity test designed to compare the detection system scanning efficiency with its static efficiency. In particular, the test was conducted to determine the maximum velocity that could be achieved to optimize surface coverage without significant degradation of detection sensitivity.

The radial matrix and velocity tests were used to justify selection of a specific FOV and maximum velocity for each system, respectively; however, the height test was performed to provide baseline information rather than to justify selection of a particular height. Operational height selection was driven primarily by physical considerations that balanced both sensitivity and maneuverability.

Field sensitivity tests also were conducted at the Walker Field Large Area Calibration Pads in Grand Junction, Colorado. At the time these tests were conducted, the equipment operating heights had yet to be established; therefore, the primary value of the calibration pad tests lay in

the detection system responses to known quantities of the naturally occurring radionuclides potassium (K)-40, thorium (Th)-232, and U-238. Field tests were subsequently performed at a set SSFL study area to evaluate the effects of soil moisture and barometric pressure on total gamma count rate measurements. Additionally, a borehole detector calibration facility is located at Walker Field in Grand Junction, Colorado. Tests were conducted at the facility to gauge borehole detector responses to known concentrations of radionuclide contaminants.

2.2 EQUIPMENT DESCRIPTION

Figure 2 is an image of a single large (4-inch by 4-inch by 16-inch) NaI detection system. The components shown in the figure are connected to form a mobile gamma scanning system that may be mounted on a variety of platforms.

Physically, field NaI detectors are sealed crystals subject to consideration of ambient temperature and moisture. For example, if the detection system is calibrated early in the morning at 70 degrees Fahrenheit (°F) and afternoon temperatures climbed to 90 °F, then the detector may be subject to significant drift (meaning the gamma spectrum would shift due to the temperature difference). The NaI crystal is chemically a salt which must be kept at very low moisture, otherwise the crystal itself degrades. The large NaI detection systems shown in Figures 2 and 3 have two design features to deal with these field conditions. First, every two minutes an internal temperature calibration is performed automatically using the K-40 signal present in the environment. Thus, electronic system drift is virtually eliminated. Second, the detector crystals are sealed in a case which excludes moisture and provides limited physical shock protection. Figure 3 shows the components inside the detector casing, which is sealed and not normally exposed to the environment.

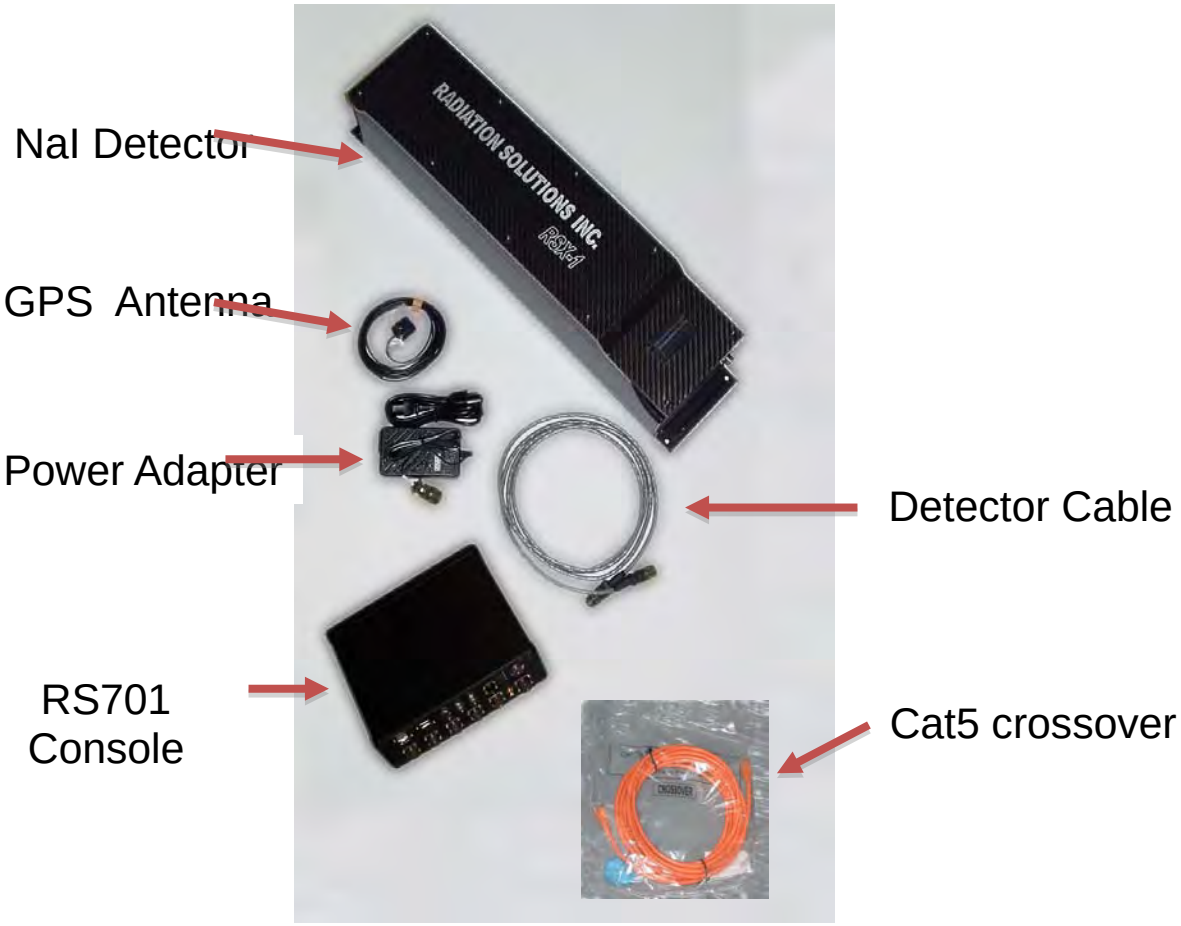

Figure 2
Outlay of Items Used for Large Detector NaI Gamma Scanning
(Images used with permission of Radiation Solutions, Inc.)

Figure 2 shows the various components required for a single large NaI detection system. Gamma spectral data is collected by the detector and stored on the RS701 or RS501 console for subsequent transfer and analysis. The global positioning system (GPS) antenna permits accurate mapping of gamma data and real-time recording of the detector path. The data is then assembled into maps showing gamma data, surface features, site and facility information.

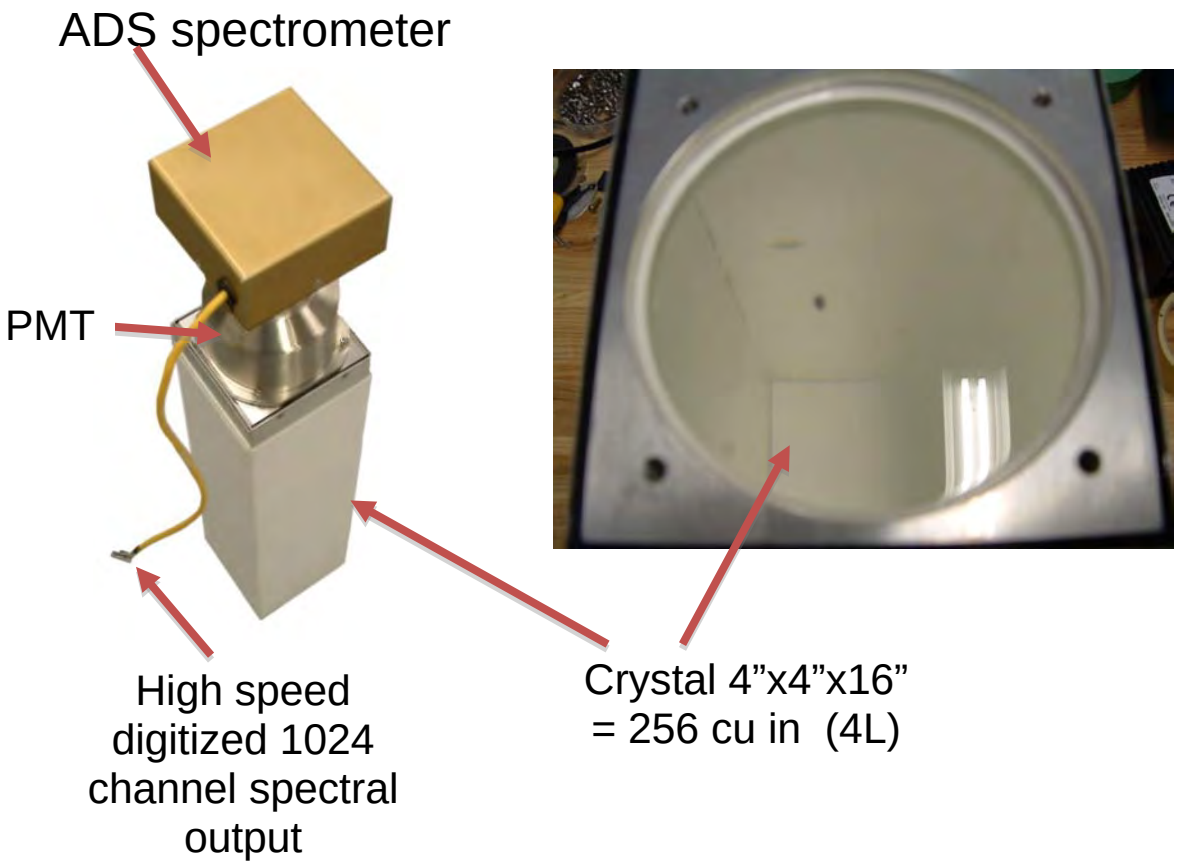

Figure 3
Exposed View of a Single NaI Scintillation Detector
(Images by permission of Radiation Solutions, Inc.)

Inside the detector case, the NaI crystal is hermetically sealed and is connected to a photo-multiplier tube and advanced digital spectrometer. In practice, the crystal shown at right is not visible. Gamma radiation interacts with the crystal, which creates scintillation or light pulses. These pulse signals are intensified through the photo-multiplier tube and recorded in the advanced digital spectrometer. The 1024 channels span gamma energies ranging from approximately 20 to 3,000 kilo electron volt (KeV) forming a gamma spectrum for each second of data.

Figures 4 through 9 show six ground scanning detection system configurations used for the study. Most feature large NaI detectors mounted beneath mobile platforms. The HHGS features a smaller NaI detector than the other systems. Each configuration is best suited to operate in specific types of terrain. The detection systems are:

- The ERGS II is an all terrain vehicle with an array of eight NaI detectors mounted on a telehandler (a telescoping forklift). Due to the size and weight of the detector array and the telehandler, the ERGS II mainly scans relatively open, flat or gently sloped terrain. The telescoping feature of the all-terrain forklift allows the detector to be extended over

ditches and up the sides of slopes, and this feature was used in certain areas where no other kind of scanning would have been possible.

- The MMGS is two large NaI detectors placed on outriggers, separated by approximately 40 inches, which are saddle-mounted on a mule. The MMGS primarily scans sloped to steeped sloped terrain which may be rocky or unsuitable for the ERGS II to scan. The MMGS supported on four relatively small hooves, can also scan biologically or culturally sensitive areas whereas the ERGS II, and, to some degree the TMGS and STGS, may cause a greater degree of soil disturbance.
- The TMGS is two large NaI detectors mounted on a gasoline-powered platform propelled by two rubber tracks. The TMGS can scan level to steep sloped terrain, but may not be the best choice for highly variable rocky surfaces because the platform required some degree of planar ground surface and the tracks tend to claw into the ground, further disturbing the surface soil.
- The STGS is one large NaI detector mounted on a gasoline-powered platform propelled by two rubber tracks. The STGS can scan on level to steep sloped terrain and it is more maneuverable than the TMGS but less sensitive. The STGS is not considered to be the best choice for highly variable rocky surfaces.
- The WMGS is a hand-propelled three wheeled cart with a single large NaI detector. This detection system mainly scans smaller areas that cannot be accessed by the other systems. It is difficult to operate the WMGS in thick vegetation.
- The HHGS is a Ludlum model 44-20 NaI detector mounted on a harness worn by the field surveyor to scan areas otherwise very difficult to access.

An important design aspect of each system is its shielding. Each system is designed to detect radiation coming from the ground, i.e., "to scan downward". This is partially accomplished by shielding the top and sides of the detectors. An important caveat for surveying the ground is that to accurately measure at low detection levels, there should be no large gamma sources nearby that could "shine" into the detectors, thus biasing the count. This issue was not observed at SSFL but could be important if systems like these were used in more of a site discovery situation. Each system, except the HHGS has a display to monitor in real time the scanning path and survey coverage, gamma data, GPS, and other information. The HHGS did not have spectral readout capabilities. An important consideration is that a balance must be struck between gamma detection sensitivity and the size, weight, and maneuverability of these detection system platforms in the field.

The detection system volume is directly proportional to the gamma detection efficiency due to an increased likelihood of interaction between a gamma ray and the detector. This is the main reason the larger systems generally have a greater sensitivity. Conversely, gamma detectors used for borehole scanning must fit inside a 2-inch internal diameter polyvinyl chloride (PVC) pipe inserted into the ground after subsurface soils samples were collected; thus, these detectors are used only for borehole gamma scanning in support of subsurface sampling activities. The borehole scanning detectors consist of a Ludlum Model 2221 meter with a Ludlum Model 44-2 or Model 44-62 NaI detector. The Model 44-2 is a 1-inch diameter by 1-

inch long cylindrical crystal with an internal photomultiplier tube. The Model 44-62 is a 0.5-inch diameter by 1-inch long cylindrical crystal with an internal photomultiplier tube. The selection of the Model 44-2 or Model 44-62 is primarily based on the diameter of the borehole being surveyed for gamma radiation.

The MMGS, TMGS, STGS and WMGS are shielded, but to a lesser degree than the ERGS II to reduce detection system weight for mobility in the field.

Figure 4
Enhanced Radiation Ground Scanner II Detection system

Figure 4 shows the ERGS II all-terrain vehicle mounted detection system that contains eight detectors and a 48-inch by 16-inch active detector surface. The detector array is encased in a metal shield with lead and copper lining to reduce radiation from above and the sides and to maximize sensitivity to radiation from the ground.

Figure 5
Mule Mounted Gamma Scanner Detection System

The MMGS has one detector on each side of a pack mule and MMGS scanning is guided by a mule handler.

Figure 6
Dual Detector Track Mounted Gamma Scanner Detection System

The TMGS has two parallel detectors mounted on a flexible platform propelled by a gasoline powered engine.

Figure 7
Single Detector Track Mounted Gamma Scanner Detection System

The STGS has one detector mounted on a flexible platform propelled by a gasoline powered engine.

Figure 8
Wheel Mounted Gamma Scanner Detection System

The WMGS has a field computer, the GPS unit (at front), and a single downward-facing detector.

Figure 9
Hand Held Gamma Scanner Detection System

The HHGS I has a compact field computer, a GPS unit (mounted on backpack), and a single downward-facing 3 inch by 3 inch detector encased in a protective polyvinyl chloride (PVC)

sleeve mounted on a harness attached to the operator's hip with a belt. In the background is an HHGS II (without a harness).

2.3 RADIOACTIVE SOURCES

Three types of gamma emitting sources were utilized in this study. The first are discrete point sources containing known quantities of Cs-137. Detector responses to Cs-137 point sources are used as a proxy for responses to individual gamma emitting radionuclides. Cesium-137 is deemed an adequate choice for response to several man-made radionuclides which may be present in Area IV. The second are considerably stronger radioactive point sources required for use in the subsurface sensitivity testing. The third are large area sources which, due to their size relative to the detection systems, are considered plane sources. The point sources were used in onsite tests whereas the plane sources were located offsite at a field calibration test facility. Each type of source is described below.

2.3.1 Sources for Laboratory Tests

National Institute of Standards and Technology (NIST) traceable Cs-137 sources were used during the sensitivity testing. Table 1 lists the activities in microCuries (μCi) and Becquerels (Bq) for four sources used in the tests. The sources were used as standalone sources or in combination to provide required activity levels.

Table 1
Santa Susana Field Laboratory Cs-137 Source Activity

Source Number	Activity (μCi)	Activity (Bq)
1405-41-9	0.9917	36,693
1405-41-10	0.9966	36,874
1429-85-11	1.131	41,847
1428-61-5	9.756	360,972

2.3.2 Sources for Subsurface Sensitivity Tests

A source container was constructed to hold radioactive sources. Two source configurations used in the tests were:

- One sealed 5 milliCurie (nominal value) radium (Ra)-226 licensed source provided by U.S. Environmental Protection Agency (USEPA)
- Twenty NIST-certified sealed 4.5 μCi Cs-137 sources combined with eight NIST-certified sealed 10 μCi Cs-137 sources

2.3.3 Field Calibration Test Facilities

Figure 10 is a diagram of the Walker Field Large Area Calibration Pads in Grand Junction, Colorado. The Department of Energy (DOE) constructed both the calibration pads and the borehole facility to calibrate radiological field instruments (Leino, et al., 1994). The pads are large area sources containing known quantities of the naturally occurring radionuclides K-40, Th-232, and Ra-226 (a progeny of U-238). The pads are concrete slabs measuring 30 feet by 40 feet and are approximately 1.5 feet thick.

The borehole test structure used in this study is concrete, cylindrical, and 30 feet deep and approximately 4 feet in diameter with a borehole pipe in the central axis having a 4.5-inch diameter. The U borehole (model U) used for the borehole detector response tests has been characterized as having "background" or uncontaminated concrete at top and bottom depths with an "enriched" or contaminated zone containing U as its Ra-226 progeny (Leino, et al., 1994).

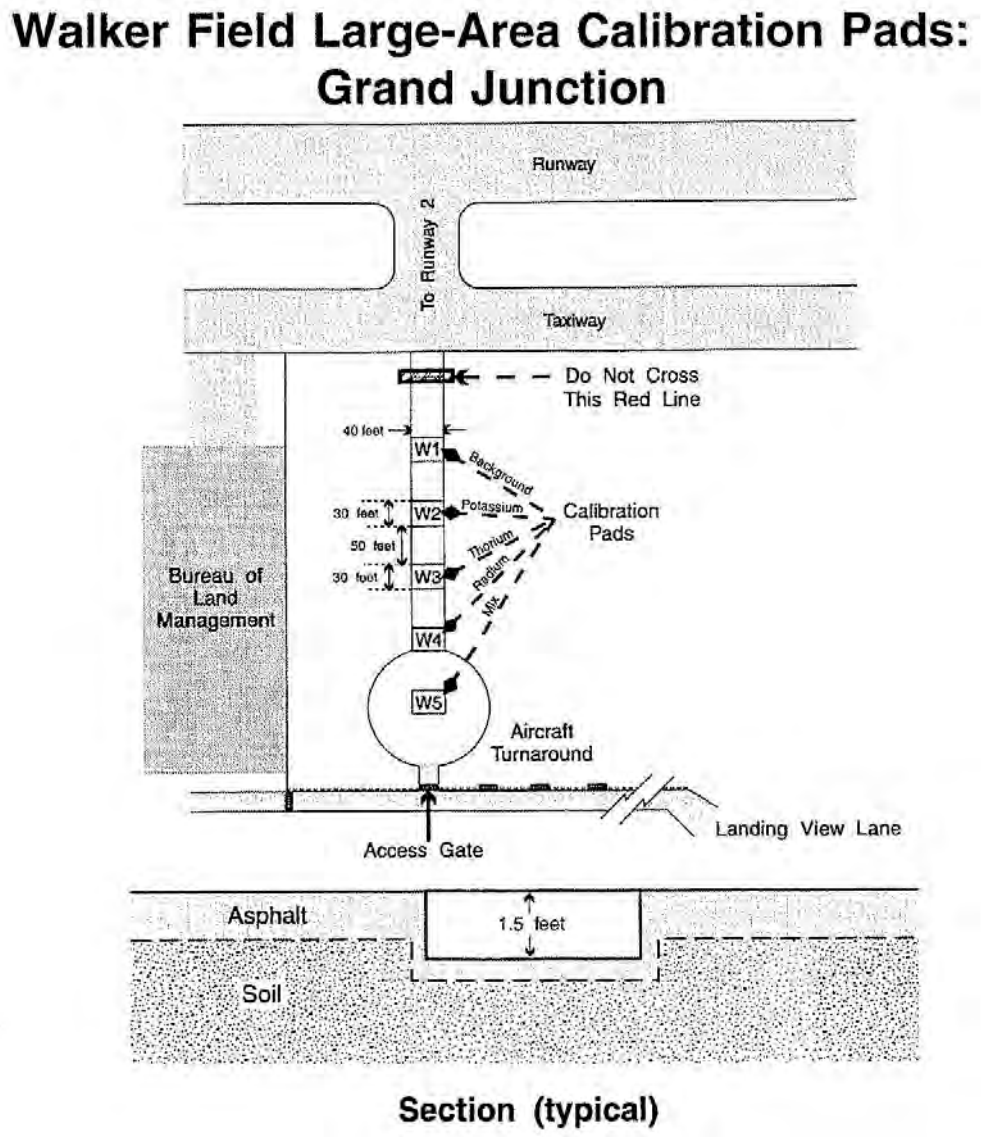

Figure 10
Map and Cross Sectional View of the Walker Field Calibration Pads
(Excerpted from Leino, et al., 1994)

These large area pads were built to facilitate detection system response calibrations for large area radiological surveys such as this study as well as aerial surveys primarily for determining the extent of mineral deposits.

2.4 ONSITE LABORATORY AND FIELD TESTING

Detector quality control analyses were performed before data collection commenced. A five minute background count rate was collected before and after each radial test plot for a specific detection system was completed. Mean background count rate data were used to calculate net Cs-137 count rates.

The detection system was leveled and placed at a specific test height. All testing required the detection systems to be supported in a fixed position. Physical replicas were utilized for the MMGS and the WMGS to simulate a mule and a human, respectively. A 35-gallon drum filled with water was used to represent the torso of a mule and was positioned on the MMGS stand. The legs of a human surveyor were simulated using 16 ounce water bottles taped to wooden supports for the WMGS tests.

A Cs-137 source was placed at a specified location in relation to the detector and data was collected at a rate of one gamma spectrum per second. Each second of data contained 1024 channels spanning approximately 3 mega electron volts (MeV), with a fixed energy to channel ratio of 3 keV per channel. For the FOV and height tests, the sources were stationary; in the velocity tests, either the sources or the detection system was moved along a specific path, meaning they were moving relative to each other to simulate a scanning mode of data collection.

Figure 11 is a diagram of radial source test locations with ray and radial distance labels. Cesium-137 sources were positioned at the locations depicted in Figure 11[1] (Bendix Field Engineering Corporation, 1981). A source position template was constructed by marking a tarpaulin as a compass rose with eight rays (labeled A through H). The tarpaulin was affixed to the floor and the center of the detector (the geometric center of the NaI crystal not including the protective casing) was positioned above the origin using a plumb line. The detectors were positioned with the forward travel direction aligned with ray "A". Each successive ray increased by 22.5 degrees clockwise from ray "A". The test locations from 180 to 337.5 degrees are denoted as negative relative to the origin. For example, test location C12 is at ray "C" which is 45 degrees clockwise from ray "A" and 12 inches from the origin and E-6 is at ray "E" 270 degrees clockwise from ray "A" at 6 inches from the origin.

[1] There are 168 radial source test locations in total. Not every location was tested on all detection systems if the test source was not detected, particularly at the most distance radial locations.

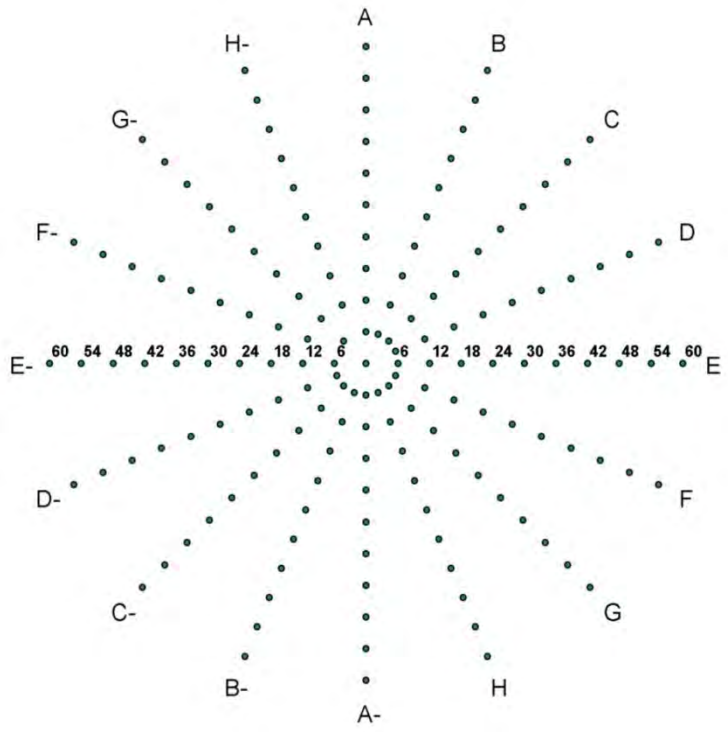

Figure 11
Diagram of Radial Source Test Positions

The origin is the central reference point. Radials are labeled as 16 rays extending from the origin, with ray "A" oriented in the detector direction of travel. The positions extend outward from the origin in 6-inch increments, up to a maximum distance of 60 inches from the origin.

In Figure 12, the MMGS is positioned on top of a saddle on a mule stand built to both support the detection system platform and physical replica of the torso of a mule. The MMGS detector positions are adjustable using the outriggers such that different mules can be exchanged and the detector scan height remains constant.

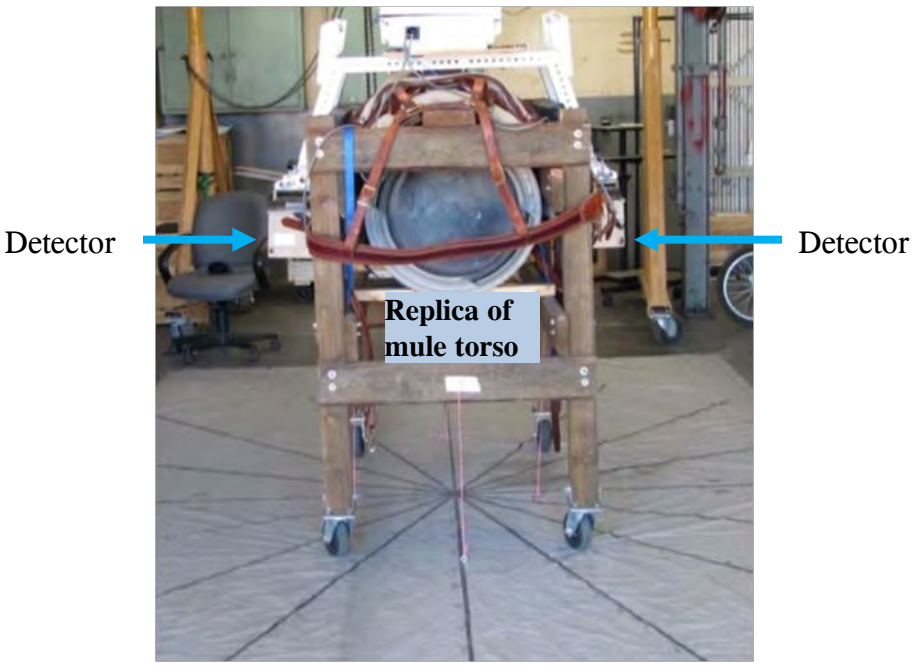

Figure 12
Mule Mounted Gamma Scanner on Radial Plot Template

The MMGS was centered over the radial source position template prior to commencing the laboratory testing. The use of a test stand was necessary because a mule cannot stand motionless during the entire testing process.

2.4.1 Field of View Testing

The detector was centered above the origin and the "A" ray of the radial template was aligned with the forward travel direction of the detector. Detector height was set at the selected operational height of each system, as indicated in Section 2.4.2. Use of a radial grid of point source positions provided an effective means to assay detection sensitivity with the activity present in any direction relative to the detection system.

One minute of data was collected for each source position with up to 168 positions measured for each detection system. The source was repositioned at the next source location and the collection process repeated until the radial test grid was completed for each system. The total distances covered in radial tests varied by the detection system; data were collected up to 60 inches from the center for the ERGS II and the MMGS, but slightly less (up to 54 inches) for the WMGS. This difference is due to the fact that Cs-137 was detected just above the mean background count rate at the most distant positions for the WMGS and had relatively high errors. Partial radial data also were recorded for the ERGS II and MMGS at two additional heights for the comparison of FOV data information from various operational heights (data not shown).

2.4.2 Height Testing

The detector was suspended while the source was lowered in fixed increments to a given distance directly below the centerline of the detector. One minute of data was collected at each source position. Height was based on distances between the detector center and the source position. The ERGS II height tests ranged from 0 to 30 inches, the MMGS height tests ranged from 5 to 35 inches, and the HHGS was height tested from 0 to 36 inches. Height was not tested for the TMGS, STGS or the WMGS because the detectors are mounted at a fixed-height for each of those systems.

2.4.3 Velocity Testing

Velocity tests were conducted by moving sources at a constant speed while maintaining detection systems in a static position for the ERGS II, WMGS, MMGS, and HHGS, and with the source in a fixed position and the detection system moving over the source at a constant velocity for the TMGS and STGS. Detector height was set to the selected operational height of each system as discussed in Section 2.4.2. A reference line was positioned at the central axis in the forward travel direction of the detector. This line ensured the source would consistently pass directly under the detector. The source was placed in a holder and attached to a string that was used to move the source under the detector. Velocity tests began with the source positioned outside the detector forward FOV and ended with the source at the rear of the detector FOV. Three tests each were recorded for velocities of 1, 1.5, 2, and 3 feet per second (ft/s) used to move the source under the detector. The string was advanced using one of two human powered methods. In both cases, one person advanced the sources under the detector as another counted a cadence aloud. In this way, the person moving the source concentrated on the source and not a clock. The string was marked with specific length intervals appropriate for the test velocities. In one case, the technician pulled the string hand-over-hand. In another case, the technician held the string and walked along an incremented pathway. In both cases it was a well practiced and timed activity.

2.4.4 Subsurface Sensitivity Testing

Tests were conducted to plot detection sensitivity versus soil depth profiles and compare these to predicted sensitivity with soil depth. The predicted sensitivities were based on calculated soil attenuation with depth and known distances from the source to the detection system. Data were collected as total counts per second (total gamma spectrum) or Cs-137 ROI counts per second from Ra-226 or Cs-137 sources, respectively.

An area was selected that had been previously surveyed and was free of detectable concentrations of contamination. This area was accessible, relatively flat, and contained grass. The testing procedure and sequence is described below.

- A borehole was created to insert the radioactive sources. A 14-foot long, 3-inch diameter borehole was drilled at a 45 degree angle as seen in Figure 13. The bottom of the borehole was 10 feet below ground surface (bgs). A 14-foot long, 2-inch inside diameter PVC pipe with a permanent end cap on the bottom and a removable end cap

on the top was inserted into the borehole. These end caps sealed the pipe from moisture, which could influence the test.

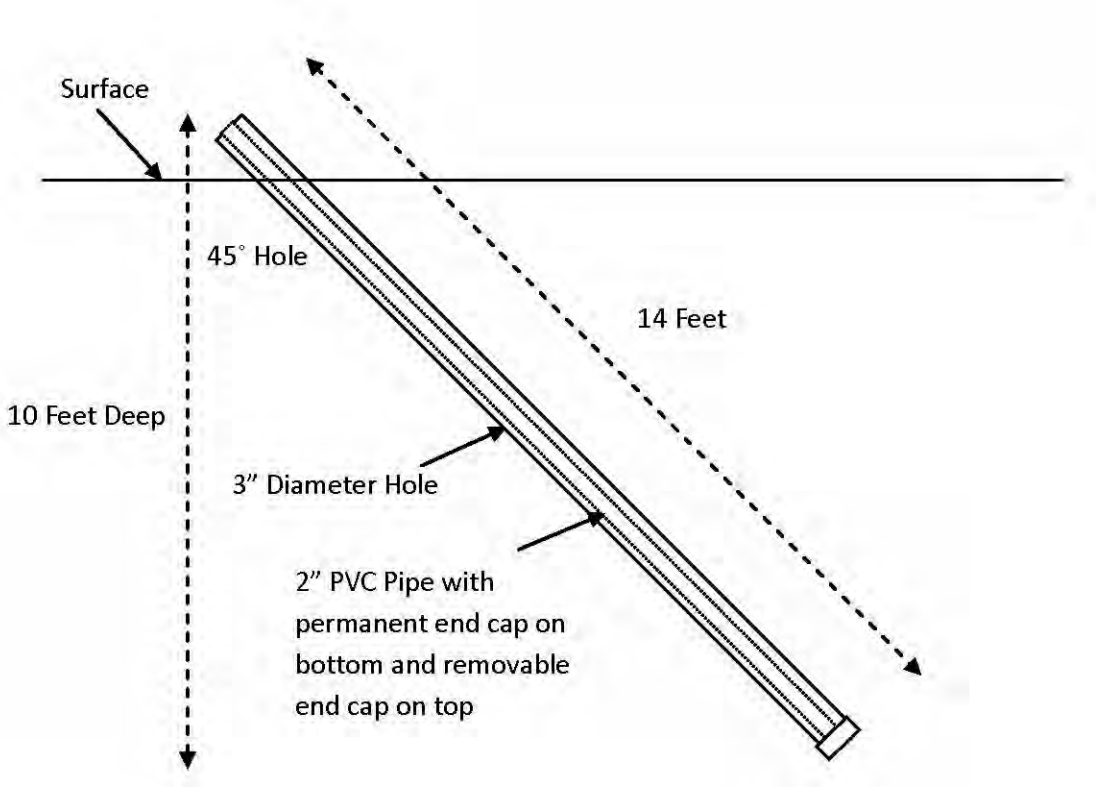

Figure 13
Subsurface Sensitivity Test Borehole Diagram

- A source container was constructed to hold radioactive sources. The source container was attached to a cord and lowered into the pipe. For each 12 inches of vertical distance through the soil, the sources traveled approximately 17 inches in total. To prevent gamma rays from passing through the open borehole and affecting the measurements, a 0.5-inch thick lead shield was placed on the pipe opening at ground level as seen in Figure 14.
- The maximum test depth was determined. A detection system was positioned in alignment with the centerline of the borehole above the 10-foot depth interval and then moved over the pipe directly above the source location in sync with the source as it was withdrawn in 1-foot increments up the pipe. Once a visible signal was detected, movement of the detector was stopped. The depth was recorded and the interval 2 feet below this increment was selected as the maximum source depth. This ensured the data collected spanned depths beyond those which were easily observed in the field.
- The background count rate was determined by performing a 3 minute static count at the 5-foot test depth position with no sources present. The background data were used to calculate net response rates.

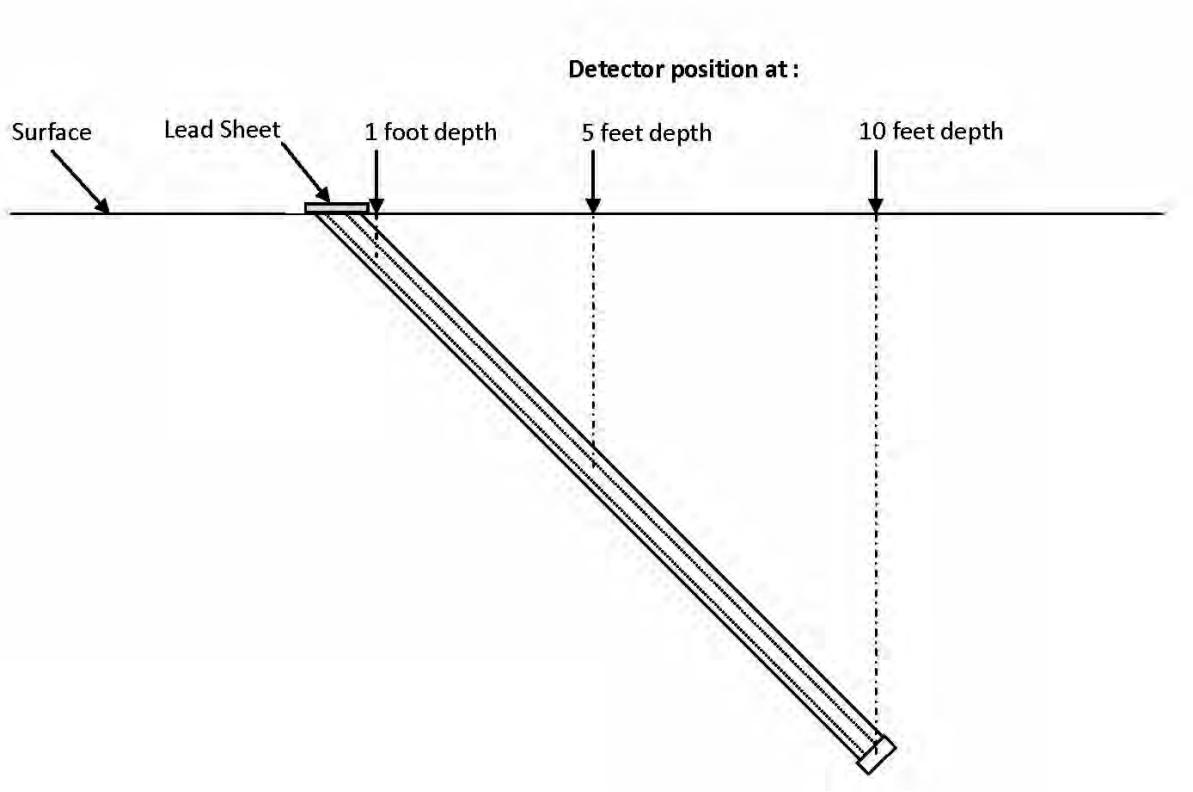

Figure 14
Detection System Position in Relation to Source Depth

- Scanning and static measurements were collected at each depth with the Ra-226 source and the Cs-137 sources. Static and scanning measurements were performed at each depth interval for all applicable detection systems. Then, the source was positioned at the next test depth and the static and scanning measurements were repeated for each applicable detection system. This procedure reduced personnel exposure to the sources in accordance with as low as reasonably achievable radiological safety practices.

For static measurements, the source was positioned at the maximum test depth. Each detection system was centered over the source such that the center of the active detection surface was perpendicular to the centerline of the borehole and directly above the source location. The detection systems collected a static measurement for one minute, except the ISGS which collected a measurement for five minutes. This process was repeated for each detection system requiring a measurement at a particular depth.

For scanning measurements, the source remained at the first static depth. A detection system was positioned approximately 20 feet from the source location and moved directly toward the source location at the maximum acceptable scanning rate of the system. The detector was orientated perpendicular to the borehole centerline such that the detector's geometric center passed over the source location. The height of each detection system was consistent with

standard operating heights of the system. The testing velocity was generally equal to the maximum velocity. An exception to the velocity was the MMGS, which utilized a test stand as a proxy for a mule because the mule could not remain stationary for a series of static counts. Since the mule test stand had hard casters that were not suited for field use, the scanning velocity was limited to 2 feet per second (compared to the MMGS maximum velocity of 4 feet per second). After passing over the borehole, data collection stopped at approximately 20 feet past the source. This step was repeated to gather two datasets for each detection system and depth combination. This allowed for discarding a dataset if there was an error in scanning velocity. This process was repeated for each detection system requiring a measurement at a particular depth. The ISGS was not used in the performance the scanning measurements as it was not a mobile detection system.

The source container was then withdrawn to the next higher one-foot depth interval. Scanning and static measurements were obtained at the new depth interval and the source depth changed until all measurements were performed. Measurements were not collected when the detector was saturated at a particular depth. This occurred at the one-foot depth increment using the Ra-226 source for all detection systems.

The responses of each detection system to known quantities of Cs-137 and Ra-226 were recorded. For each system, a detection capability profile based on depth was generated.

2.5 PROCESSING OF SANTA SUSANA FIELD LABORATORY DATA

Raw test data was transferred from the detection system data acquisition console and inspected using the manufacturer's (Radiation Solutions, Inc.) gamma spectrometry software, RadAssist, version 3.15.1. The software is designed for gamma scanning such that each second of data contains a full spectrum of 1024 channels. However, only the total gamma spectrum and Cs-137 ROI data were used for evaluation and analysis. Cesium-137 emits a gamma peak at 662 keV. The Cs-137 ROI was defined as lower and upper energy limits of 600 and 735 keV, respectively, which covers the entire Cs-137 energy range for NaI detector resolution. Cesium-137 was the source gamma radiation for all tests, thus evaluations and comparisons were based on net Cs-137 data; i.e., background values for the Cs-137 energy range were subtracted from gross measurements.

The purpose of the testing is to gauge detection system response to the presence of known quantities of gamma radiation. Spectra are composed of a continuum of gamma energies. Even if no source is present, the detector will have count data present in the Cs-137 ROI; exclusive use of net Cs-137 data ensures that evaluations will be based on signal contributions from a Cs-137 source only.

It is important to note that the data from the NaI scanning detectors was used to identify locations having either anomalous total gamma count rates or preferably, anomalous data within a specific radionuclide ROI. Data within a particular ROI are generally more useful than the total gamma count rate because the energy-specific data may be used to identify presence of a gamma emitting radionuclide.

Test data was collected as a series of detector-source positions with time stamps recorded to identify specific test conditions. For FOV tests, 1 minute of data was collected at each source location; from these sixty, 1-second gamma spectral files, the central 20 seconds of data was selected for data analysis. This allowed for the technician to position the source, then record information in a logbook, and to move clear of the source and detector area as not to influence the measurements. Total count rate, Cs-137 count rate, and time stamp data were selected and exported to Microsoft Excel for data manipulation and evaluation. The data were correlated with their test conditions and were uniquely identified. Consistent data processing and evaluation was performed for each detection system.

Data processing is illustrated in the following discussion, using ERGS II background and radial plot test data as an example. Table 2 shows a summary of statistical background results from positions A36 through A0 to illustrate an initial data processing step. The ERGS II background data was collected from a 15 inch operating height.

Table 2
Enhanced Radiation Ground Scanner II
Background Data from a 15-inch Operating Height

Value	Total Spectrum (cps)	Cs-137 ROI (cps)
Mean	10432	437.7
1 SD	110.4	19.9
2 SD	220.7	39.9
3 SD	331.1	59.8
1 SD/Mean	1.1%	4.6%

Table 3 shows a subset of ERGS II net Cs-137 data because the entire radial test data would require several pages to display. It contains data from positions A36 through A0 to illustrate an initial data processing step. Table 3 lists the ERGS II mean, net Cs-137 count rate, and one SD of the mean data generated from 20 seconds of consecutive count rate data from each test location. Raw data include count rate contributions from gamma radiation from both the source and any ambient "background" radiation. Net Cs-137 count rate is the mean Cs-137 value ($n = 20$, where n denotes the number of observations) less the mean Cs-137 background ($n = 600$), which was 437.7 cps. (Data comprising the background, gross counts, and other raw data supporting this document are provided contained in a supporting information compact disc.)

Table 3
Enhanced Radiation Ground Scanner II
Cs-137 Data from Select Radial Test Locations

Radial Location	A36 (cps)	A30 (cps)	A24 (cps)	A18 (cps)	A12 (cps)	A6 (cps)	A0 (cps)
Mean Gross Cs-137	619.6	768.2	994.1	1309.0	1652.3	1913.0	1929.4
Mean Net Cs-137	182.0	330.5	556.4	871.3	1214.7	1475.3	1491.7
Mean 1 SD	19.9	25.1	30.1	30.8	41.0	38.7	37.1
1	635.3	758.4	1001.6	1304.0	1737.3	1888.3	1865.7
2	595.4	733.5	929.6	1368.0	1597.4	1885.4	1970.7
3	604.4	790.5	967.7	1239.0	1618.4	1997.6	1927.4
4	658.4	785.6	1021.6	1301.8	1656.4	1950.8	1879.4
5	620.4	769.5	982.8	1319.9	1669.4	1879.6	1927.4
6	596.3	792.6	966.5	1292.2	1667.2	1858.5	1916.3
7	646.5	788.4	988.6	1335.8	1683.3	1888.5	1940.6
8	603.3	768.5	1012.7	1313.0	1600.3	1973.5	1988.8
9	632.5	730.6	1021.6	1305.0	1651.1	1906.4	1990.7
10	626.4	738.5	1004.5	1318.9	1677.5	1841.4	1952.7
11	621.3	800.5	1028.8	1305.8	1675.3	1889.5	1881.6
12	649.4	786.5	987.6	1308.8	1605.2	1924.7	1925.4
13	596.3	775.4	956.6	1312.9	1664.2	1919.7	1914.4
14	625.5	768.5	983.7	1356.8	1641.2	1920.7	1927.2
15	630.4	792.8	1017.7	1307.9	1662.4	1880.6	1950.4
16	595.4	741.4	1038.8	1294.1	1650.1	1924.5	1915.5
17	626.4	728.5	941.8	1358.9	1673.3	1921.5	1985.6
18	588.4	767.4	995.7	1294.9	1689.2	1918.4	1915.5
19	622.3	806.5	1030.8	1261.8	1676.5	1924.6	1873.3
20	618.4	740.4	1002.5	1280.0	1551.0	1965.6	1939.8

Note:
Notice the increase in mean Cs-137 count rates as the positions are closer to the center of the detector (located at position A0). The term 1 SD is one standard deviation of the mean of the 20 observations.

2.6 GAMMA RADIATION TRANSMISSION THROUGH SOIL

Many of these large NaI detection systems were assembled and developed for this study, thus a central question was at what depths could known quantities of radiation be detected? In lieu of rigorous depth testing, the gamma ray transmission through soil was calculated using NIST gamma energy attenuation coefficients. However due to the project schedule and utilization of the systems for data collection, field testing to answer this question was not conducted until after gamma scanning was completed. The results of this testing did not impact gamma measurements as this data provided only an estimate of the depth detection capability of each system.

2.6.1 Estimated Gamma Ray Transmission through Soil

Figure 15 shows the gamma transmission (the percentage of gamma radiation which penetrates the soil) as a function of gamma energy and selected soil thicknesses[2] (NIST, 2010). Gamma transmission is calculated using Equation 1, for soil depths of 1, 2, 4, 8, and 16 inches.

Equation 1:

$$T = \frac{I}{I_0} = Be^{(-\mu x)}$$

Where:

T is transmission which is the attenuated gamma photon intensity (I) divided by the source gamma photon intensity (I_0)

B is the buildup factor, and the attenuation at a particular energy is calculated using applicable linear attenuation coefficients (μ) and soil thicknesses (x).

Equation 1 is often described as two forms of equations, without and with the buildup factor. The form without the buildup factor applies to a radiation beam (radiation is detected in a straight line from the source) with a relatively thin absorber (soil thickness). Buildup is applied when the soil thicknesses are large and radiation is detected from a variety of directions (as in these field tests).

The buildup factor accounts for the probability of gamma radiation which collides with material between a source and a detection system to be detected. Figure 16 is a cross-sectional diagram that illustrates gamma ray buildup in soil with similar dimensions to the experimental setup of subsurface sensitivity testing. Buildup is a function of the thickness and density of the medium (soil), the source to detector distance, the size of the detector, and gamma energy (thus the radionuclide or radionuclides being detected). Buildup increases the count rate from what would be expected from attenuation alone. Rigorous calculations of buildup are beyond the scope of this document.

For the sole purpose of estimating overall gamma transmission through soil over a wide range of gamma energies, buildup can be ignored. The transmission of gamma radiation is comparatively much lower at low gamma energies. Inspecting Figure 15, the gamma transmissions through a 1-inch thick soil column are 88 percent at 3 MeV, 80 percent at 1 MeV, 69 percent at 0.3 MeV, and drops to 55 percent at 0.1 MeV. At energies below 0.1 MeV (100 KeV), the transmission of gamma radiation through soil is limited.

[2] Gamma attenuation in soil was approximated using NIST photon attenuation coefficients. The coefficients for ordinary concrete were used as a proxy for soil with each coefficient reduced by the proportionate difference in density. NIST reference concrete has a density of 2.30 grams per cubic meter (g cm^{-3}) and the median local SSFL soil density is 1.76 g cm^{-3}, hence coefficients were reduced by 0.77 (= 1.76/2.30).

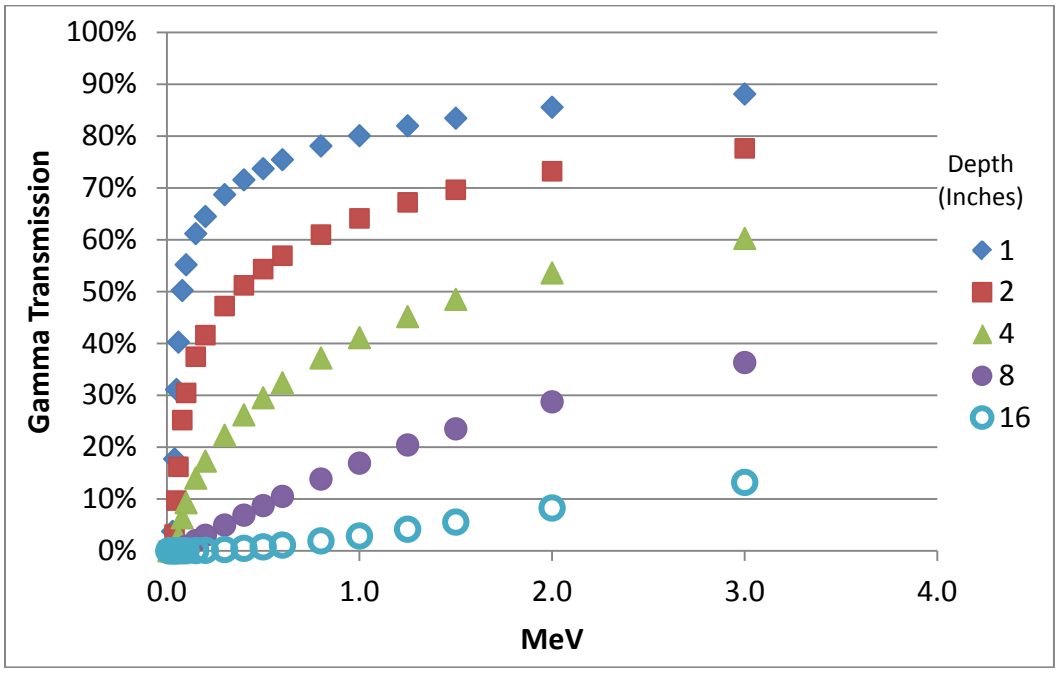

Figure 15
Gamma Transmission Estimates Through Various Soil Thicknesses

Gamma transmission through soil depends on both the gamma energy and the soil thickness.

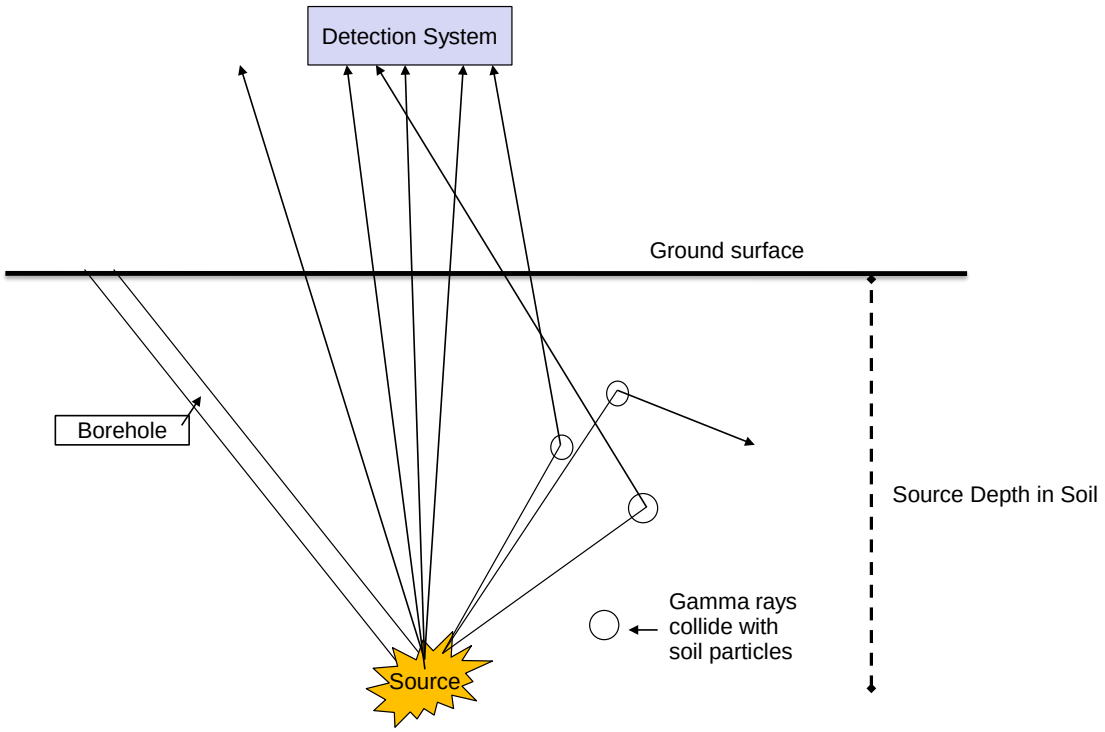

Figure 16
Conceptual Diagram Illustrating Gamma Ray Buildup

Buildup accounts for gamma rays which strike nuclei of soil particle elements and some of those rays are re-directed to the detection system. Thus, the count rate can be greater than that predicted from the source strength and transmission through soil alone.

2.6.2 Methods to Compare Observed Subsurface Sensitivity Count Rates with Predicted Count Rates

Detection system responses to known quantities of Cs-137 and Ra-226 at discrete depths in soil were observed for static and scanning measurements. The purpose of these tests was to compare field count rate data to predicted results. Calculation of these requires correlation of count rate data with distance and soil depth. As discussed in subsequent sections, increasing the distance between a radioactive source and a detection system decreases the count rate. Increasing source depth dramatically decreases count rate due to gamma ray attenuation by soil.

Accounting for these factors required approximating the source to detection system distance approximations and calculating the transmission of gamma radiation through soil. Three equations apply to source to detector distance approximations for commonly encountered situations and to count rate estimations. These are based on the respective geometries of source and detection system and are known as point – point, point – line, and point – plane

approximations. They are a function of both the distances between the source and detector and the geometries of each.

The most appropriate equation for the subsurface sensitivity test distances is the point - line approximation (Gollnick, 2006). This normally describes a situation in which a small detector (point geometry) is used to measure a relatively large radioactive source, such as a contaminated pipe (line geometry). However for these tests, the small radioactive source is approximated as a point and the relatively large detection systems are approximated as lines.

Equation 2 describes the approximation for a point - line geometry. Count rate (R) is inversely proportional to the distance (D) between the source and the detection system.

Equation 2:

$$R_a D_a = R_b D_b$$

Equation 3 incorporates the soil attenuation of Equation 1 and describes the relationship between count rate and the transmission of gamma rays through a specific depth of soil. Count rate is proportional to the gamma ray transmission through the soil (T).

Equation 3:

$$R_a / T_a = R_b / T_b$$

Equation 4 is the mathematical combination of Equations 2 and 3.

Equation 4:

$$R_a D_a / T_a = R_b D_b / T_b$$

Equation 4 allows approximation of an expected or predicted count rate based on count rate measured at a known distance, known source strength, and estimated transmission through soil.

2.7 SCANNING DETECTOR RESPONSES TO THE WALKER FIELD CALIBRATION PADS

Figure 17 is a photograph of the Walker Field calibration pads which are also shown schematically in Figure 10. Of these pads, gamma count rate data was collected from pads W1 (the background pad) and W5 (the mixed isotope pad). ERGS II data was collected in three inch increments beginning at zero inches and ending at a height of 36 inches. MMGS data was collected in three inch increments starting a zero inches and ending at a height of 30 inches from the surface. WMGS data was collected at only 12 inches from the surface. Height data were collected to be informative of the detection system responses to large area distributed sources, and were not intended to support decisions related to operating height in the field.

The gamma spectral data was processed and evaluated according to the radionuclide ROI, based on primary gamma peak energies for K-40, Th-232, and U-238 (as Ra-226).

Figure 17
Calibration Pads W1 through W5 in Grand Junction, Colorado

These pads were designed and constructed to provide large area sources for the calibration of field gamma detection equipment, including both ground and aerial scanning systems.

2.8 SCANNING DETECTOR RESPONSES TO ENVIRONMENTAL CONDITIONS[3]

2.8.1 Soil Moisture

The SSFL Area IV Radiological Study Gamma Radiation Scanning Sampling and Analysis Plan stated gamma scanning would cease if soil moisture exceeded 15 percent soil moisture (HGL and TPC, 2010). This value was selected based on the standard American National Standards Institute (ANSI) N42.23 (ANSI, 2006) which recommended a 15 percent soil moisture maximum limit for the calibration of in situ gamma radiation detectors (Institute of Electrical and Electronics Engineer, 1997).

An on-site field reference area (FRA) was selected to study the effect of soil moisture on total gamma count rates. The FRA is a 1.26 acre area located in Area IV which was selected based on its representative physical, radiological, and geological characteristics and its close proximity to the USEPA field office. The FRA is flat, open, and vegetated with predominately grasses.

[3] The environmental study methods, results, and discussions are all excerpted and edited from the Technical Memorandum: Effect of Soil Moisture on Gamma Radiation Count Rate Measurements (TPC, 2011).

An approximately 6-foot by 4-foot area within the FRA was selected as a soil moisture study location, its perimeter was marked, and gamma count rate data were collected at this specific location over a period of seven weeks during the wet season. Soil moisture readings using a nuclear density gauge require the removal of a small area of vegetation as part of the data collection process. Denuding vegetation in such a small surface area would very likely alter the soil moisture content of the area over the duration of the study. Therefore, the soil moisture tests were collected in the FRA closely neighboring yet not precisely at the study location. This way, the vegetation in the soil moisture study location remained intact during and beyond the study.

Soil moisture measurements were taken with a Troxler, model 3430, nuclear density gauge which is shown in Figure 18. The gauge uses an americium-241-beryllium neutron source and a tritium detector tube to measure soil moisture. Caution was exercised to keep the Troxler at a sufficient distance to prevent interference with the ERGS II while gamma radiation measurements were collected. An approximately 12-inch by 6-inch area within the FRA was scraped clear of vegetation and leveled for nuclear density gauge measurements. Each measurement was recorded for one minute. The percent soil moisture read from the gauge display was recorded into the Troxler logbook.

A total of 25 gross gamma radiation count rate and soil moisture measurements were collected over the period of December 1, 2010, through January 24, 2011. Measurements were usually collected in the morning between 7:00 a.m. and 10:00 a.m. However, in a few cases measurements were collected later in the day. Gamma total count rate data (spanning an energy range from approximately 6 to 3,000 keV) was collected using the ERGS II. Daily quality control checks were performed on the ERGS II and Troxler prior to use to verify instruments proper function. The ERGS II was positioned within the moisture study location and gamma measurements were collected with the detector parallel to the ground at a height of 15 inches for a 10 minute static count. The start and stop count times were recorded as displayed in RadAssist. The radiation data were automatically saved to the detector's data storage console for later file transfer and data processing.

Figure 18
Nuclear Density Gauge

The nuclear density gauge can use both neutron and gamma sources to measure soil density and calculate soil moisture.

Meteorological data collected at The Boeing Company's onsite weather station was supplied by The Boeing Company. The monitoring station participates in an external certification and performance audit program, in accordance with USEPA specifications (USEPA 454/R-99-005). Meteorological observations were noted in the field logbook.

The raw data collected by the ERGS II was transferred from the data storage console and processed through RadAssist. Data were entered into a Microsoft Excel spreadsheet. The average total gamma count rates were calculated in cps. Soil moisture data were plotted with the corresponding gamma count rates. Data were evaluated to remove outliers which were determined by statistical analysis using the USEPA's Scout 2008 Version 1.0 statistical software program (USEPA, 2009).

2.8.2 Barometric Pressure

Barometric pressure may affect the emanation of natural radon-222 from surface soils. The effect of barometric pressure on the gamma radiation count rate was studied at the FRA. The same total gamma count rate data collected and processed as described in the soil moisture section were used to evaluate correlations with barometric pressure.

Atmospheric pressure data was obtained from The Boeing Company's onsite meteorological station using a Climatronics digital pressure sensor barometer Model #102663. Pressure data

is automatically recorded on the hour by the barometer. The total gamma count rate data were correlated to the barometric data based on the times the gamma measurements were collected.

2.9 BOREHOLE DETECTOR RESPONSES TO THE DEPARTMENT OF ENERGY GRAND JUNCTION CALIBRATION MODEL

A DOE borehole facility constructed with a depth zone of known concentrations of radionuclide contaminants was used to test the detectors which measure borehole gross gamma activity at the SSFL. Figure 19 is a diagram of the borehole model used for field testing. The borehole detectors are operated in a total count mode only, thus the test data consist of total counts on each detector in response to the borehole model U. In short, a static one-minute count was collected each depth increment, proceeding from the surface to 10-foot depth.

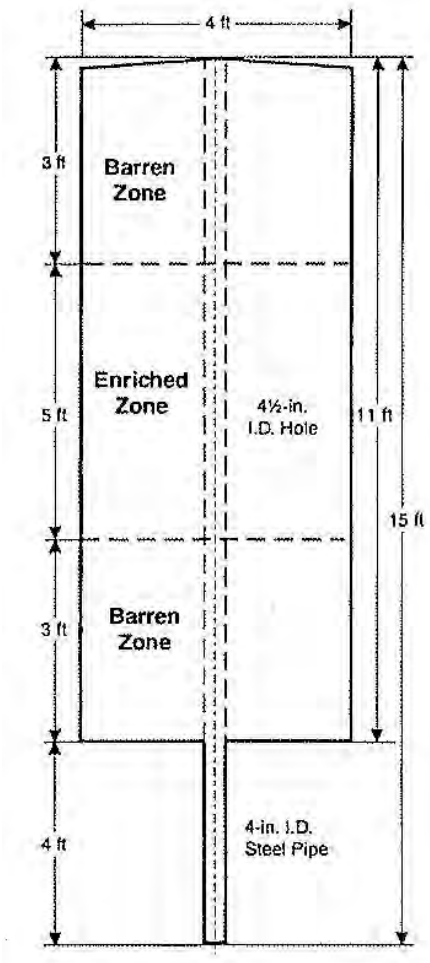

Figure 19
Plan Drawing of Grand Junction, Colorado Borehole Test Model U

The drawing depicts barren or uncontaminated zones extending both from 0 to 3 feet below ground surface and below 8 feet and a central contamination or enriched zone extending from 3 to 8 feet below ground surface. The borehole pipe inside diameter is 4.5 inches.

3.0 RESULTS AND DISCUSSION

Several different types of gamma detection systems and experiments are contained in this report. The results will be discussed in the following order:

- Contour plots showing each detection system net Cs-137 count rates relative to the detector positions
- Detection systems key operational scanning parameters:
  - FOV
  - Scanning Height
  - Maximum Scanning Velocity
- Calculated scanning MDAs and MDCs in soil
- Subsurface sensitivity test results
- Detection system responses to Walker Field calibration pads
- Detection system responses to environmental conditions
  - Total gamma count rate correlation with percentage soil moisture
  - Total gamma count rate correlation with barometric pressure
  - Borehole detector responses to borehole test calibration facility

The process for testing the systems, collecting test data, and evaluating the test data to establish the FOV, scan height, and maximum scan velocity is presented in the same order for each scanning detection system; therefore, detailed process descriptions are presented for the ERGS II as an example. For the MMGS, TMGS, STGS, WMGS, and HHGS only results are presented. For the HHGS only total count data was obtained as the instrument has no gamma spectroscopy capability. This is an important factor when field detectable MDCs are calculated because the MDCs from region-specific spectra do not directly compare to a total gamma spectrum.

Table 4 provides a definition of terms that are discussed to process and interpret data. These are described briefly here for familiarity, and will be presented in greater detail in this section.

Table 4
Definition of Terms

Term	Meaning
Field Of View	A soil surface area (length and width) under a detection system which is the extent in which the integrated relative efficiency is 0.5. Operationally, a FOV width is larger than a scanning transect width, to ensure some overlap between transects and to ensure complete surface coverage.
Relative efficiency (RE)	The efficiency at a surface source location divided by the maximum detection efficiency which occurs directly under the center of the active surface of a detector.

Table 4 (Continued)
Definition of Terms

Term	Meaning
Integrated relative efficiency	The efficiency over a particular surface area. The integrated relative efficiency will be compared to and normalized to the efficiency directly under the detector surface area.
Absolute efficiency	The measured efficiency for the detection of Cs-137 in the FOV of the detection system. It is understood that the detection efficiency of Cs-137 will differ from those of other gamma emitting radionuclides.
Scanning efficiency ratio	The ratio of velocity count rates to static count rates. The scanning efficiency ratio accounts for decrease in count rate data collected as a function of time the detection system may be near a radioactive source.
Overall field efficiency	The product of the absolute efficiency and the scanning efficiency ratio.
Gamma transmission	The percentage of gamma radiation (at a particular energy) which penetrates a specific thickness of soil.

3.1 ENHANCED RADIATION GROUND SCANNER II

With the data from the multiple radial test locations assembled into a detector response field, Figure 20 shows the net Cs-137 contour intervals for the ERGS II. This type of illustration gives a 'snapshot' of net count rates and provides intuitive information about detector response, yet it is not useful for quantitatively defining a FOV which is the focus of the following sections. The design of the shield also shows no dramatic (undue) shielding effects due to construction.

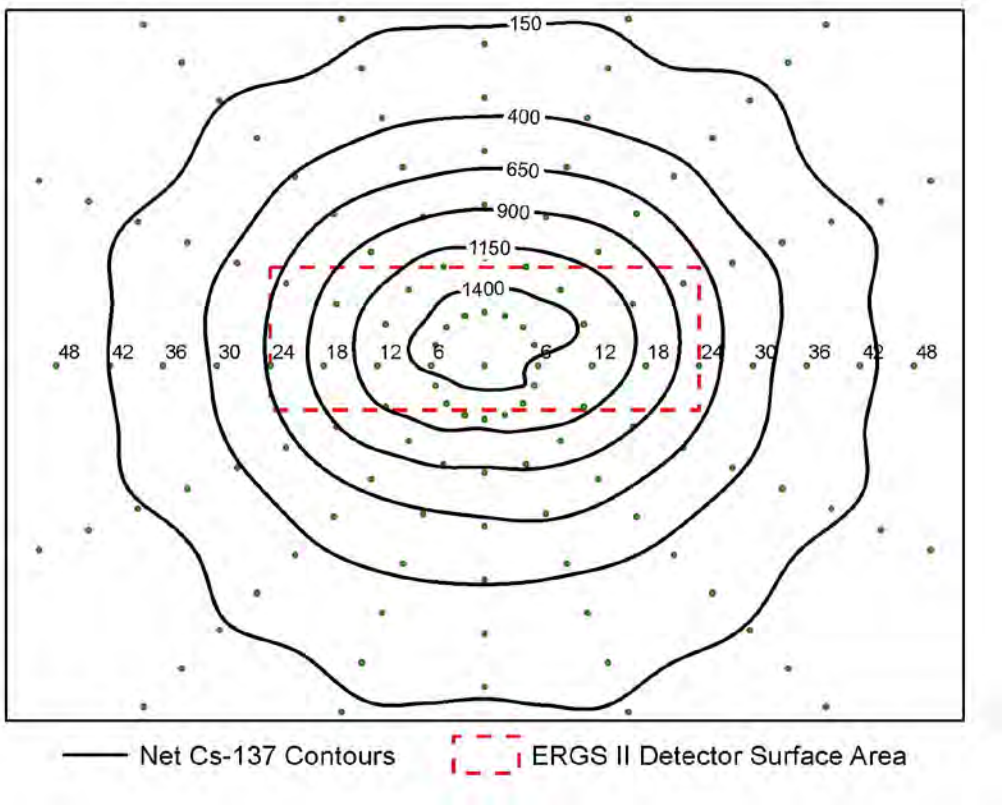

Figure 20
Enhanced Radiation Ground Scanner II Net Cs-137 Count Rate Contours with the Active Detector Surface Area

Figure 20 has a plot of contour lines of net Cs-137 count rates relative to the center of the radial source locations. The contour intervals were produced using Arc Geographic Information System (ArcGIS) Software (version 10) and a spline data interpolation. The superimposed red dashed line approximates the active detector surface area. Each contour line or count rate isopleth indicates the same count rate detected relative to the detector.

3.1.1 Field Of View

The detection of gamma radiation is strongly influenced by the source to detector distance, amongst other variables. Neglecting the dimensions of the detector, the inverse distance squared law governs radiation flux from a point source. As an example of this radiation flux – distance relationship, if the unit distance from a source increases from one to two (doubles), then the flux decreases by a factor of four (one quarter of original flux). If the unit distance increases by a factor of four (quadruples), then the flux decreases by a factor of 16 (one sixteenth of original flux), and so on.

Based on the flux–distance relationship, the maximum efficiency is expected at the minimum source to detector distance. This condition occurs when the detector center is directly above a radiation source, which is at the origin (0 inch) source location.

The ratio of data collected at any test location to the origin is meaningful; it provides a direct comparison of a positional efficiency and the maximum efficiency. However, this ratio does not allow direct comparisons between different detection systems or different operating heights. The RE is described in Equation 5. It is the ratio of the net Cs-137 count rate at a specific test location (for example A36) to the net Cs-137 count rate at the origin (A0).

Equation 5:

$$Relative\ Efficiency\ (RE) = \frac{net\ \mathrm{Cs137}_{\,i}}{net\ \mathrm{Cs137}_{0}}$$

Where *net* Cs-137 $_i$ is the net count rate for Cs-137s at position *i,*
net Cs-137 $_o$ is the net count rate for Cs-137 at the origin

Net Cs-137 data from individual test locations were assembled into a matrix of gamma source location responses, based on the radial test positions shown in Figure 21. Sub-dividing the radial test matrix into contiguous polygons and assuming the point efficiency at the center represents the efficiency over the discrete area of the polygon, efficiencies can be calculated and summed or distributed over specific areas (for example, a group of polygons). Figure 21 illustrates this division of the radial test locations into discrete polygons. This, in turn, can be used to examine detection system efficiency in a particular direction.

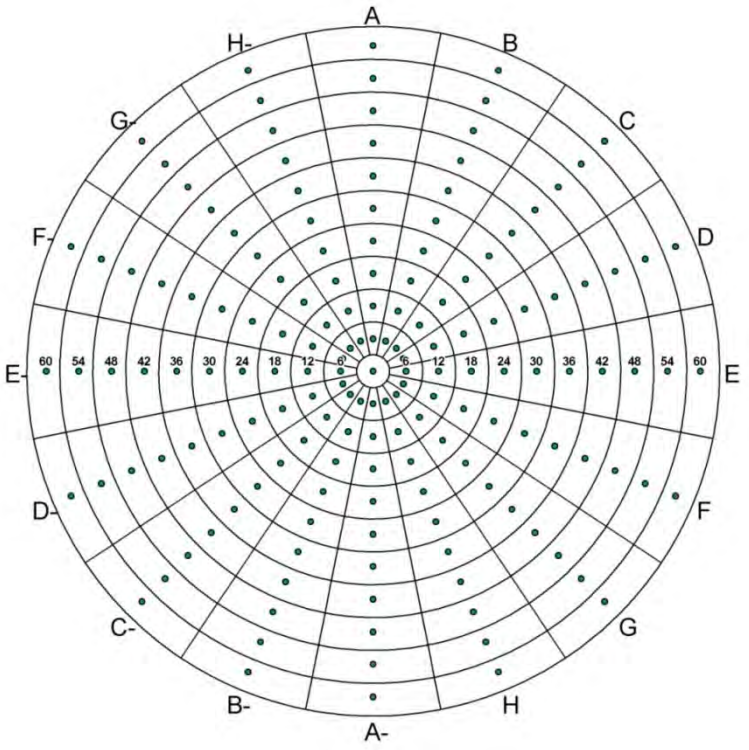

Figure 21
Radial Matrix Shown with Point Source Locations and Sub-Divided Areas

There are several ways to evaluate an array consisting of so many data. A logical first step is to compile and evaluate RE data in each concentric ring at each radial distance. As illustrated in Figure 21, from 0 to 3 inches around the origin is the first ring, the second concentric ring is from 3 to 9 inches formed by the six inch radial position, and the third concentric ring is from 9 to 15 inches as formed by the 12 inch radial position, and so on.

Table 5 is a comparison of cumulative Cs-137 count rates for all radial position at a particular distance from the origin (i.e., concentric rings) for the ERGS II. Each row of data is calculated from all radial distance positions in a concentric ring; e.g., radial position 12 is compiled from A12, B12, C12, to H-12 and consists of 16 measurements. Position 0 is compiled from eight observations (A0, B0, C0, to H0) collected at the origin. The RE for each concentric ring shows the comparative detector efficiency at a particular distance from the origin. For example, the relative efficiency at 24 inches is 0.404. The combined area covered by the 24-inch concentric ring is much larger than the origin area (905 versus 28.3 square inches, respectively). The column to the right of the radial ring area is the summed area which is the sum of each concentric ring from the origin to the perimeter of the concentric ring; i.e., from 0 to 27 inches for the 24-inch concentric ring.

The integrated relative efficiency (Equation 6) is important because it measures the efficiency over an area. Practically, the integrated relative efficiency is the efficiency over a contiguous surface area compared to the efficiency at the origin. Whereas the 24-inch RE is the efficiency of a 24-inch concentric ring (between 21 and 27 inches), the integrated relative efficiency is the RE over the entire surface area from the origin (with a 27-inch perimeter). In this example, it is important to note the integrated relative efficiency at 24 inches (0.592) is greater than the relative efficiency (0.404), which is to be expected.

Equation 6:

$$Integrated\ Relative\ Efficiency = \frac{\sum(RE_i \times area_i)}{total\ area}$$

The value of the integrated relative efficiency is that it permits comparison of the detection efficiency of a specific surface area to the efficiency of either another surface area or even a point location. The initial discussion uses regular shapes, such as the concentric circles depicted in Figure 21, to describe the data analysis process. Later, other shapes will be compared using the integrated relative efficiency.

Table 5
Enhanced Radiation Ground Scanner II Radial Position Count Data, Relative Efficiency, Area, Summed Area, and Integrated Relative Efficiency

Radial Position (inch)	Mean net Cs-137 (cps)	Standard Deviation (cps)	Standard Deviation /Mean	Relative Efficiency	Radial Area (in^2)	Summed Area (in^2)	Integrated Relative Efficiency
0	1494	6.1	0.41%	1.000	28.3	28.3	1.000
6	1391	100	7%	0.931	226.2	254.5	0.939
12	1165	160	14%	0.779	452.4	706.9	0.837
18	880.5	158	18%	0.589	678.6	1385.4	0.715
24	603.2	121	20%	0.404	904.8	2290.2	0.592
30	387.3	74	19%	0.259	1131.0	3421.2	0.482
36	236.1	47	20%	0.158	1357.2	4778.4	0.390
42	144.1	28.3	20%	0.096	1583.4	6361.7	0.317
48	87.2	16.6	19%	0.058	1809.6	8171.3	0.260
54	56.8	8.4	15%	0.038	2035.8	10207.0	0.216
60	38.5	8.4	22%	0.026	2261.9	12469.0	0.181

Note:
in^2 – square inch

Figure 22 is a plot of ERGS II integrated relative efficiencies and relative efficiencies versus radial distance. The plot shows that the integrated relative efficiency at 30 inches drops below 0.5. This means that the ERGS II efficiency integrated over the entire 30-inch radius surface area is less than one-half of its detection efficiency at the origin. The relative efficiency and integrated relative efficiency are useful for calculating field efficiencies of a detection system.

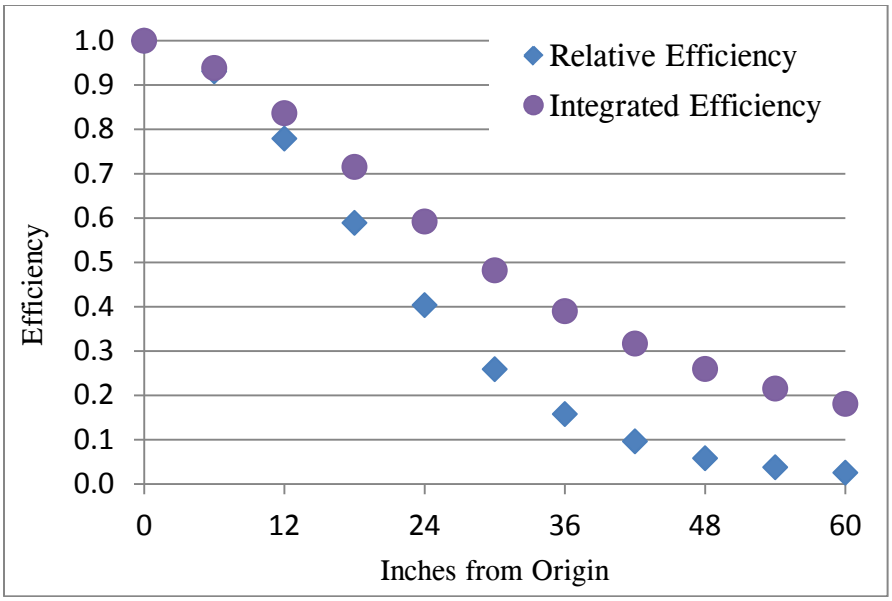

Figure 22
Enhanced Radiation Ground Scanner II Efficiency versus Radial Distance

Figure 22 includes plots of RE and integrated RE from the origin to 60 inches from the origin. The reason why the integrated RE data are greater than the RE is based on their definitions; the RE includes only the data for that distance from the origin whereas the integrated RE spans the entire area up to a stated distance from the origin.

Figure 23 compares the ERGS II relative radial efficiency with the forward travel direction and lateral direction REs. The forward travel data are the average REs for the "A" ray (for example, 12-inch data consists of A12 and A-12), and the lateral data are from the "E" ray. Figure 23 shows that the RE is higher in the lateral direction than in the travel direction from 12 to 42 inches. As described in Section 2.1, the ERGSII is a 16-inch by 48-inch array of eight large NaI detectors. Due to its shape and the radiation flux to distance relationship, the REs are not expected to be uniform over the entire radial template. This is the case for the other detection systems as well. Considering the dimensions of each detection system, comparing the integrated REs to the detector surface area is more meaningful than comparison to a radial distance.

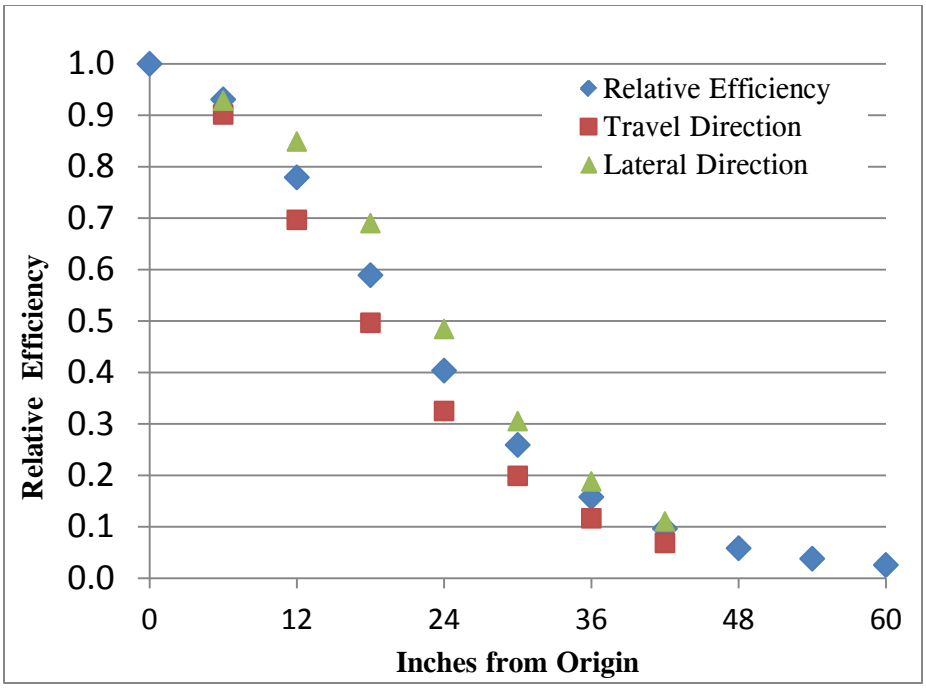

Figure 23
Enhanced Radiation Ground Scanner II Directional Relative Efficiency versus Distance

With the RE shown as diamond symbols, the ERGS II has a greater efficiency in the lateral (or side to side) direction as compared to the direction of travel. This is particularly easy to see from about 12 to 36 inches from the origin. The main reason the relative efficiency is greater laterally than in the direction of travel is that the detector array is about three times as wide as it is long.

It is not logical or practical to limit a detection system FOV to an area smaller than its detector surface area. In effect, large volume gamma detectors can and do detect beyond the boundaries of their "footprints", although how much they detect is a function of detector size and shielding. Quantification of the detection efficiencies beyond the footprint is essential to compute the lowest overall acceptable sensitivity, to increase confidence that radioactivity present in the field would not go undetected.

Comparing areal detection efficiencies to the detector surface area or footprint is logical. The integrated relative efficiency decreases with increasing surface area. As the soil surface size increases relative to the detection system footprint, an operational limit or cut-off must be chosen to balance effective coverage in the field with detectability.

A limit of the integrated relative efficiency of a soil surface area of 0.5 was chosen relative to the integrated relative efficiency of the detector footprint. This means that it is acceptable to have a much larger effective soil surface area with the detection efficiency one-half of that directly under the detector footprint. One constraint on evaluation of the FOV is that the starting dimensions used is the detector footprint and dimensional increases are equal in all

directions from the footprint, e.g., if the footprint was 16 inches long by 48 inches wide and a 12-inch increment was evaluated, then the surface area integrated was 40 inches long by 72 inches wide. Thus, an iterative approach was used to calculate the resultant FOV.

It is important to note that the FOV is conservative because field surface scanning efficiencies represent the full extent of the FOV, yet surface coverage of each transect includes some overlap which increases the overall sensitivity.

The integrated relative efficiency for the ERGS II FOV is 0.50 normalized to the integrated RE of the detector surface area. The resultant ERGS II FOV measures 54 inches long by 86 inches wide. Figure 24 shows the ERGS II integrated Res of the active detector surface area, and the length and width of the FOV in which the integrated RE is precisely equal to 0.50 of that of the active detector surface area. To calculate this FOV dimensions, the radial source location template was sub-divided into 1-inch by 1-inch square grid cells. The relative efficiency value for each 1 inch square grid cell was calculated using ArcGIS (version 10) kriging interpolation based on measured efficiency data. By sub-dividing the point source data into discrete areas, efficiencies can be combined to represent the efficiency over a specific area of interest (this is similar to mathematical integration). In Figure 24, the REs for the areas have been summed and normalized to the integrated relative efficiency of the detector surface area.

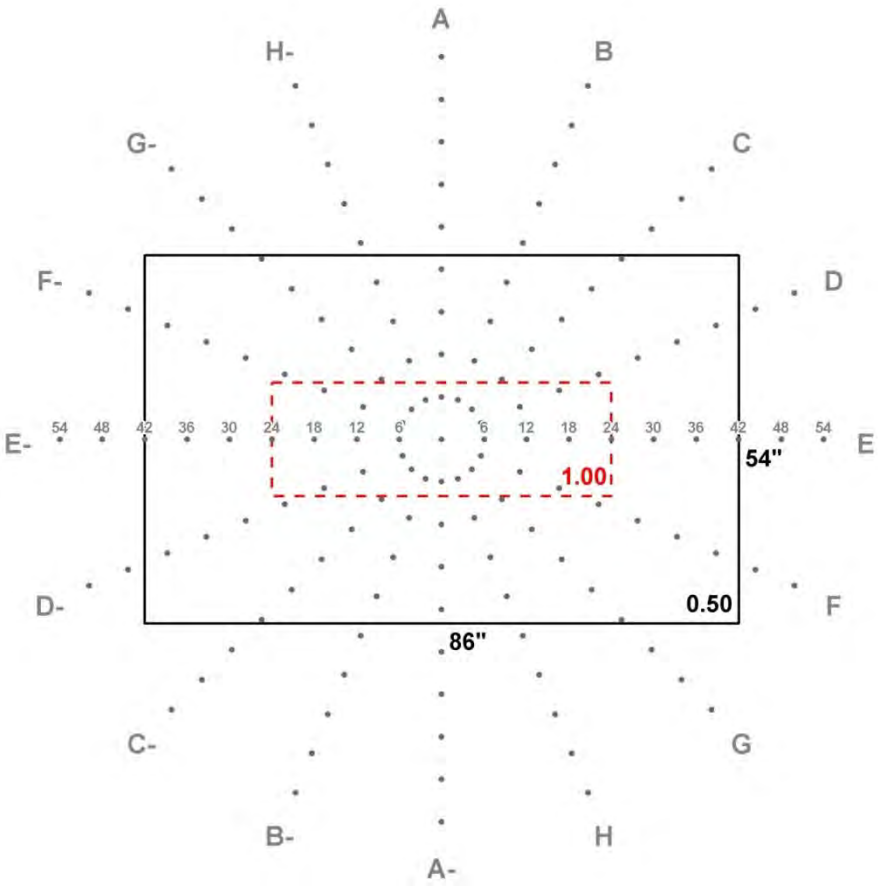

Figure 24
Enhanced Radiation Ground Scanner II Field of View Dimensions and the Active Detector Surface Area

Figure 24 illustrates the extents of both the FOV (wherein the integrated RE equals 0.50 of that of the active detector surface area) and the active detector surface area. The operational width of the ERGS II is set to 6 feet (72 inches) for the purpose of ensuring transects overlap in the field even though the FOV defines the width as 86 inches.

By defining a normalized areal efficiency limit of 0.50, the FOV of different detection systems are selected using the same process criteria. The FOV is based on efficiency. An additional benefit of this approach is that the efficiencies of various configurations can be compared directly using the efficiency at the origin.

By establishing a detector swath of 86 inches, the field personnel can mark ERGSII transects and ensure complete spatial coverage of the survey area. For example, with a 7-foot wide FOV, transects could be marked at 6 feet, ensuring transect overlap for more complete coverage.

3.1.2 Height

The selection of an operational height is driven by both the detection sensitivity and equipment maneuverability in the field. Therefore, height ranges were anticipated for particular detection systems before conducting the tests. Hence, the data shown here are simply the count rates versus source to detector distance. Figure 25 shows the net Cs-137 count rate data from the ERGS II detection system collected at a series of source to detector distances. Note that the greatest count rate is obtained from the least distance. Based on the overall efficiency, FOV, and operational considerations (vegetation clearance, avoidance of obstacles, safety, etc.), 15 inches was selected by the USEPA as an optimum height for the ERGS II (R. Shura, USEPA, personal communication, 2010).

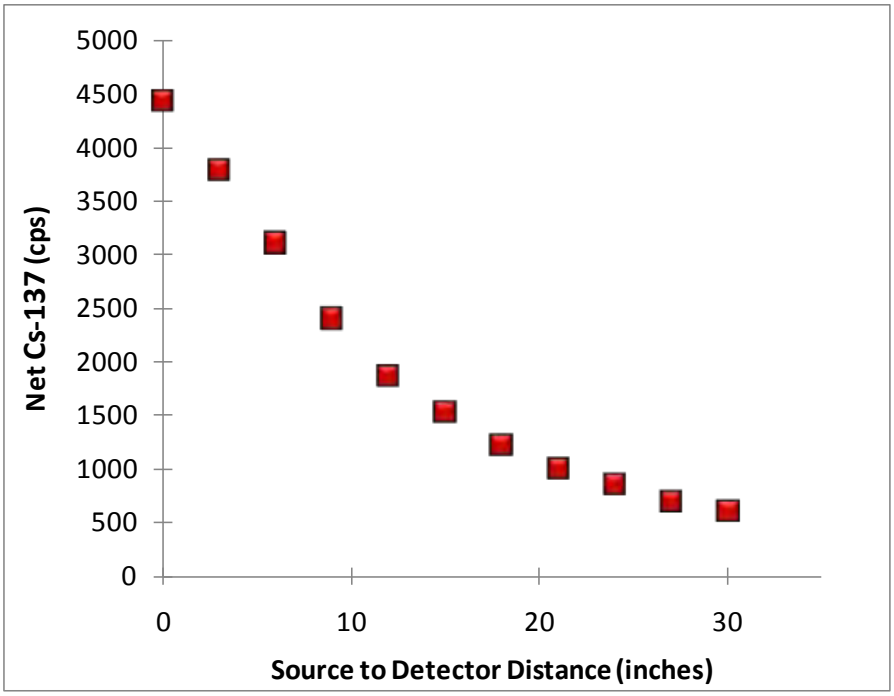

Figure 25
Enhanced Radiation Ground Scanner II Count Rate versus Height

For the ERGS II, the count rate decreases logarithmically as the source to detector distance increases.

3.1.3 Velocity

In velocity tests, sources were moving whereas they were in fixed positions for the static tests, such as FOV and height. The detector was stationary while Cs-137 sources were moved at a specific velocity under its centerline in the direction of travel. The scanning efficiency ratio is the ratio of velocity count rates to static count rates. The scanning data consist of one second time increments or "snapshots" taken as the source moved directly under the detector. The snapshot of data could *occur when the moving source was located at any point on the*

centerline. For this reason, the data is not directly equivalent to static data collected at fixed positions. Therefore, scanning count rates were compared to integrated static count rate data from radial "A" (the centerline in the direction of travel).

Radial "A" data was assembled to produce an integrated static count rate for calculation of a scanning efficiency ratio. For example, during the 1 ft/s velocity tests, the source was moving along radial "A" for 10 seconds (equivalent to traveling from positions A60 to A-60), thus scan count rates were relatively higher because the moving source had a longer time in the detector FOV. During the 3 ft/s tests, the source transited the same distance in approximately 3.3 seconds.

Table 6 shows the data used to calculate the ERGS II scanning efficiency ratio. The ratios are plotted in Figure 26 which shows scanning efficiency ratios for 1.0, 1.5, 2.0, and 3.0 ft/s velocities. Data in both Table 6 and Figure 26 are mean results of three velocity tests.

Table 6
Enhanced Radiation Ground Scanner II
Data for Scanning Efficiency Ratio

Velocity (ft/s)	Integral of Counts Per Second		Scanning Efficiency Ratio (Scanning Net Cs-137/ Radial A Net Cs-137)
	Scanning Net Cs-137 (cps)	Radial A Net Cs-137 (cps))	
1	4872	5073	0.96
1.5	3132	3419	0.92
2	2246	2589	0.87
3	1282	1839	0.70

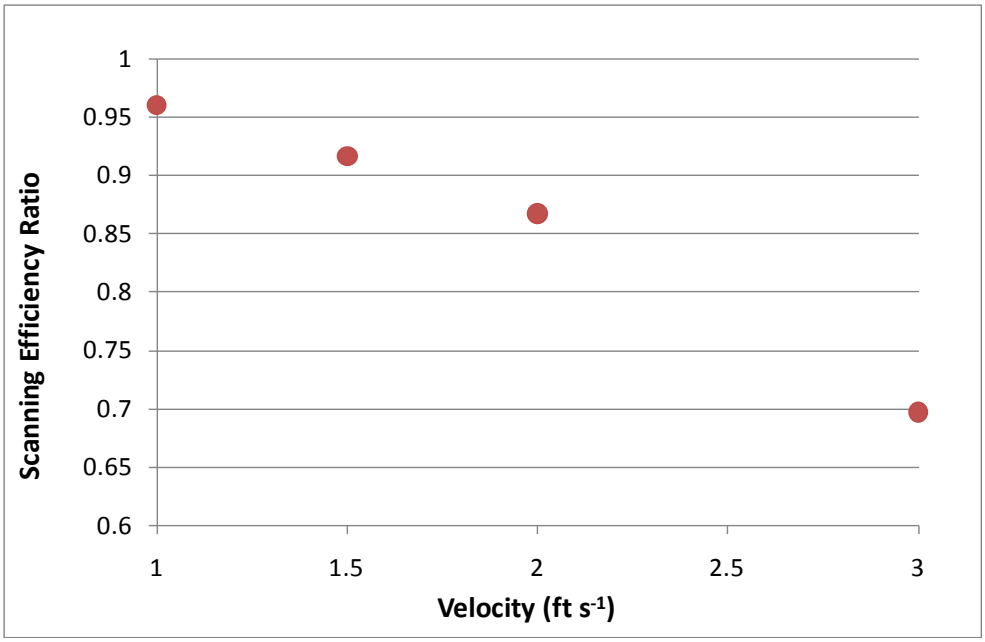

Figure 26
Enhanced Radiation Ground Scanner II Scanning Efficiency Ratio versus Velocity

The ratio permits establishment of a maximum velocity for field scanning efficiency. For the ERGS II, an a priori estimate of scanning efficiency ratio of 0.8 was assumed. The data indicate velocities of 2 to approximately 2.5 ft/s will meet this criterion. Therefore, a constant scan speed of 2 ft/s with minor velocity excursions above 2 ft/s is acceptable. The scanning efficiency ratio influences field detection sensitivity. That is, the overall field sensitivity is the product of the static test efficiency at the FOV and the scanning efficiency ratio.

3.2 MULE MOUNTED GAMMA SCANNER

The data evaluation processes for the MMGS, TMGS, STGS, and WMGS are analogous to those of the ERGS II; therefore, only results are presented.

Figure 27 shows the net Cs-137 contour intervals for the MMGS. It is roughly oval-shaped and also shows the deviations about the legs of the test stand due to attenuation of gamma signal.

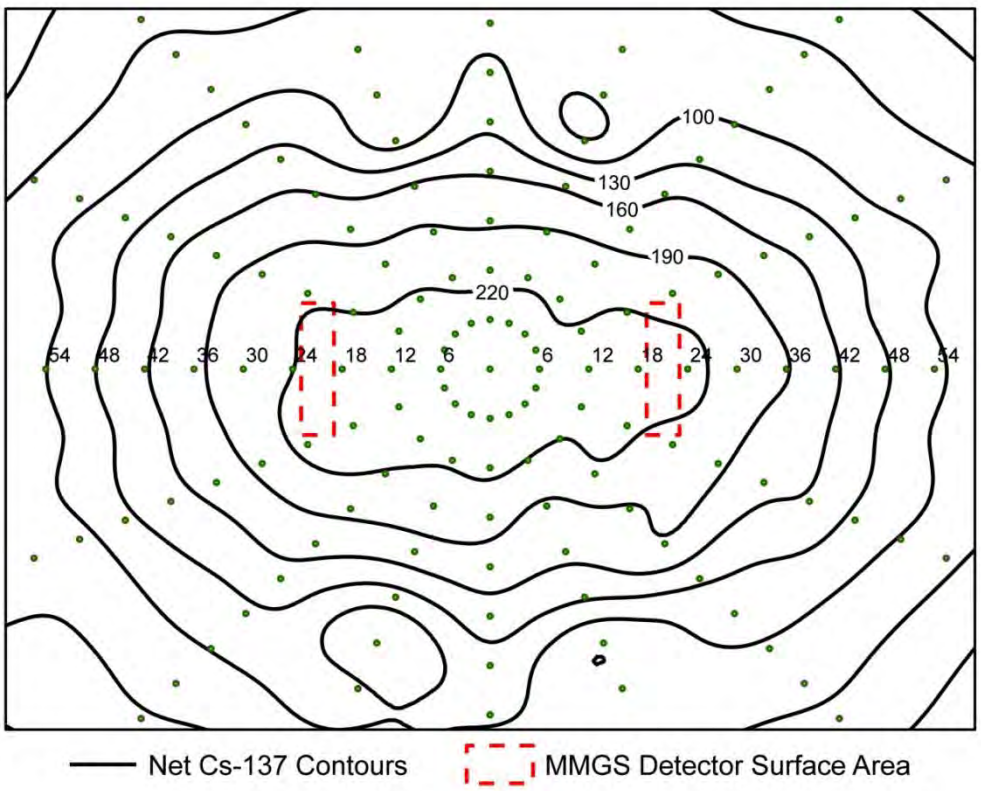

Figure 27
Mule Mounted Gamma Scanner Net Cs-137 Count Rate Contours with the Active Detector Surface Area

The contour lines for the MMGS are more irregular than those of the ERGS II. This is due to the shape of active detector areas (two individual detectors suspended on outrigger for the MMGS versus essentially a block of eight detectors for the ERGS II). Notice that the contour lines are wider than they are long. Additionally, the positions of the mule test stand 'legs' can be seen at the isopleths lower than 100 cps, which are each approximately positioned at the B, H, B-, and H- rays. This shielding effect is very important when considering field of view.

3.2.1 Field Of View

Figure 28 is a plot of the MMGS REs for radial, the travel direction, and the lateral direction versus distance. The RE is greater laterally than in the direction of travel. Considering the arrangement of the mule-mounted detectors (Figures 5 and 12) with detectors suspended on outriggers approximately 46 inches apart, this is expected.

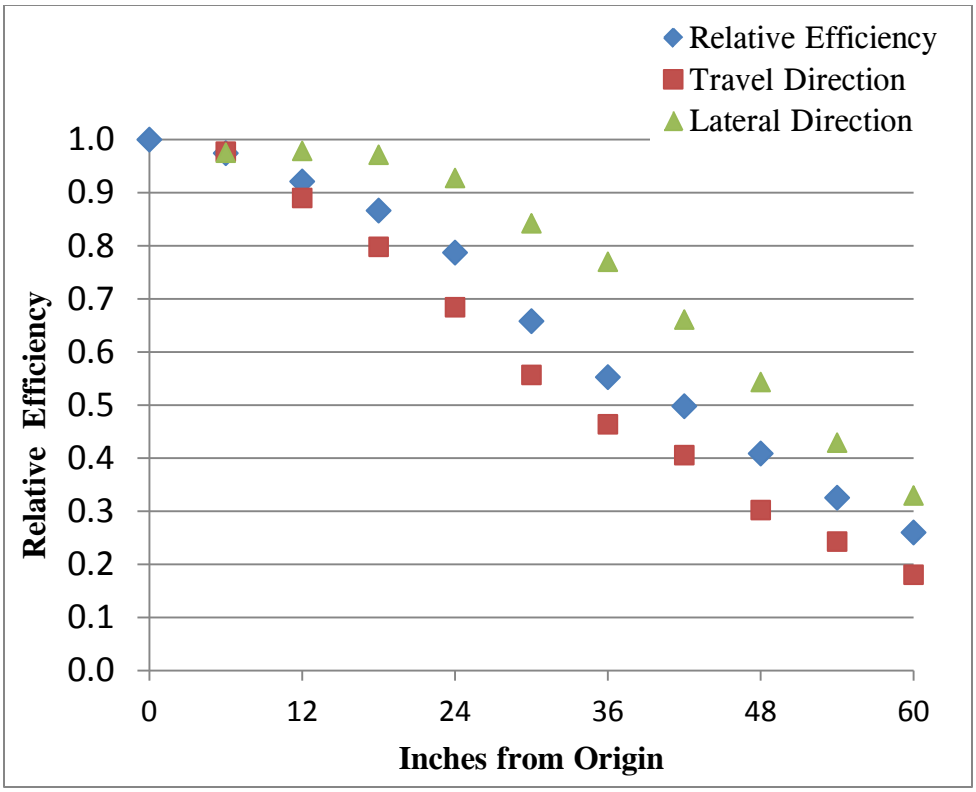

Figure 28
Mule Mounted Gamma Scanner Directional Relative Efficiency versus Distance

The MMGS RE data are greater laterally than in the forward travel direction at 12 inches and greater positions, due to the arrangement of the detectors.

Figure 29 shows the MMGS FOV in which the integrated RE is precisely 0.50 of that of the combined active detector surface areas. This figure also indicates the right detector is slightly more efficient than the left detector. The FOV for the MMGS is 104 inches wide by 76 long with a total FOV area of 7,904 square inches. The FOV of the MMGS is greater than the FOV of the ERGS II even though the ERGS II has a larger number of detectors. This is because of the operational height. The ERGS II scans at 15 inches and the MMGS scans at 35 inches.

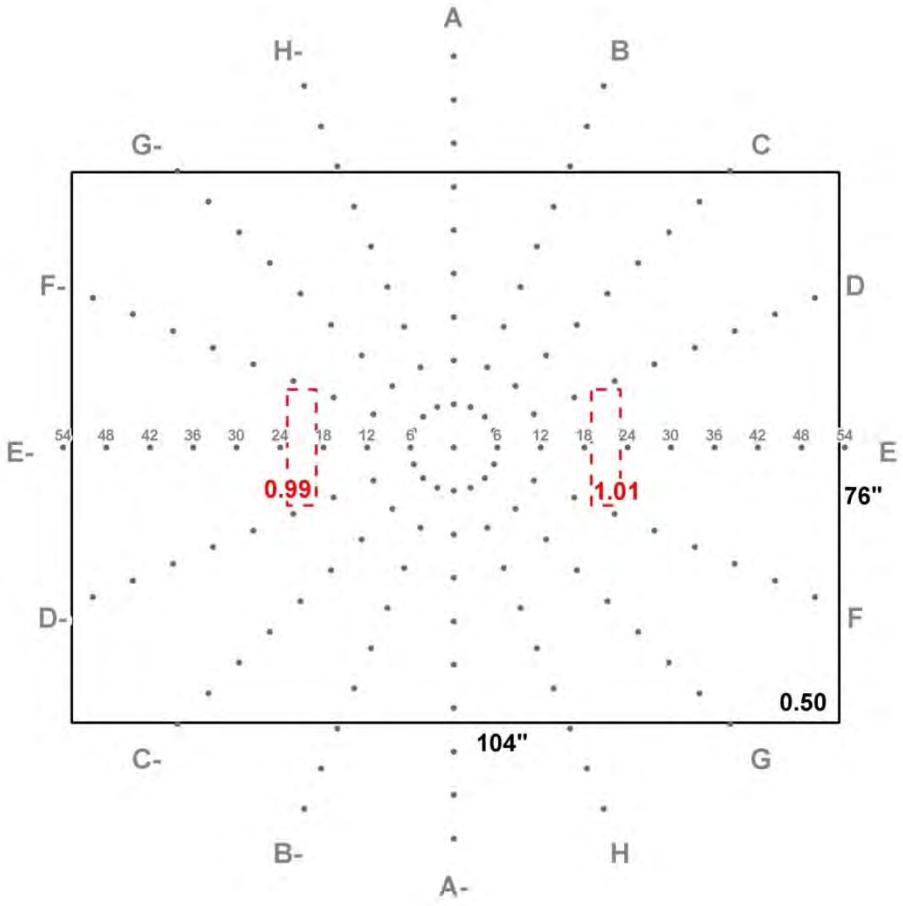

Figure 29
The Mule Mounted Gamma Scanner Field of View Dimensions and the Active Detector Surface Area

The MMGS has a larger FOV than the ERGS II which is mainly because the ERGS II scans at 15 inches height and the MMGS scans at 35 inches height. The overall sensitivity of the MMGS is much lower than that of the ERGS II. The operational transect width of the MMGS is set to 7 feet, 6 inches (90 inches) for the purpose of ensuring transects overlap in the field even though the FOV defines the width as 104 inches.

3.2.2 Height

Figure 30 exhibits two notable features. First, the closest source to detector distance (5 inches) does not have the greatest count rate. This is because the two detectors are placed relatively far apart (to straddle the animal) and the mule torso actually attenuates the gamma signal at this distance. Second, the net Cs-137 count rate does not change substantially from 32 to 35 inches.

The operating height chosen for the mules is actually the farthest distance tested in this experiment (35 inches). This height was largely based on locating the detectors next to the

mule without creating discomfort for the animal. There were practical considerations when mounting the detectors on the animal. The saddle had to be able to support the weight of the detectors, the detectors couldn't be mounted too low to impede walking or sway widely so that it would affect the animal's balance in uneven terrain. The overall size of the mule was important as well as its chest cavity size which influenced how far apart the detectors ultimately were. Mules were trained to walk with the handler and follow commands, which also influenced which mules were selected for the rough site terrain. Lower heights were attempted but caused discomfort by obstructing the range of motion of the mule's legs. The MMGS is specifically designed for deployment in difficult and rocky terrain, where wheeled detection systems cannot readily access.

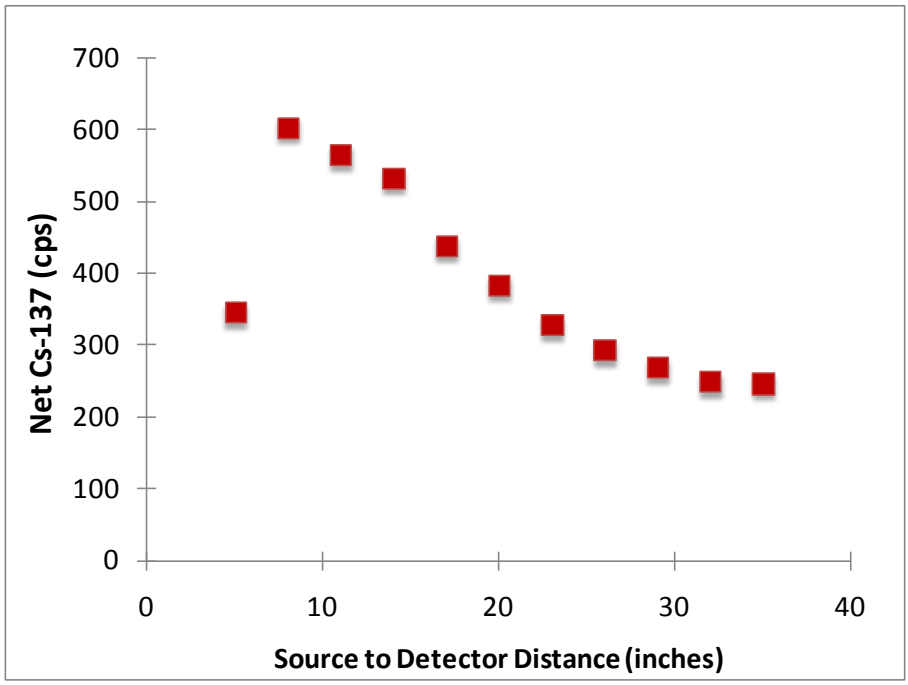

Figure 30
Mule Mounted Gamma Scanner Count Rate versus Height

At the lowest source to detector distance, the mule stand actually shields the source. As the height increases to approximately 8 inches, the net Cs-137 also increases, and as the height increases, the count rate decreases with increasing distance.

3.2.3 Velocity

The fact that the MMGS has a large FOV is directly related to its operating height. In the same sense, the scanning velocity of the MMGS does not significantly decrease over the velocities tested. In fact, it is possible that the MMGS may be operated at a greater velocity than 3 ft/s without decreasing scanning efficiency.

Figure 31 is a plot of scanning efficiency ratio versus velocity. No distinguishable trend is described from this data; therefore, the mean of the scanning efficiency ratios from all velocities is computed and shown for comparison. The data may be interpreted as there is little correlation between scan velocity and scan efficiency ratio. For this reason, the mean scan efficiency ratio is selected and the maximum velocity is set at 3 ft/s. It appears that excursions above this value may not significantly decrease the scanning efficiency ratio. Mules were trained to walk at this gait, which was significantly slower than their natural pace.

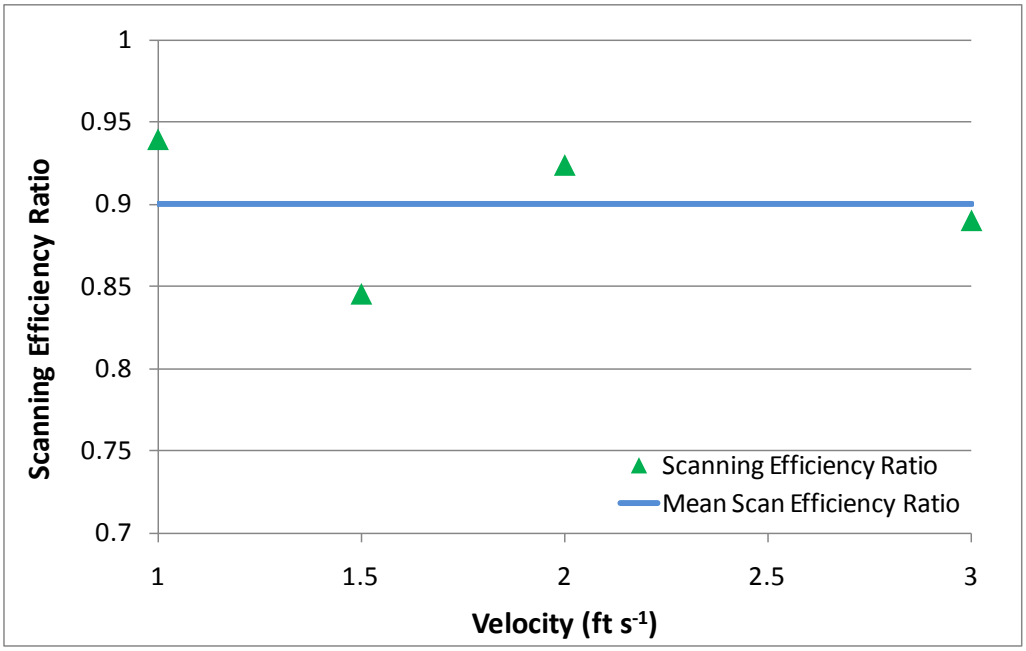

Figure 31
Mule Mounted Gamma Scanner Scanning Efficiency Ratio versus Velocity

The scanning efficiency ratio plot for the MMGS includes a trend line which is the mean of the data. Because the ratio does not decrease below 0.8, any of these velocities is acceptable. The MMGS operates at a higher scan height than the other systems, and this effectively increases the FOV while decreasing sensitivity to scan velocity.

3.3 TRACK MOUNTED GAMMA SCANNER

The TMGS is mounted to a platform base with a cantilevered plate extending forward with a weight bearing wheel. Due to this fixed position, height testing was not performed. Figure 32 shows net Cs-137 contour intervals relative to the positions of the NaI detectors. As expected, the greatest net Cs-137 count rates are observed near the center of the two detectors, and the count rates drop as a function of distance from the detectors. The count rate decreases proportionately more in the direction of travel than laterally. Also, the gamma signal attenuation due to the wheel is noticeable. In the relatively distant forward and rear directions, the shielding of the wheel and the track deck and tracks are noticeable.

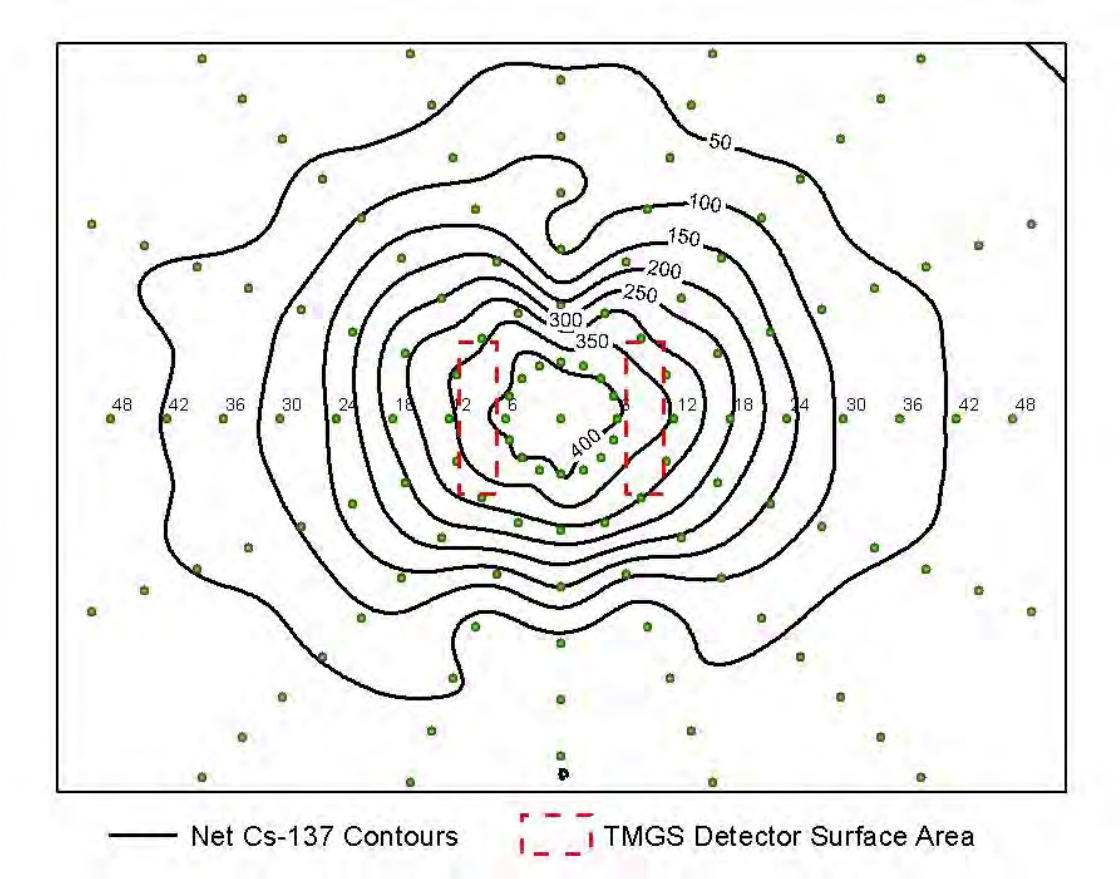

Figure 32
Track Mounted Gamma Scanner Net Cs-137 Count Rate Contours with the Active Detector Surface Area

The net Cs-137 contour lines of the TMGS are symmetrical and somewhat uniform about the center of the detection system with count rate contours closer together in the direction of travel than laterally. The signal attenuation due to the position of the front wheel and the detector proximity to the tracks are seen on the A, H, and B- rays.

3.3.1 Field Of View

Figure 33 is a plot of the TMGS REs for radial, the travel direction, and the lateral direction versus distance. The RE is greater laterally than in the direction of travel. This is particularly noticeable between 12 and 24 inches, and is this difference is due mainly to the positions of the tracks, the deck, and the front wheel.

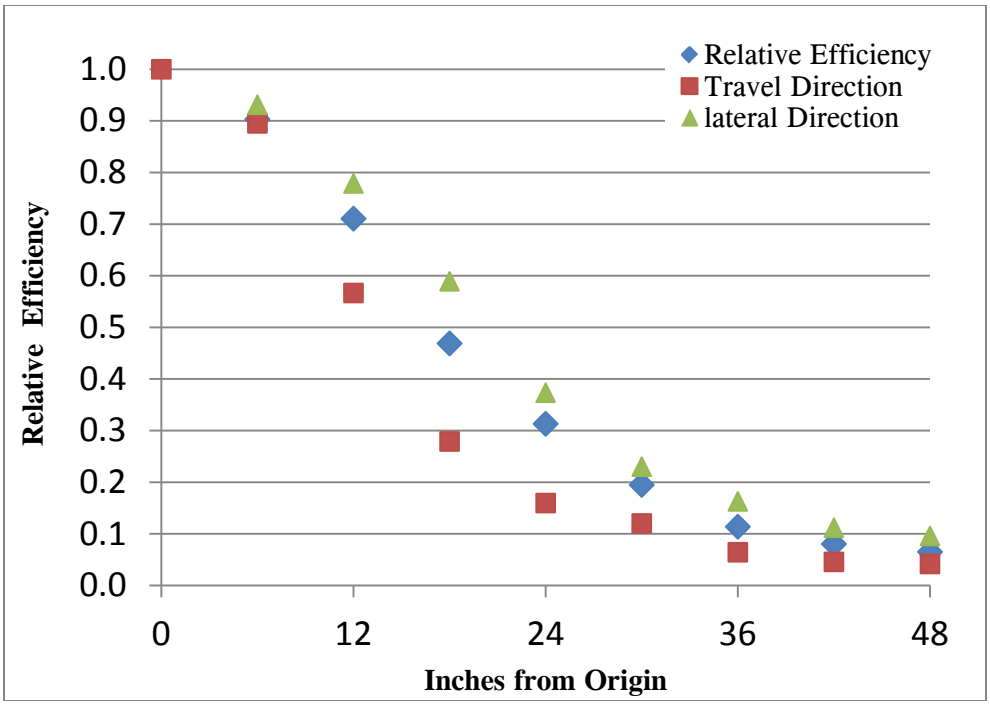

Figure 33
Track Mounted Gamma Scanner Directional Relative Efficiency versus Distance

Figure 34 shows the TMGS FOV of 50 inches long by 56 inches wide for a total area of 2,800 in^2. The FOV of the TMGS is less than the FOV of the ERGS II and the MMGS. This is because of both the number of detectors and the operational height. It is important to understand that FOV is only one parameter to consider in the calculation of detection sensitivity. One primary objective in the development of the TMGS was its ability to scan and maneuver in steep terrain safely. A hinged deck and front wheel were added for these reasons, and FOV considerations for the position of the front wheel relative to the detector were taken into account.

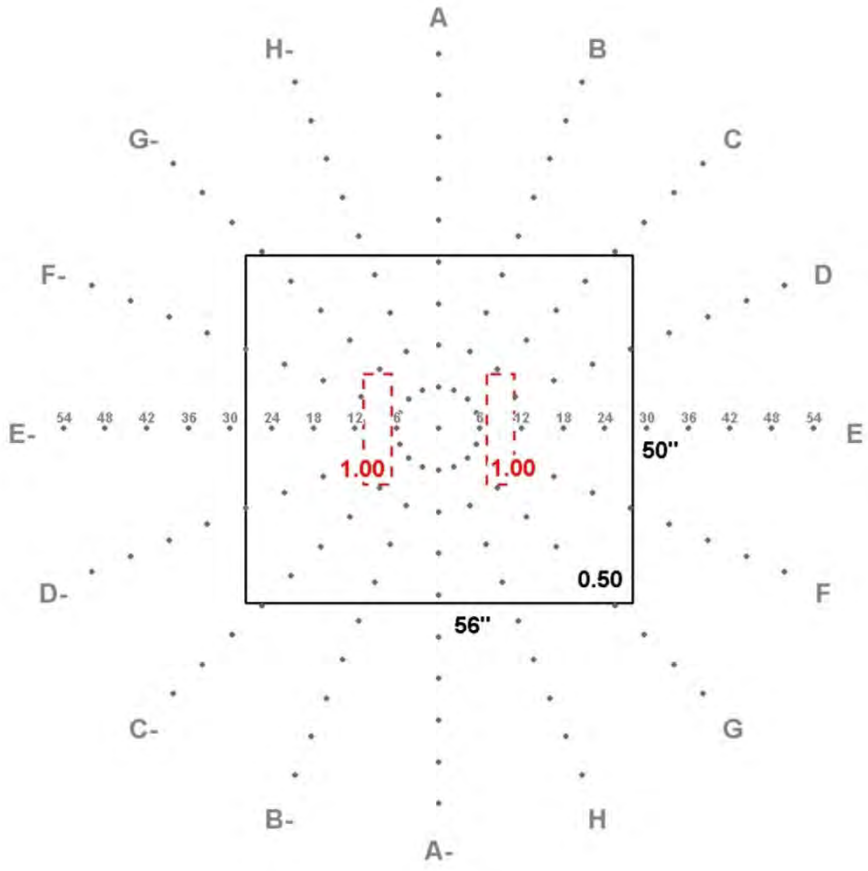

Figure 34
Track Mounted Gamma Scanner Field of View Dimensions and the Active Detector Surface Area

The TMGS FOV of 50 inches by 56 inches is less than the ERGS II due to the number of detectors and the MMGS due to detector height. However, with the TMGS closer to the surface the sensitivity will be much greater than that of the MMGS. The operational transect width of the TMGS is set to 4 feet (48 inches) for the purpose of ensuring transects overlap even though the FOV width is 56 inches.

3.3.2 Velocity

The TMGS scanning efficiency ratios at 1, 1.5, 2, and 3 ft/s are shown on Figure 35. These data represent combined scanning data of three separate tests at each velocity. There is some noise in the data as it is not possible to have a scanning efficiency higher than the static count efficiency. However, the amount of error in the data is approximately 4 percent, which is acceptable given the conditions of the tests (one second counts with the detection system moving relative to the source) and statistical errors associated with counting. As shown in Table 5, repeated counts of static radial plot positions for the ERGS II resulted in standard deviations of approximately 20 percent at positions 12 inches and greater from the origin. Therefore, the 4 percent degree of uncertainty is minor.

The data as a whole indicate that the scanning efficiency is acceptable at 2 ft/s, but unacceptable (a scanning efficiency ratio of less than 0.8) at 3 ft/s.

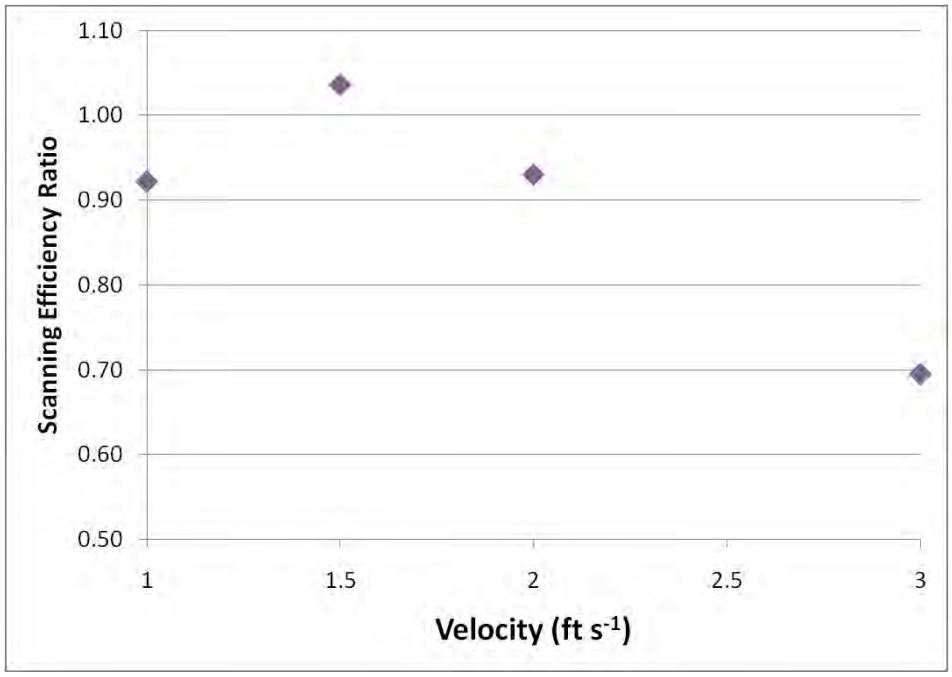

Figure 35
Track Mounted Gamma Scanner Scanning Efficiency Ratio versus Velocity

The TMGS scanning efficiency drops below 0.8 at 3 ft/s, but is well above that limit at 2 ft/s and slower. The data trend such that occasional slight excursions above 2 ft/s are acceptable.

3.4 SINGLE DETECTOR TRACK MOUNTED GAMMA SCANNER

The STGS is mounted to a platform base with a cantilevered plate extending forward with a weight bearing wheel. Due to this fixed position, height testing was not performed. Figure 36 shows net Cs-137 contour intervals relative to the position of the NaI detector. As expected, the greatest net Cs-137 count rates are observed near the center of the detector, and the count rates drop as a function of distance from the detector. The count rate decreases proportionately more in the direction of travel than laterally. Also, the gamma signal attenuation due to the wheel is noticeable. In the relatively distant forward and rear directions, the shielding of the wheel and the track deck and tracks are noticeable. In this case, the single wheel design more significantly attenuated the forward FOV.

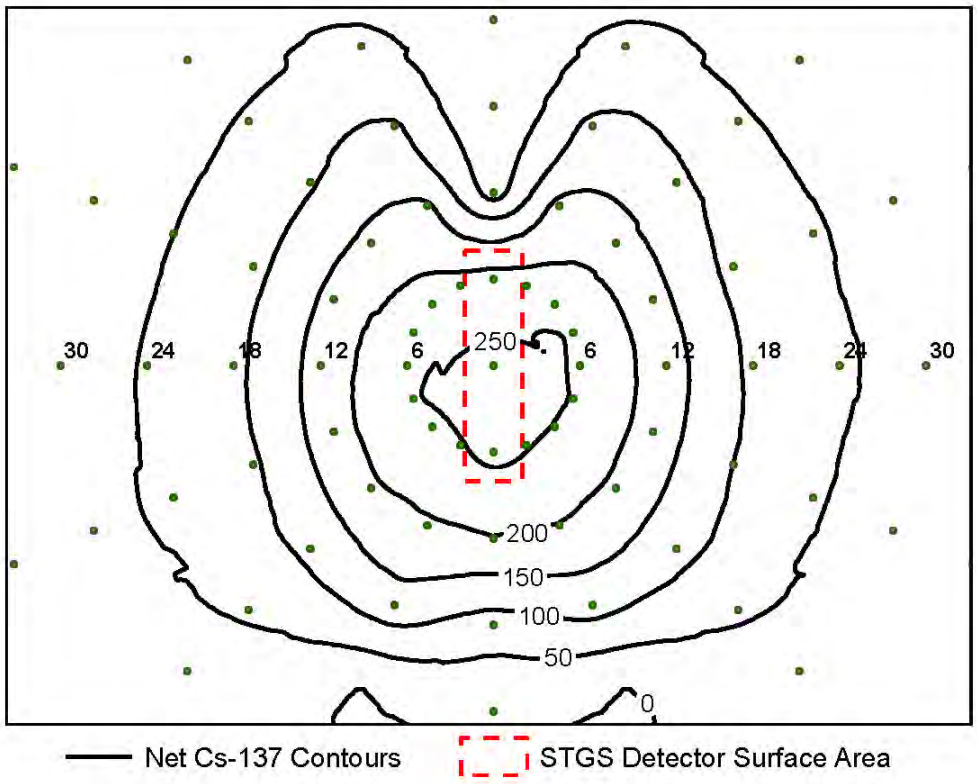

Figure 36
Single Detector Track Mounted Gamma Scanner Net Cs-137 Count Rate Contours with the Active Detector Surface Area

The net Cs-137 contour lines of the STGS are symmetrical and uniform about the center of the detection system with count rate contours closer together in the direction of travel than laterally. The signal attenuation due to the position of the front wheel and the detector proximity to the tracks are seen on the A, H, and B- rays.

3.4.1 Field Of View

Figure 37 is a plot of the STGS REs for radial, the travel direction, and the lateral direction versus distance. The RE is greater laterally than in the direction of travel. This is particularly noticeable between 12 and 24 inches, and is this difference is due mainly to the positions of the tracks, the deck, and the front wheel.

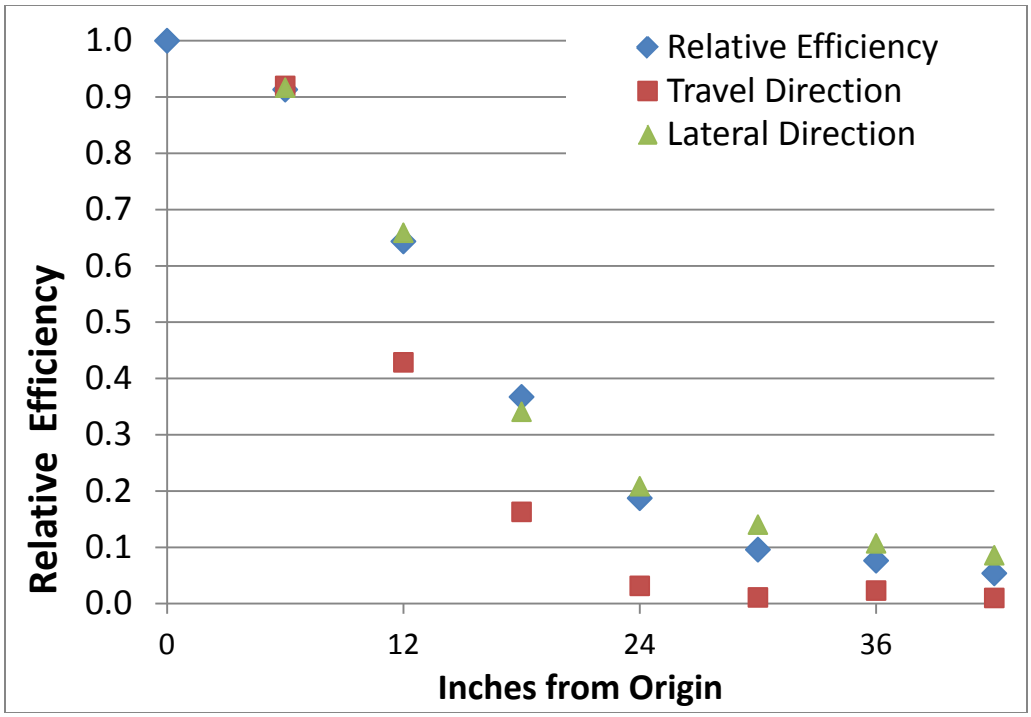

Figure 37
Single Detector Track Mounted Gamma Scanner Directional Relative Efficiency versus Distance

Figure 38 shows the STGS FOV of 48 inches long by 36 inches wide for a total area of 11,728 square inches. The FOV of the STGS is less than the FOV of the ERGS II, TMGS and the MMGS. This is because of both the number of detectors and the operational height. It is important to understand that FOV is only one parameter to consider in the calculation of detection sensitivity. One primary objective in the development of the STGS was its ability to scan and maneuver in steep terrain safely.

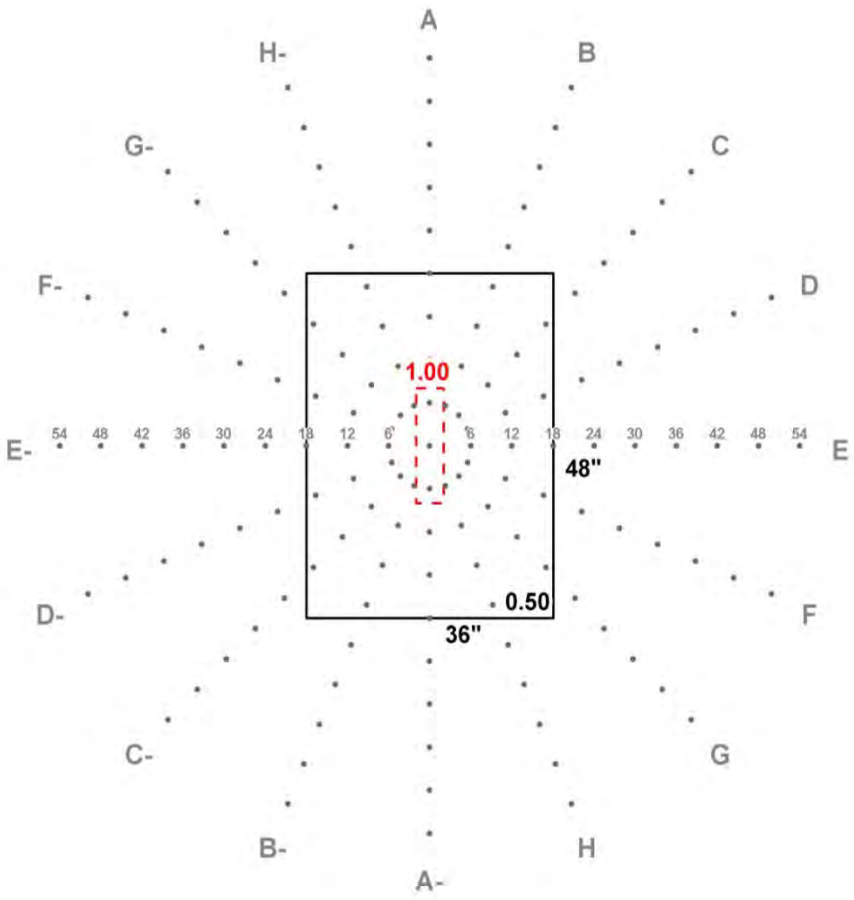

Figure 38
Single Detector Track Mounted Gamma Scanner Field of View Dimensions and the Active Detector Surface Area

The STGS FOV of 48 inches by 36 inches is less than the ERGS II and TMGS due to the number of detectors and the MMGS due to detector height. However, with the STGS closer to the surface, the sensitivity is much greater than that of the MMGS. The operational transect width of the STGS is set to 30 inches for the purpose of ensuring transects overlap even though the FOV width is 36 inches.

3.4.2 Velocity

The STGS scanning efficiency ratios at 1, 1.5, 2, and 3 ft/s are shown in Figure 39. These data represent combined scanning data of three separate tests at each velocity. There is some noise in the data as it is not possible to have a scanning efficiency higher than the static count efficiency. However, the amount of error in the data is approximately 4 percent, which is acceptable given the conditions of the tests (one second counts with the detection system moving relative to the source) and statistical errors associated with counting. As shown in Table 5, repeated counts of static radial plot positions for the ERGS II resulted in standard

deviations of approximately 20 percent at positions 12 inches and greater from the origin. Therefore, the 4 percent degree of uncertainty is minor.

The data as a whole indicate that the scanning efficiency is acceptable at 2 ft/s, but unacceptable (a scanning efficiency ratio of less than 0.8) at 3 ft/s.

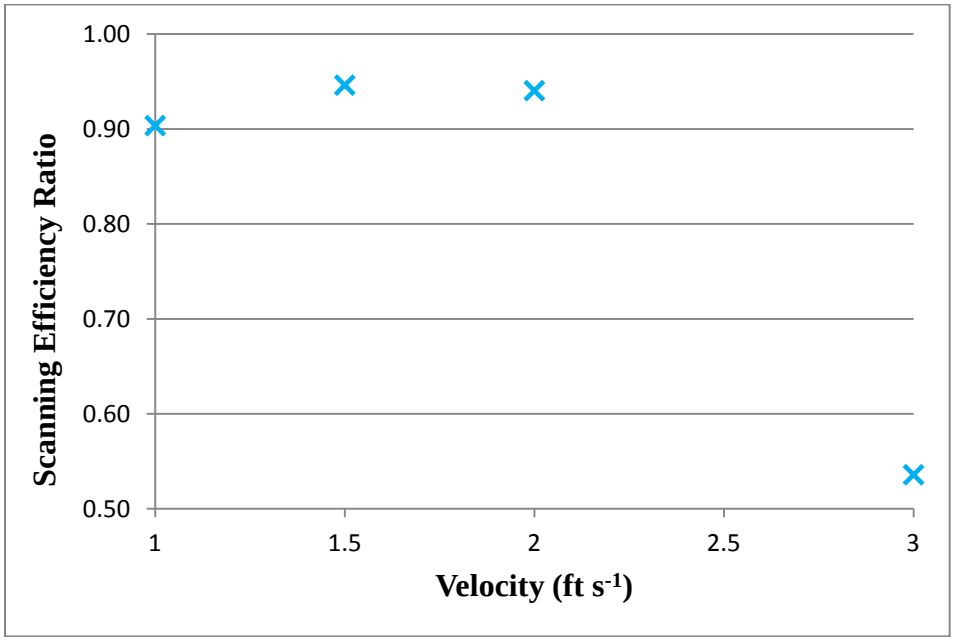

Figure 39
Single Detector Track Mounted Gamma Scanner Scanning Efficiency Ratio versus Velocity

The STGS scanning efficiency drops below 0.8 at 3 ft/s, but is well above that limit at 2 ft/s and slower. The data trend such that occasional slight excursions above 2 ft/s are acceptable.

3.5 WHEEL MOUNTED GAMMA SCANNER

In the case of the WMGS, the operational height is 12 inches which was constrained by the configuration of the wheeled cart used to mount the detector. Thus, height tests were not conducted for the WMGS.

Figure 40 is the count rate contour intervals of the WMGS with the detector superimposed over the radial source positions. One can see that, unlike the ERGS II, MMGS, TMGS, and STGS, the count rates are slightly greater in the direction of travel than laterally.

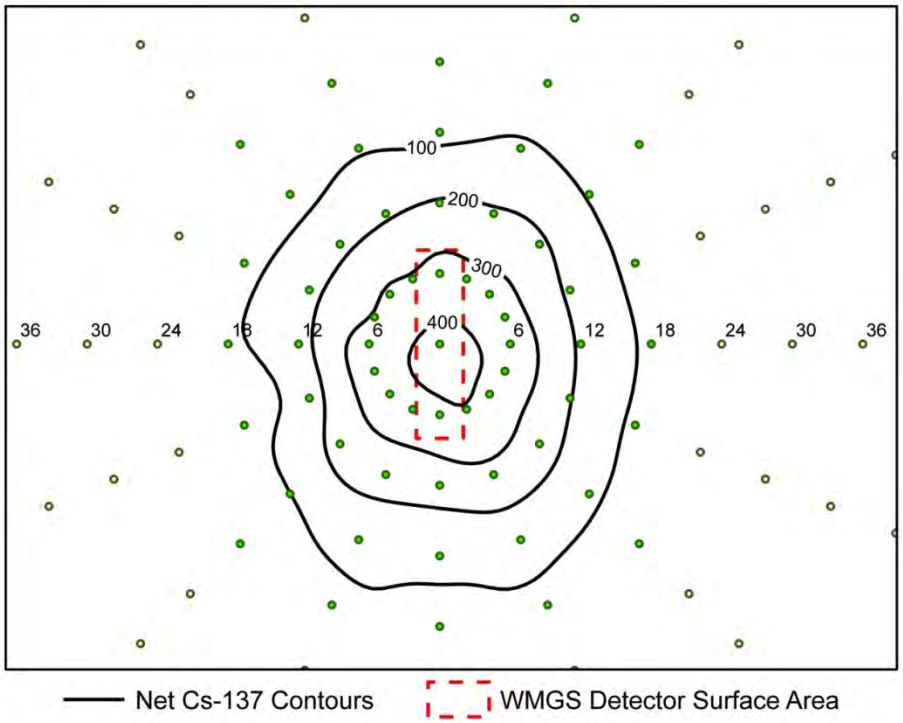

Figure 40
Wheel Mounted Gamma Scanner Net Cs-137 Count Rate Contours with the Active Detector Surface Area

The WMGS contour lines are fairly consistent with the single detector shape and orientation.

3.5.1 Field Of View

Figure 41 shows that with differences in radial, forward travel direction and lateral direction, REs are not as pronounced for the WMGS as for other detectors. Some small differences are observed at 12 and 18 inches where the wheels begin to impact the count rate. Figure 42 illustrates the WMGS FOV and its active detector surface area. The FOV for the WMGS is 40 inches long by 28 inches wide resulting in an FOV area of 1,120 in^2.

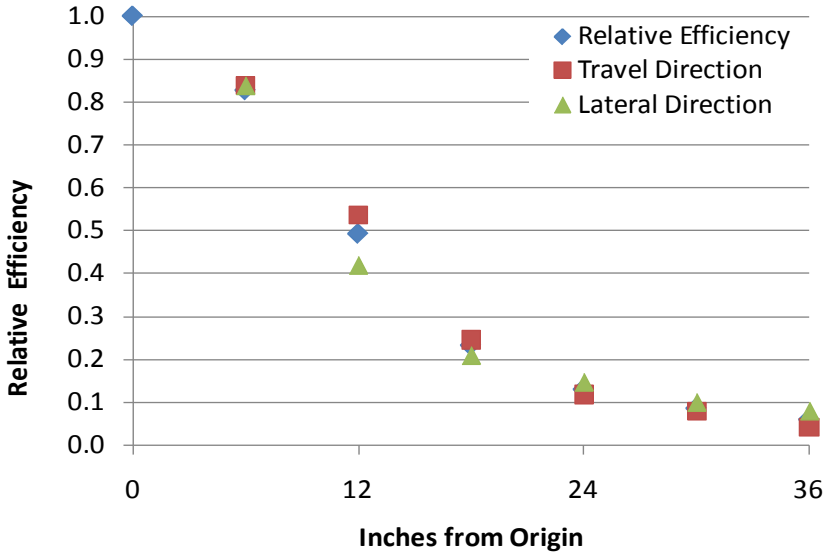

Figure 41
Wheel Mounted Gamma Scanner Directional Relative Efficiency versus Distance

The WMGS shows relatively little effect due to its orientation. Notice that at 12 inches, the RE is higher in the direction of travel than it is laterally.

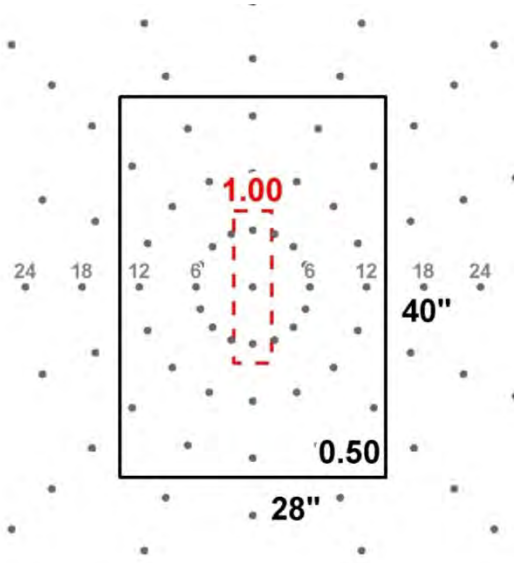

Figure 42
Wheel Mounted Gamma Scanner Field of View Dimensions and the Active Detector Surface Area

The WMGS FOV length is greater than its width, unlike the other detection systems. The transect width of the WMGS is set to 2 feet (24 inches).

3.5.2 Velocity

The data for the WMGS indicate that the scanning efficiency ratio drops off significantly at 3 ft/s. Therefore, a maximum velocity of 2 ft/s is selected. Some experimental error is observed in this dataset as noted in Figure 43 by the scan efficiency ratio of greater than one for the 1 ft/s test.

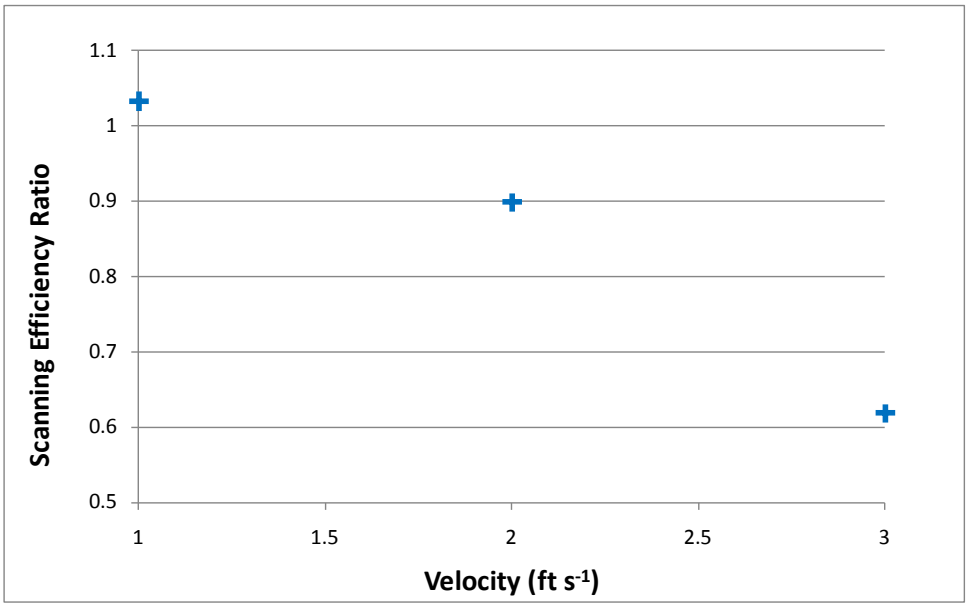

Figure 43
Wheel Mounted Gamma Scanner Scanning Efficiency Ratio versus Velocity

3.6 HAND HELD GAMMA SCANNER

The data collection and evaluation processes for the HHGS are nearly analogous to those of the ERGS II; however, the HHGS does not have the ability to set ROIs. Thus, MDC results discussed below are unique for the HHGS and are not directly comparable to radionuclide-specific MDCs. Figure 44 shows the net total count contour intervals for the HHGS. It is roughly circular-shaped due to the cylindrical shape of the uncollimated HHGS NaI crystal.

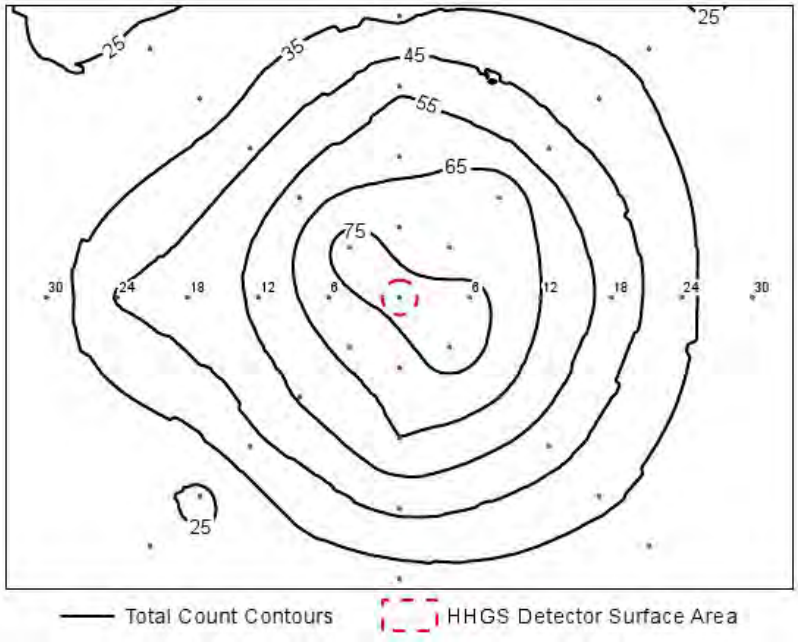

Figure 44
Hand Held Gamma Scanner Net Total Count Rate Contours with the Active Detector Surface Area

The contour lines for the HHGS are approximately circular due to the cylindrical configuration of the detector.

3.6.1 Field Of View

Figure 45 is a plot of the HHGS REs for radial, the travel direction, and the lateral direction versus distance. A shield was not included for weight considerations (i.e., ergonomics) as the equipment was used in areas very difficult to access and carried by personnel. Operating the HHGS as an uncollimated detection system resulted in an increased FOV area.

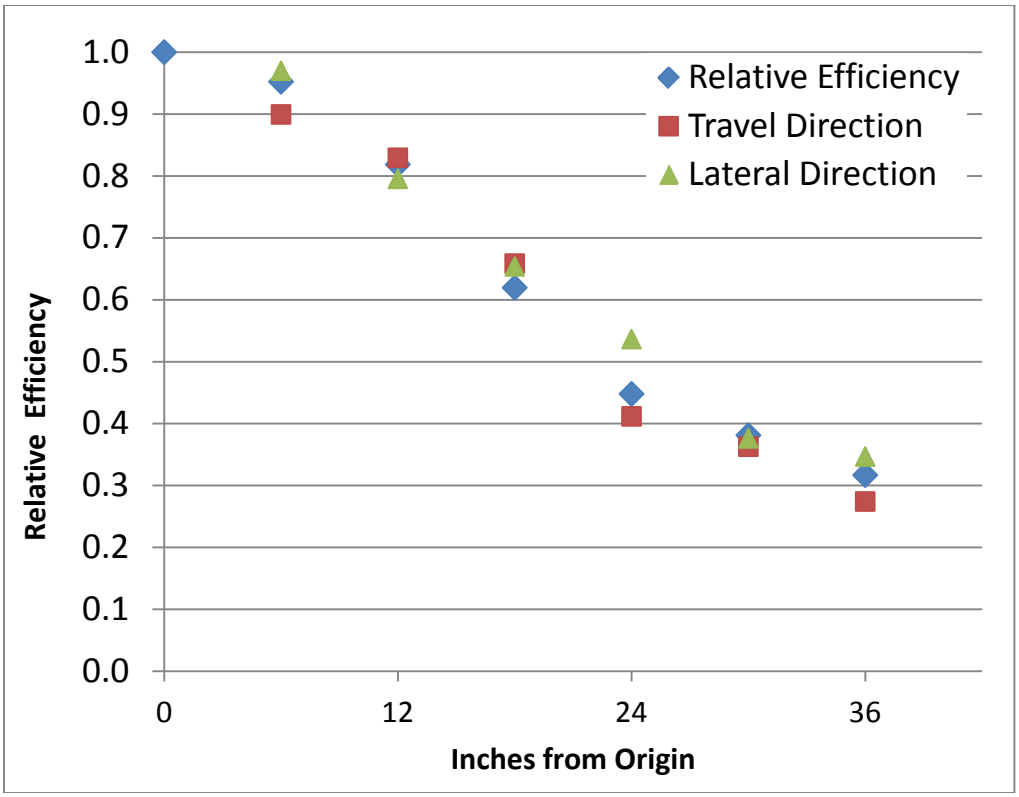

Figure 45
Hand Held Gamma Scanner Directional Relative Efficiency versus Distance

The HHGS RE data are roughly equal laterally and in the forward travel direction due to the arrangement of the detector.

Figure 46 shows the HHGS FOV in which the integrated RE is approximately 0.68 of that of the combined active detector surface areas.

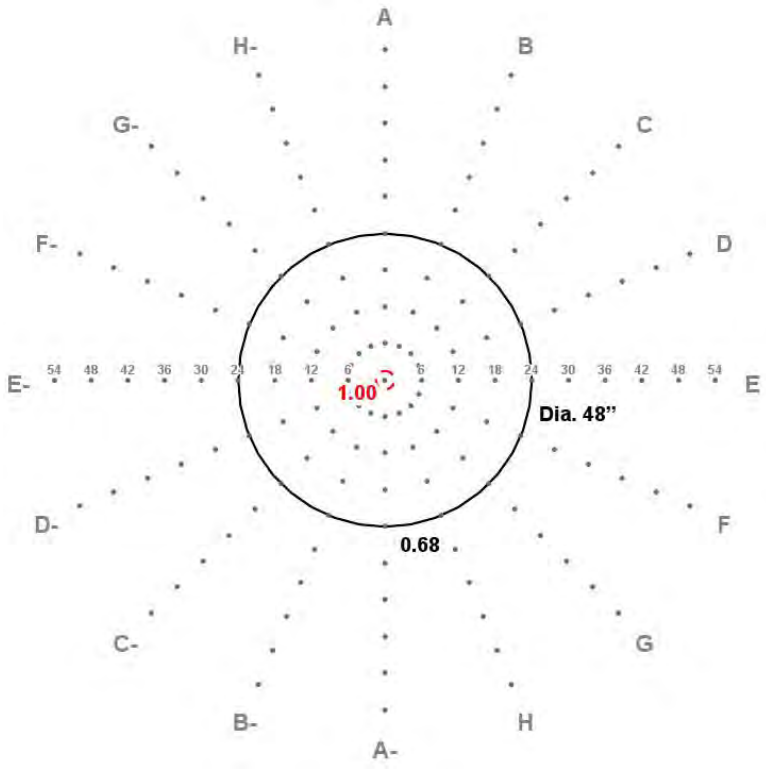

Figure 46
The Hand Held Gamma Scanner Field of View Dimensions and the Active Detector Surface Area

The HHGS has a FOV consistent with the large NaI detection systems due to the absence of a shield. The overall sensitivity of the HHGS is much lower than that of the other detection systems due to its much smaller crystal volume and absence of a shield. The operational transect width of the HHGS is set to 2 feet (24 inches) for the purpose of ensuring transect overlap in the field even though the FOV defines the width as 48 inches.

3.6.2 Height

The operating height chosen for the hand held is 18 inches. This height was largely based on locating the detector at a distance from the ground to avoid incidental contact between the detector and the terrain when traversing steep rocky slopes. Lower heights were attempted but could have lead to detector damage. The HHGS is specifically designed for deployment in very difficult and rocky terrain where wheeled and mule mounted detection systems cannot readily access.

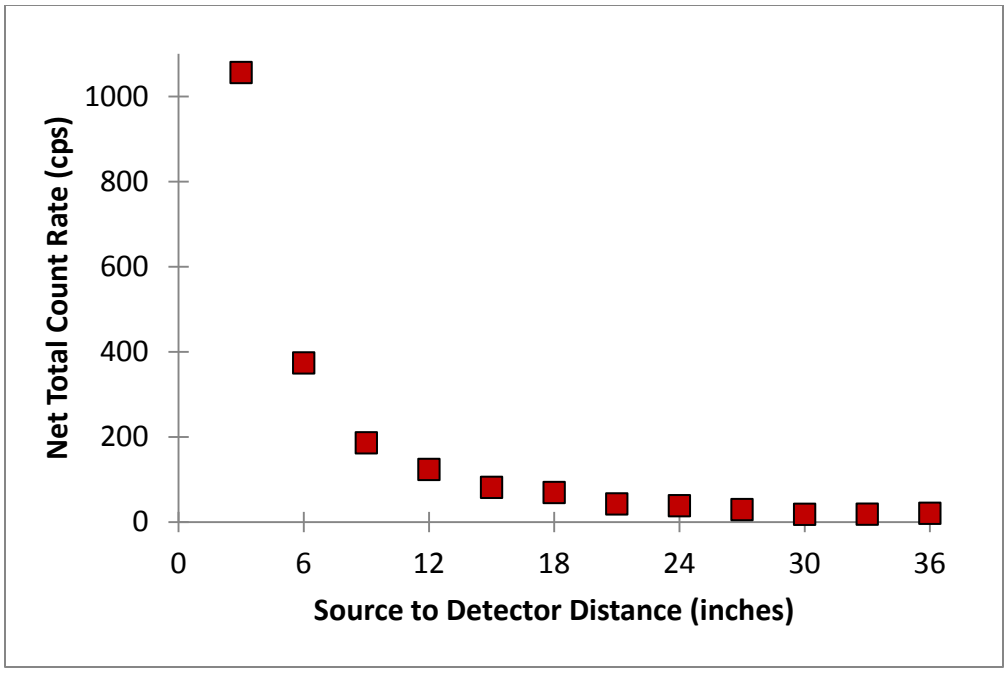

Figure 47
Hand Held Gamma Scanner Count Rate versus Height

3.6.3 Velocity

The fact that the HHGS is used by personnel on very steep slopes means that scanning velocity will sometimes increase beyond an established limit. For personnel safety this velocity cannot consistently be maintained at a slow pace when scanning downhill. Whenever possible the scanning will occur uphill at a slower pace.

Figure 48 is a plot of scanning efficiency ratio versus velocity. A downward trend is described from this data. For this reason, the mean scan efficiency ratio is selected and the maximum velocity is set at 1 ft/s. It appears that excursions above this value may not significantly decrease the scanning efficiency ratio.

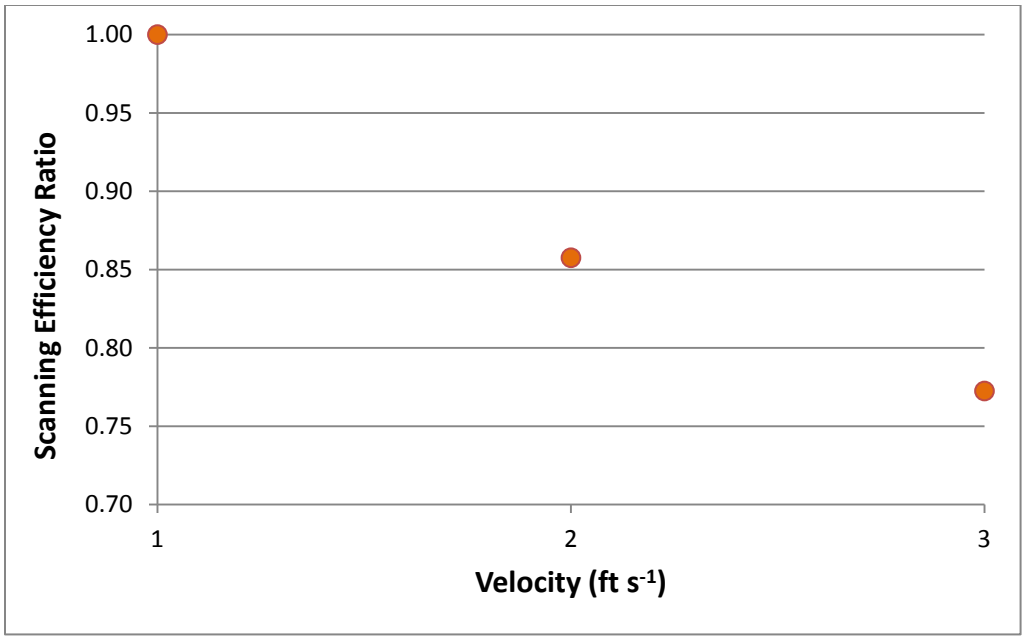

Figure 48
Hand Held Gamma Scanner Scanning Efficiency Ratio versus Velocity

The scanning efficiency ratio permits establishment of a maximum velocity for field scanning efficiency. For the ERGS II, an a priori estimate of scanning efficiency ratio of 0.8 was assumed. The data indicate velocities of 1 to approximately 2 ft/s will meet this criterion. For personnel safety, a slower scan velocity is desired with fluctuations above normal on down sloping surveys. Therefore, a constant scan velocity of 1 ft/s with minor excursions above 1 ft/s is acceptable. The scanning efficiency ratio influences field detection sensitivity. That is, the overall field sensitivity is the product of the static test efficiency at the FOV and the scanning efficiency ratio.

3.7 SUMMARY OF FIELD OF VIEW, HEIGHT, AND VELOCITY FOR SCANNING SODIUM IODIDE DETECTION SYSTEMS AND CALCULATIONS OF MINIMUM DETECTABLE ACTIVITY AND MINIMUM DETECTABLE CONCENTRATION

The FOV, absolute efficiency, scanning efficiency ratio, and overall efficiency for each detection system are shown in Table 7. The FOV is the area for which each detection system has an integrated relative efficiency greater than 0.5. The FOVs vary by a factor of seven with the MMGS having the largest FOV at 7,904 in^2 and the WMGS having the smallest at 1,120 in^2. This is due to the number and arrangement of detectors and the operating height of each system, which varied from 12 inches for the WMGS to 35 inches for the MMGS.

Table 8 includes the operating parameters: FOV width, transect width, height, and maximum velocity. In each case, the transect width is less than the FOV width. Transect width is influenced by the height, amount of shielding, as well as the FOV. The transect width is used

in scanning graphics to display the correct size of each detection system transect in the field. Gamma scanning personnel can also monitor velocity with the real-time field computers.

Table 7
Tested Parameters for Each Detection System

Detection System	FOV ($inch^2$)	Length (inch)	Width (inch)	Absolute Efficiency	Scanning Efficiency Ratio	Overall (Field) Efficiency
ERGS II	4,644	54	86	0.0219	0.87	0.0191
MMGS	7,904	76	104	0.0015	0.90	0.00137
TMGS	2,800	50	56	0.0083	0.93	0.00770
STGS	1,728	48	36	0.0039	0.94	0.00366
WMGS	1,120	40	28	0.0062	0.90	0.00557
HHGS I and II	1,810	48	48	0.0015	0.86	0.00129

Table 8
Operating Parameters for Each Detection System

Detection System	FOV Width (inch)	Transect Width (inch)	Operating Height (inch)	Maximum Velocity (ft/s)
ERGS II	86	72	15	2
MMGS	104	90	35	3
TMGS	56	48	15	2
STGS	36	30	15	2
WMGS	28	24	12	2
HHGS I and II	48	24	18	1

Absolute efficiency is the measured efficiency for the detection of Cs-137 in the FOV of the detection system. It is calculated by dividing the Cs-137 net count rate (for the FOV) by the emission rates of the Cs-137 sources (Equation 7). The absolute efficiency is affected both by the number of detectors (i.e., the total detector surface area and volume) and the scanning height. The overall efficiency is the product of the absolute efficiency and the scanning efficiency ratio. The maximum velocities are listed for reference. Note for the HHGS, net total count rate was used in place of Cs-137.

Equation 7:

$$Absolute\ Efficiency\ = \frac{(net\ Cs\ cps)_{FOV}}{I_\gamma\ \times dps}$$

Where $I\gamma$ is the branching ratio and dps is the gamma emission rate of the Cs-137 source in disintegrations per second. Using the ERGS II as an example, the absolute efficiency for Cs-

137 is calculated as 780.1 cps (net count rate measured)/ 0.851 (Cs-137 branching ratio) x 41,847 dps (the Cs-137 source emission rate) = 0.0219.

In this case, even though the MMGS has a larger FOV than the ERGS II, its sensitivity is one fourteenth that of the ERGS II, based on its overall efficiency. The WMGS has about 30 percent of the overall efficiency as the ERGS II and has a smaller detector surface area and is operated closer to the ground. Although the WMGS is more than four times more efficient than the MMGS, it has coverage of only one seventh of the surface area due to its FOV which is greatly influenced by its scan height.

The scanning efficiency ratio results are shown in Figure 49 for each detection system. The ERGS II has a smooth decrease in scanning efficiency with velocity. The WMGS is most sensitive to velocity increases, and the MMGS is the least sensitive to velocity. In general, the scanning efficiency ratio is dependent on both the height and size of the detector. The ERGS II and WMGS have acceptable scanning efficiencies up to 2 ft/s, and the MMGS is acceptable up to 3 ft/s. Data from a single test, the WMGS at 1.5 ft/s, data have been omitted due to an experimental error. Examining all detection systems, the order from most to least affected by scanning velocity is: STGS, WMGS, TMGS, HHGS, ERGS II, and MMGS. This is mainly due to the operating height of each detection system and gamma ray attenuation from the TMGS and STGS platforms.

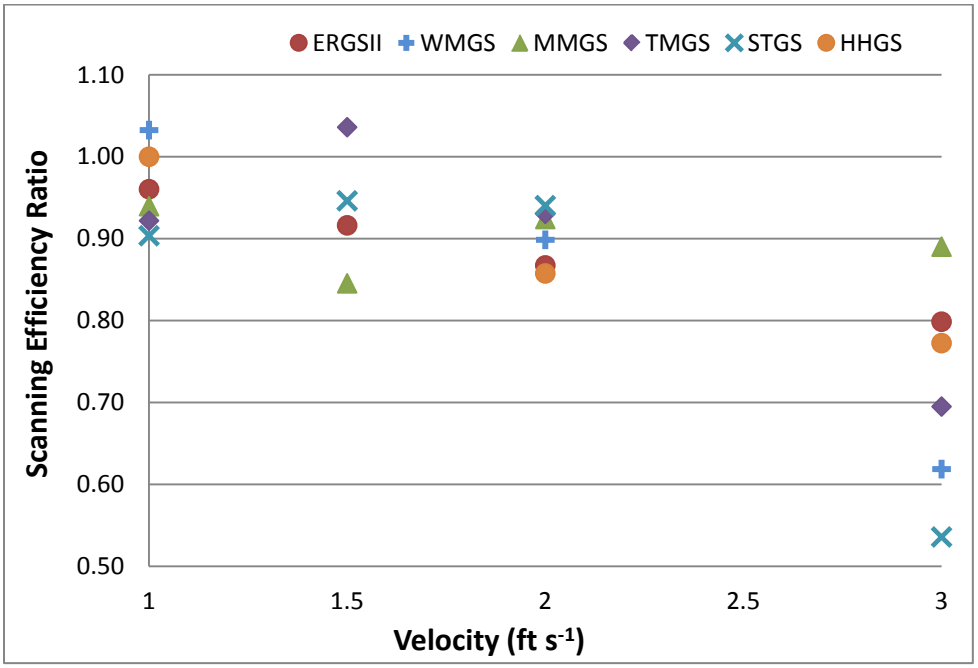

Figure 49
Summary of Detection System Scanning Efficiency Ratios versus Velocity

Figure 50 is an illustration of the FOV of the ERGS II. This figure provides an intuitive, easy to understand depiction of FOV. The FOV area is used in conjunction with a specific soil depth to calculate estimated MDCs. As a first approximation, MDC values will be calculated

assuming that the radionuclide concentration is uniformly distributed throughout a soil volume. Using the ERGS II as an example, the total volume of soil scanned is calculated by multiplying the FOV by a specific soil depth.

Figure 50
Illustration of Enhanced Radiation Ground Scanner II Field of View
(Detector footprint in blue and FOV in red.)

The ERGS II FOV illustrated is to scale. This figure is an aid to visualize the physical FOV.

Table 9 lists the area, volume, and soil mass of several possible contamination volumes. Areas were converted into volumes of cubic centimeters (cm^3) and soil masses were calculated assuming a bulk density of 1.6 g cm^{-3} or 26.2 grams per cubic inches (in^3). A point source is calculated as a 1-inch diameter by 1-inch thick volume, a small area source is 12-inch diameter by 1-inch depth, and the FOV area multiplied by 1-inch thick depth are calculated for each detection system. The MDC calculations discussed in detail later in this section are inversely proportional to the soil mass, (i.e., the greater the mass of soil contamination, the lower the MDC value).

Table 9
Soil Masses for Selected Contamination Volumes for a One Inch Depth

Parameter	Point Source (1" diameter)	Small Area (12" diameter)	ERGS II FOV	MMGS FOV	TMGS FOV	STGS FOV	WMGS FOV	HHGS FOV
Area (in^2)	0.79	113.1	4,644	7,904	2,800	1,728	1,120	1,810
Volume (cm^3)	12.9	1,853	76,102	129,523	45,884	28,316	18,354	29,661
Mass (grams)	21	2,965	121,762	207,237	73,414	43,305	29,366	47.457

Note:
These calculations are not rounded using significant figures to avoid introduction of rounding errors to subsequent MDA and MDC calculations.

MDC values also depend on transmission of gamma radiation through a specific soil depth. This relationship was first illustrated in Figure 15. Table 10 shows the gamma transmissions at various energies for homogenous radionuclide distributions of various soil depths. Table 10 has the gamma energy transmissions for Cs-137 and Co-60. Their transmission data were interpolated linearly using the nearest neighboring energies. The data in Table 10 clearly illustrate that the detection of gamma emitting radionuclides varies greatly based on the transmission through soil.

Table 10
Gamma Transmission as a Function of Energy and Soil Depth
(Calculated using the NIST gamma attenuation coefficients as described in Figure 15)

Gamma Transmission	Homogeneously Contaminated Soil Depth (inches)				
Energy (MeV)	**1**	**2**	**6**	**12**	**24**
0.01	0.0%	0.0%	0.0%	0.0%	0.0%
0.03	19.4%	3.8%	0.0%	0.0%	0.0%
0.06	63.5%	40.3%	6.5%	0.4%	0.0%
0.10	74.3%	55.2%	16.8%	2.8%	0.1%
0.15	78.2%	61.2%	22.9%	5.3%	0.3%
0.20	80.3%	64.5%	26.8%	7.2%	0.5%
0.30	82.9%	68.7%	32.4%	10.5%	1.1%
0.50	85.9%	73.7%	40.1%	16.0%	2.6%
0.60	86.9%	75.5%	43.0%	18.4%	3.4%
0.662 **(Cs-137)**	87.3%	76.3%	44.4%	19.8%	3.9%
0.80	88.4%	78.1%	47.6%	22.7%	5.2%
1.00	89.5%	80.1%	51.4%	26.4%	7.0%
1.25	90.5%	82.0%	55.1%	30.4%	9.2%
1.333 **(Co-60)**	91.2%	83.1%	57.4%	32.9%	10.9%
1.50	91.4%	83.5%	58.1%	33.8%	11.4%
2.00	92.5%	85.6%	62.7%	39.3%	15.4%
3.00	93.9%	88.1%	68.4%	46.8%	21.9%

With the FOV established for each system, masses of specific contamination volumes, and the calculated gamma transmission through the soil, detection sensitivities can be computed in terms of MDA and MDC. The MDA is a minimum activity which may be detected for each system. Its calculation is equivalent to that of the MDC without a sample quantity in the denominator. MDC data are computed using Equation 8 which is a modified form of the Currie Equation (Currie, 1968; Brodsky and Gallaghar, 1991). The modifications reflect two considerations pertinent to scanning surveys of soil:

- Background count time is the same as the sampling count time. This condition is based on the fact that during gamma scanning, the data from one second intervals potentially contain both ambient background and radionuclides of interest (i.e., contaminants).
- The MDC calculation accounts for the gamma energy transmission through soil.

There is a relatively large degree of uncertainty about the potential locations or distributions of radionuclides in soil in the project study area, therefore the MDC values calculated below are based on a number of assumptions which may not represent actual field conditions (for example, a source distribution located deeper in the soil will result in a different MDC). These

MDC calculations do not account for the relatively small changes in gamma signal associated with environmental conditions, which are discussed in Section 3.5.

Equation 8:

$$Minimum\ Detectable\ Concentration_{DS,\gamma}(MDC) = \frac{3.0 + 4.65 \times \sqrt{CR \times t}}{\varepsilon \times I_{\gamma} \times M \times t \times CF \times GTS}$$

Where DS, γ refers to a specific detection system and gamma emitting radionuclide

CR	-	count rate (cps) in the ROI of the radionuclide
t	-	time (set at the scan cycle of 1 second)
ε	-	overall detector efficiency (cps/Bq)
Iγ	-	branching ratio of a radionuclide (unitless)
M	-	contaminated soil mass (grams)
CF	-	conversion factor (0.037 Bq/picocuries [pCi])
GTS	-	gamma energy transmission through a specific soil depth (unitless)

For an example of the MDC calculation, the MDC for the ERGS II for Cs-137 in a homogeneously contaminated 1 inch soil volume is:

$$\text{MDC} = \frac{3.0+4.65\times\sqrt{600\times1}}{0.0191\times0.851\times121762\times1\times0.037\times0.873} = 1.8 \text{ picocuries per gram (pCi/g)}$$

The corresponding MDA calculation has neither a soil quantity nor a GTS term and is expressed:

$$\text{MDA} = \frac{3.0+4.65\times\sqrt{600\times1}}{0.0191\times0.851\times1\times0.037} = 194{,}381 \text{ pCi}$$

Table 11 lists the Cs-137 and Co-60 MDA and MDC values for each detection system. The MDCs presented include a point source, small area source, and volumes of the areal extent of each detection system's FOV at 1, 2, 6, and 12 inch depths. The MDA and MDC data were computed using the data presented in Tables 7 through 10 and approximate count rates for the regions of interest for Cs-137 and Co-60. Gamma energy transmission through each depth of soil has been taken into account.

Table 11
Minimum Detectable Activities and Minimum Detectable Concentrations of Cs-137 and Co-60

Radionuclide and Detection System		Count Rate (cps)	MDA (pCi)	MDC Point Source	MDC Small Area	MDC FOV 1" Depth	MDC FOV 2" Depth	MDC FOV 6" Depth	MDC FOV 12" Depth
Cs-137	ERGS II	600	190,000	10,800	75	1.8	1.0	0.6	0.7
	MMGS	200	1,600,000	88,700	620	8.8	5.0	2.9	3.2
	TMGS	170	260,000	14,600	100	4.1	2.3	1.3	1.5
	STGS	170	390,000	21,500	150	9.8	5.6	3.2	2.7
	WMGS	100	280,000	15,700	110	11.0	6.3	3.6	4.0
Co-60	ERGS II	450	140,000	7,700	53	1.3	0.7	0.3	0.3
	MMGS	150	1,200,000	63,000	440	6.3	3.4	1.7	1.4
	TMGS	130	200,000	10,500	73	2.9	1.6	0.8	0.4
	STGS	67	290,000	15,200	105	6.9	3.8	1.8	1.2
	WMGS	80	222,000	11,500	80	8.1	4.4	2.1	1.9

Notes:
All MDCs measured in pCi/g.

Examining Table 11, the results span approximately six orders of magnitude. This difference is due first to the fact that the MDA does not account for mass and second that the contaminant masses vary greatly as shown in Table 9. The masses of the FOV columns increase with soil depth, i.e. the 6 inch depth is six times the mass of the 1 inch depth. MDC results assume detection of areas in which the soil under the detector FOV is homogeneously volumetrically contaminated, which may be unlikely or highly unlikely to encounter in the field. If the contaminated soil mass decreases, then the MDC increases proportionately. For example, the calculated Cs-137 MDC for the ERGS II for a 2-inch deep volume uses approximately 244,000 grams of soil. Consider the possibility that the entire 2-inch deep volume under the ERGS II FOV was not uniformly contaminated, but only 2,500 grams of soil was contaminated. In that case, the MDC calculated would increase from 1.0 pCi/g to approximately 100 pCi/g.

The HHGS does not compare with the MDCs calculated in Table 11 using Equation 8 because for all other detection systems, MDCs were calculated using a radionuclide-specific region (i.e., Cs-137 or Co-60) of the gamma spectrum. In general, HHGS equivalent MDCs were approximately one to two orders of magnitude higher than those of the large NaI detection systems, depending greatly on the contaminant distribution.

The sensitivities of each detection system reflect both their dimensions and operating parameters, particularly the height and FOV. For point and small area contaminant distributions, the ERGS II is the most sensitive detection system, followed by the TMGS, WMGS, STGS, MMGS, and lastly the HHGS. However, for large contaminant distribution MDCs, the ERGS II is still the most sensitive, followed by the TMGS, STGS, MMGS,

WMGS and lastly the HHGS. This shift of the MMGS and WMGS is because the FOV of the MMGS represents seven times as much soil as the WMGS and these calculations are considering the entire soil mass being contaminated. The HHGS is useful for detecting relatively small areas of surface contamination.

A notable finding is that the MDCs do not automatically increase as the sample mass increases. This is illustrated by the ERGS II Cs-137 results for the FOV at all depths, which have different calculated MDCs. Though the soil mass increases with each successive depth increase, between 6 and 12 inches the MDC actually increases. This is because the Cs-137 gamma transmission through the soil decreases to the point that the top six inches of the soil shields the bottom six inches and the MDC increases. This effect is also seen for Cs-137 results of the WMGS and the MMGS, but not for the corresponding Co-60 MDCs. Cobalt-60 has a higher gamma energy which penetrates soil to a greater extent than Cs-137 gamma radiation.

3.8 SUBSURFACE SENSITIVITY TEST RESULTS

3.8.1 Validation of Point-Line Distance Approximation

Detection system height data are useful to verify that the detection system distance approximations described in Section 2.6.2 are appropriate for predicting results at one particular soil depth relative to another depth.

To demonstrate that the point – line approximation is valid, Figures 51 and 52 are plots of count rates versus source to detector distances for the ERGS II and the MMGS, respectively. Each figure plots trend lines predicted using Equation 2. In Figure 51, expected count rates over the range of distances were calculated based on the count rate at 15 inches. Similarly, in Figure 52, the expected count rates were calculated based on 26 inches distance. The distances selected were approximately the midpoint of the height distance range for each detection system, respectively.

The observed count rate data deviate from the data predicted from the point – line approximation when the source to detector distance becomes relatively very close. This is because the approximation is no longer valid as distances decrease markedly. The deviations from the approximation occur when the source is less than approximately nine to 12 inches for the ERGS II and approximately 16 inches for the MMGS. However, the source to distance ranges of the subsurface sensitivity tests were much greater than very close distances where the approximation fails. Thus, the point – line approximation is valid over the distance ranges used for subsurface sensitivity testing.

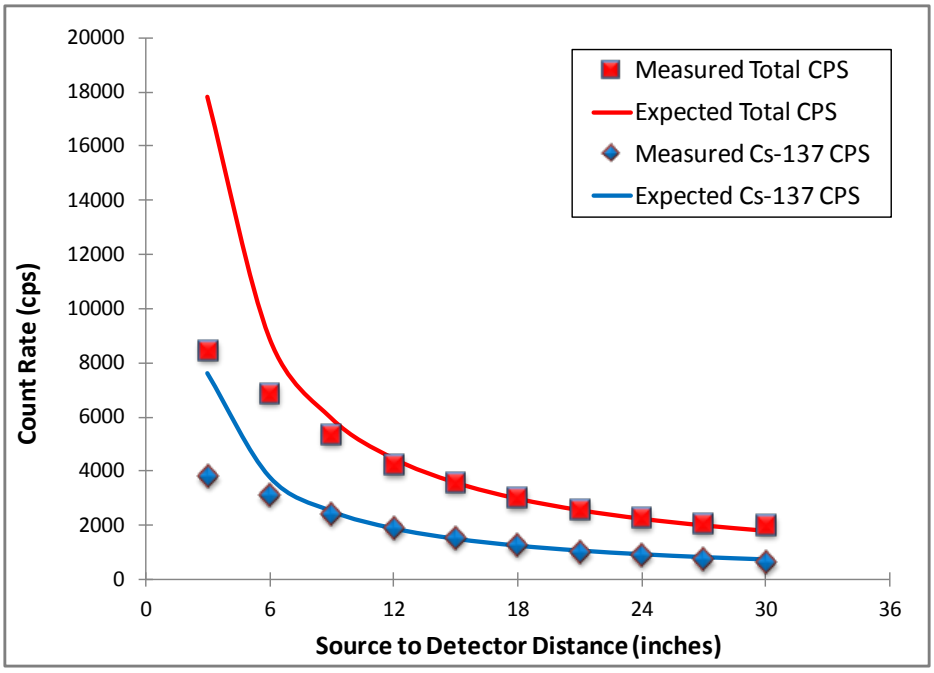

Figure 51
Comparison of Enhanced Radiation Ground Scanner II Height Test Count Rates with Count Rates Expected using the Point – Line Distance Approximation

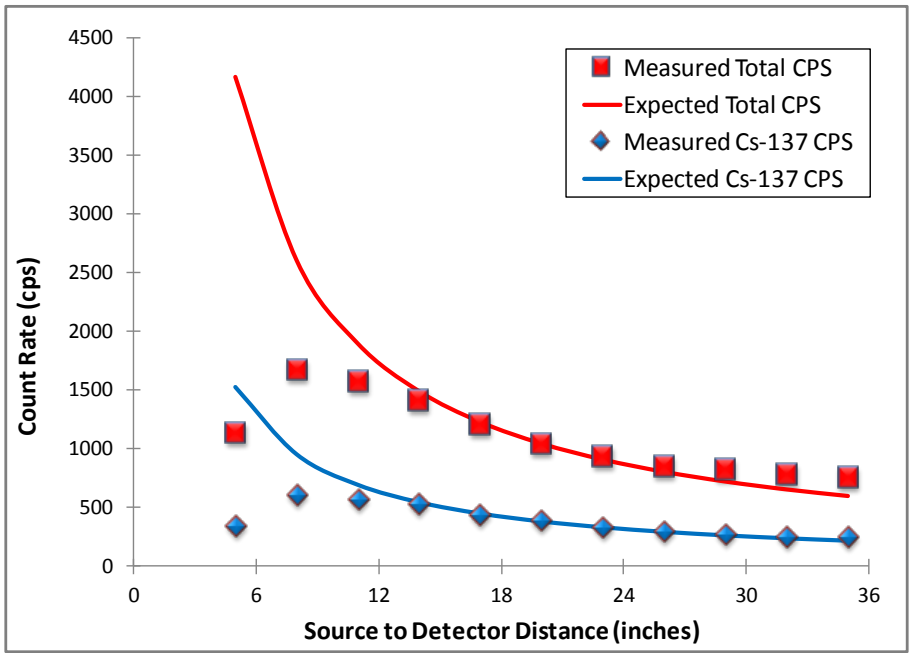

Figure 52
Comparison of Mule Mounted Gamma Scanner Height Test Count Rates with Count Rates Expected using the Point – Line Distance Approximation

Equation 4 was applied to count rate data collected from shallowest depth measured for Cs-137 (1 foot bgs) and Ra-226 (2 feet bgs). As an example, count rates for the 2 and 3-foot depths were calculated (based on the shallowest depth of 1 foot) to predict expected count rates from moving the Cs-137 source from 1 foot to 2 or 3 feet bgs.

Predicted results are presented along with measured data in Tables 12 and 13 and results are expressed as ratios to the count rates collected at the respective shallowest depth. For Cs-137, measured data closely matched the expected results. However, for Ra-226, measured results were significantly higher than expected due to buildup and to Compton scattering. Total Counts (used to analyze Ra-226) encompasses a large energy window and is therefore more significantly affected by these effects.

The Ra-226 source has gamma peak energies emanating from a number of Ra-226 progeny, which also have strong gamma peaks, such as bismuth-214 at 1765 keV and others. In fact, the combination of buildup and Compton scattering from Ra-226 progeny contribute much more to the total count rates observed than does Ra-226 itself. These factors complicate discussion of Ra-226 results; however, the most important consideration is that in each case, measured Ra-226 data far exceed predicted count rate. This is important because, if the reverse were true, then the detection systems would have been predicted to detect greater concentrations of activity than their capability. In this case, Ra-226 and its progeny are measured much more readily than predicted. This affirms that use of total count rates as a general means of detection is valid.

These tests verified that gamma radiation was attenuated by soil as expected for Cs-137 and this supports the calculation of MDCs discussed in Section 3.5. Figure 53 through 57 are a combination plot of Cs-137 and Ra-226 static count data from the ERGS II, MMGS, TMGS, STGS, and WMGS, respectively. As shown on Figure 53, due to the source strength and attenuation of soil, Cs-137 was detected at 2 feet bgs but not at 3 feet bgs. Radium-226 was detected several orders of magnitude greater than predicted, enabling detection of the stronger Ra-226 source at 5 feet bgs.

Table 12
Static and Scanning Cs-137 Region of Interest Count Rate Ratios

Static	Mean Net Cs-137 Region of Interest			
Detection System	**Measured from 12 - 24**	**Expected from 12 - 24**	**Measured from 12 - 36**	**Expected from 12 - 36**
ERGS II	3.19E-02	2.84E-02	1.94E-04	9.31E-04
TMGS	5.28E-02	2.84E-02	5.19E-04	9.31E-04
WMGS	1.19E-02	2.74E-02	3.94E-04	8.79E-04
STGS	2.28E-02	2.84E-02	6.38E-04	9.31E-04
MMGS	5.84E-02	3.27E-02	7.07E-03	1.16E-03
Scanning	**Peak Net Cs-137 Region of Interest**			
Detection System	**Measured from 12 - 24**	**Expected from 12 - 24**	**Measured from 12 - 36**	**Expected from 12 - 36**
ERGS II	3.55E-02	2.84E-02	8.68E-03	9.31E-04
TMGS	4.73E-02	2.84E-02	2.96E-02	9.31E-04
WMGS	1.50E-02	2.74E-02	6.81E-03	8.79E-04
STGS	2.71E-02	2.84E-02	1.35E-02	9.31E-04
MMGS	5.78E-02	3.27E-02	5.15E-02	1.16E-03

Table 13
Static and Scanning Ra-226 (Total cps) Count Rate Ratios

Static	Mean Net Total					
Detection System	**Measured from 24 - 36**	**Expected from 24 - 36**	**Measured from 24 - 48**	**Expected from 24 - 48**	**Measured from 24 - 60**	**Expected from 24 - 60**
ERGS II	5.54E-02	3.78E-03	2.84E-03	1.54E-05	3.51E-04	6.63E-08
TMGS	4.98E-02	3.78E-03	3.30E-03	1.54E-05	2.70E-04	6.63E-08
WMGS	4.00E-02	3.71E-03	2.86E-03	1.50E-05	2.32E-04	6.37E-08
STGS	4.20E-02	3.78E-03	2.80E-03	1.54E-05	1.84E-04	6.63E-08
MMGS	7.45E-02	4.11E-03	6.34E-03	1.77E-05	1.35E-03	7.91E-08
Scanning	**Peak Net Total Counts Region of Interest**					
Detection System	**Measured from 24 - 36**	**Expected from 24 - 36**	**Measured from 24 - 48**	**Expected from 24 - 48**	**Measured from 24 - 60**	**Expected from 24 - 60**
ERGS II	5.02E-02	3.78E-03	3.61E-03	1.54E-05	5.44E-04	6.63E-08
TMGS	4.85E-02	3.78E-03	3.49E-03	1.54E-05	1.10E-03	6.63E-08
WMGS	4.17E-02	3.71E-03	4.42E-03	1.50E-05	8.08E-04	6.37E-08
STGS	4.50E-02	3.78E-03	2.47E-03	1.54E-05	1.09E-03	6.63E-08
MMGS	6.45E-02	4.11E-03	6.17E-03	1.77E-05	7.67E-04	7.91E-08

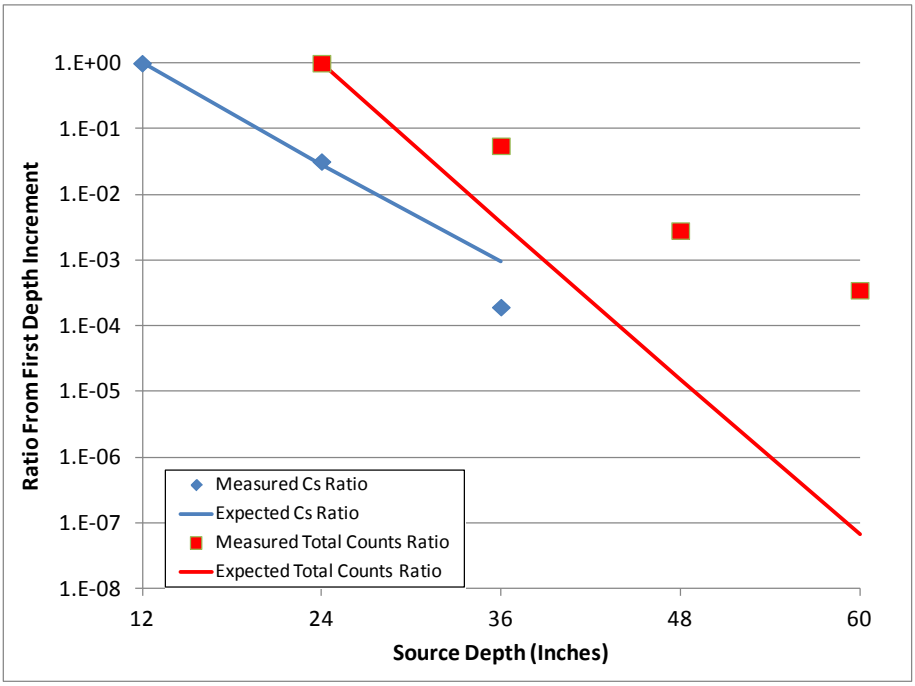

Figure 53
Enhanced Radiation Ground Scanner II Static Count Rates Ratio Relative to the Shallowest Depth Measured

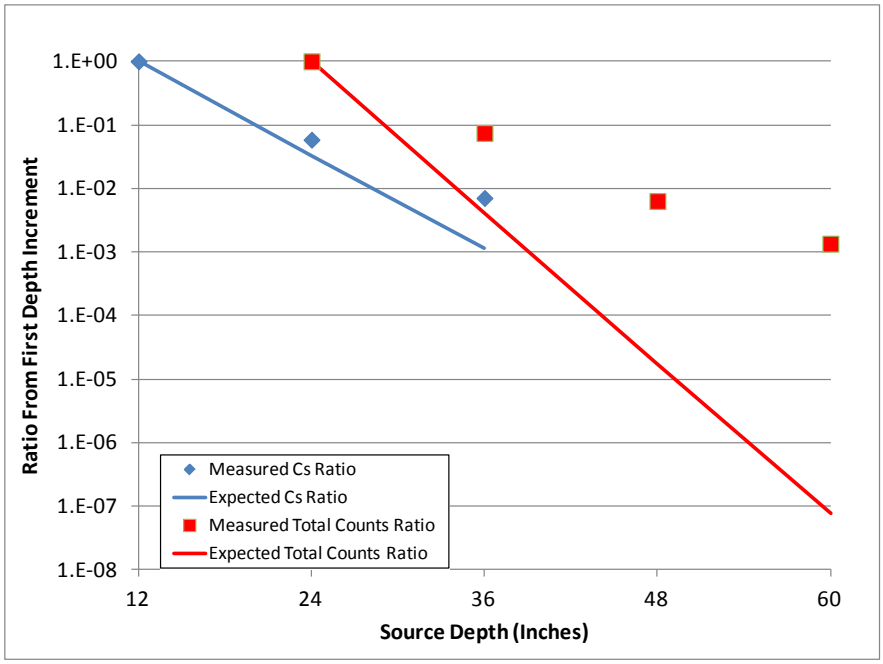

Figure 54
Mule Mounted Gamma Scanner Static Count Rates Ratio Relative to the Shallowest Depth Measured

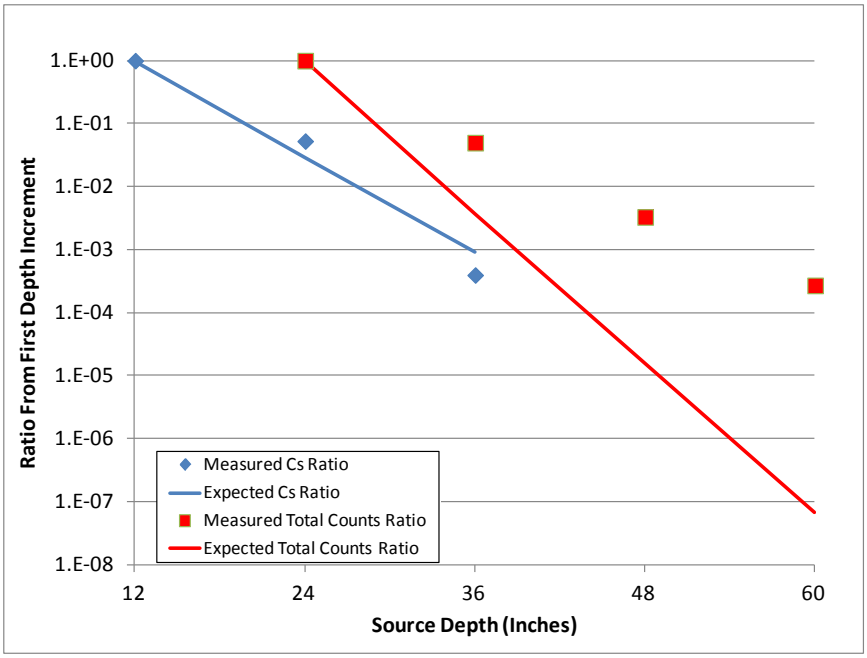

Figure 55
Track Mounted Gamma Scanner Static Count Rates Ratio Relative to the Shallowest Depth Measured

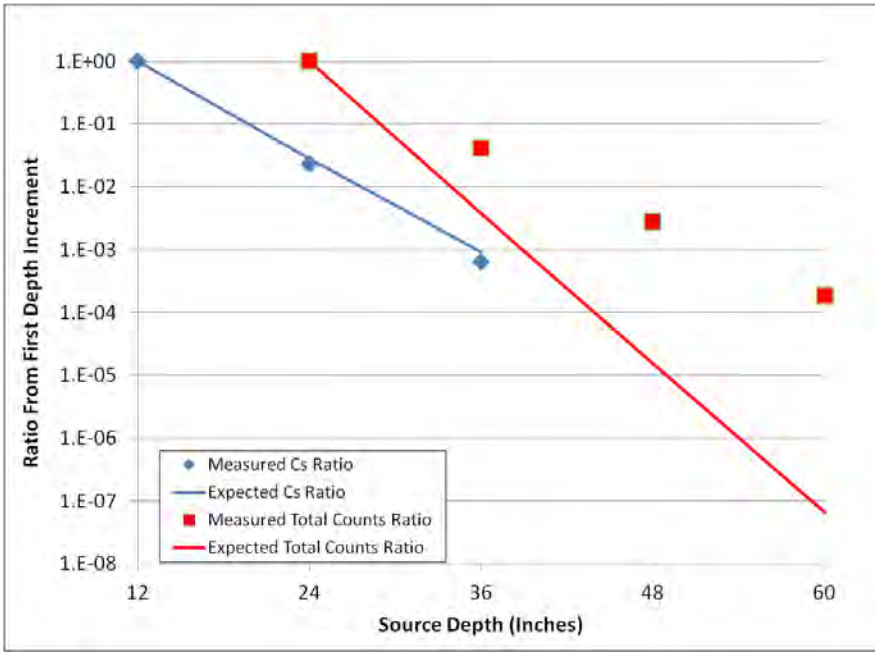

Figure 56
Single Detector Track Mounted Gamma Scanner Static Count Rates Ratio Relative to the Shallowest Depth Measured

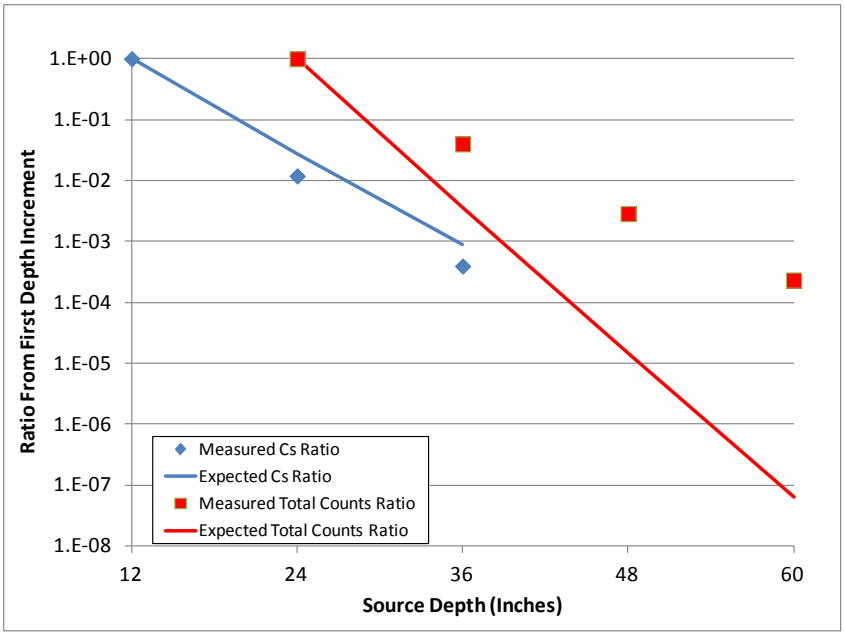

Figure 57
Wheel Mounted Gamma Scanner Static Count Rates Ratio Relative to the Shallowest Depth Measured

3.9 DETECTOR RESPONSES TO THE WALKER FIELD CALIBRATION PADS

Table 14 lists the measured concentrations and uncertainties (at the 95 percent confidence interval) of K-40, Th-232, and Ra-226 as the progeny of U-238 (Leino, et al. 1994). The dry bulk density and partial density values indicate very little structural differences between these two pads. For each radionuclide, the concentration is listed in pCi/g and the uncertainty is listed in both in pCi/g and expressed as a percentage of the concentration. It is important to note that the Ra-226 concentrations have a very high degree of uncertainty compared to K-40 and Th-232.

Table 14
Radionuclide Concentrations in Tested Calibration Pads
(Adapted from Leino, et al., 1994)

Pad	Concentration									Dry Bulk Density (g cm^{-3})	Partial Density H_2O (g cm^{-3})
	K-40			Th-232			Ra-226 (U-238)				
	pCi/g	uncertainty		pCi/g	uncertainty		pCi/g	uncertainty			
		95%	unc/conc		95%	unc/conc		95%	unc/conc		
W1 Background	12.7	0.72	5.7%	0.67	0.10	15%	0.82	1.02	124%	1.91	0.256
W5 Mixed Radionuclide	34.7	1.46	4.2%	1.91	0.16	8.4%	8.36	3.52	42%	1.97	0.244

Note:
The uncertainty data are expressed as the stated 95 percent values (pCi/g) and the uncertainty divided by the radionuclide concentration (unc/conc).

Table 15 lists detection system responses for each radionuclide ROI as cps data and as cps (per region) divided by the pCi/g of each calibration pad. The ratios of cps per pCi/g are ideally consistent for detection system responses to both pads, especially if the tests were conducted identically (for example, tests were conducted at the same heights). To examine the response consistency, the cps per pCi/g for each detection system are compared using the relative percentage differences which are presented following each set of measurements.

As shown on Table 15, the cps data are expected to vary because the pad concentrations vary from one pad to another. Focusing on the cps per pCi/g data (herein referred to as detector response), each detection system has similar response patterns for both calibration pads. The Th-232 and K-40 responses are acceptable, which is to state that the detection system accurately responds to the concentration present in each pad. This is supported by comparing the relative percent difference (RPD) of response data in Table 15 with stated percentage uncertainties in Table 14. For instance, checking the MMGS Th-232 responses to pads W1 and W5, the RPD is 14 percent and the individual pad uncertainties are 15 percent and 8.4 percent. Propagating those two pad errors as $((15 \text{ percent})^2 + (8.4 \text{ percent})^2)^{0.5}$, the overall error is 17.2 percent which is equivalent to the RPD. For U-238, the uncertainties in pad concentrations are quite high, especially for the W1 background pad. The detection systems count rate ratios differ by a factor of five to six between the mixed pad and the background pad whereas the pad concentrations, 0.82 and 8.36 pCi/g, differ by an order of magnitude. However, U-238 concentration errors for the pads are $((124 \text{ percent})^2 + (42 \text{ percent})^2)^{0.5} = 131$ percent. Thus, although higher than those of K-40 and Th-232, the RPD values of detection system response data for U-238 are also acceptable.

Table 15
Detector Region of Interest and Total Count Rate Responses to Calibration Pads

Detector and Pad	K-40			Th-232			U-238			Height (inches)
	cps	cps/ pCi/g	RPD	cps	cps/ pCi/g	RPD	cps	cps/ pCi/g	RPD	
ERGS II W1	391	30.8	14%	73	109.5	6%	70	85.7	52%	**15**
ERGS II W5	1233	35.6		197	103.1		420	50.2		**15**
WMGS W1	66	5.2	7%	13	18.9	17%	13	15.7	66%	**12**
WMGS W5	196	5.6		31	16.0		66	7.9		**12**
MMGS W1	134	10.6	5%	25	36.9	14%	24	29.2	61%	**30**
MMGS W5	386	11.1		61	31.9		130	15.6		**30**

Notes:
RPD is relative percentage difference applied to the cps per pCi/g data.
It is defined as: $RPD = \frac{absolute\ difference\ of\ two\ measurements}{mean\ of\ two\ measurements} \times 100\ (\%)$

3.10 DETECTOR RESPONSES TO ENVIRONMENTAL CONDITIONS

3.10.1 Soil Moisture

Figure 58 is a plot of total gamma radiation count rate versus soil moisture percentage data. The study was conducted during December 2010 and January 2011 which are wet season months, and there was appreciable precipitation over this period. This resulted in a relatively high range of soil moisture (13.4 percent to 25.7 percent), whereas 3 percent soil moisture is typical during the dry season.

The overall total gamma count rate mean was 11,517 cps for 25 observations. The dataset was statistically analyzed for outliers using the Scout 2008 Version 1.0 software program (USEPA, 2009). Data outliers were determined by five robust methods: sequential classical method, Huber estimation method, minimum covariance determination, multivariate trimming, and proposed estimation method, as described in the Scout User's Guide (USEPA, 2009). All outlier methods identified measurement number 12 on December 16, 2010, as an outlier, except the sequential classical method. With four of the five outlier tests indicating the subject data point was an outlier, it was removed from the dataset and further analysis of the remaining dataset was conducted.

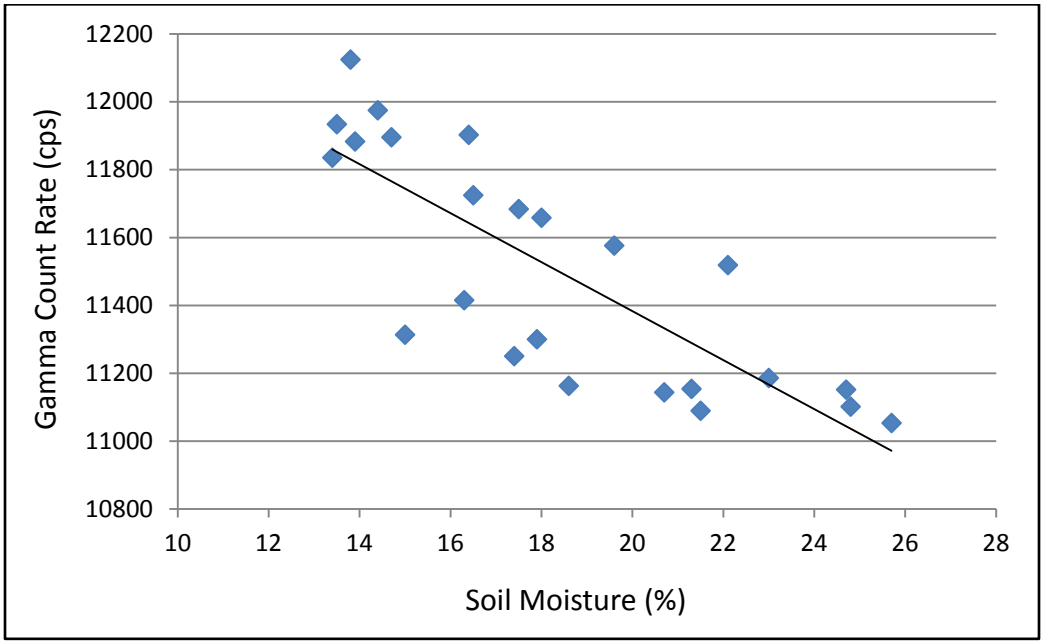

Figure 58
Total Gamma Count Rate versus Percentage Soil Moisture

Total gamma count rate is negatively correlated with soil moisture. The attenuation of total gamma count rate is about 3 percent (e.g., a 3 percent decrease in count rate) as soil moisture increases from 15 to 20 percent.

The data set, without the outlier, was plotted using the Microsoft Excel 2007. The coefficient of determination (R^2) of the linear regression was 0.6441 with a formula for the line as follows:

$$y = -72.207x + 12{,}827$$

Where y = gamma count rate (cps) and x = percent soil moisture

The slope of the line is -72.207. Thus, an increase in soil moisture of 1 percent should result in a count rate decrease of 72 cps. Based on the linear regression, derived gamma count rates were calculated for several soil moistures. The results were normalized to the total count rate at 15 percent moisture by calculating the relative percent differences as summarized in Table 16.

Table 16
Summary of Soil Moisture and Derived Gamma Count Rates

Soil Moisture (%)	Derived Gamma Count Rate (cps)	RPD in Gamma Count Rate (%)
15	11,744	0.0
20	11,383	-3.1
23	11,166	-5.0
25	11,022	-6.3

This study indicates that a negative correlation exists between soil moisture and gamma radiation total count rate. However, the rate of decrease in gamma radiation count rate data is relatively minimal with increasing soil moisture from approximately 13 percent to 26 percent. Comparison of gamma radiation count rate at 15 percent and 23 percent soil moisture indicates a 5.0 percent decrease in gamma count rate. Even so, a practical moisture cutoff was set at 15 percent for field crews so consistent MDCs and count rates could be maintained because the moisture effect was not studied at a 25 percent moisture level.

3.10.2 Barometric Pressure

The barometric pressure and total gamma radiation count rate data are summarized in Figure 59. The data set was statistically analyzed for data outliers using the Scout 2008 Version 1.0 statistical software program. Data outliers were determined by five robust methods: sequential classical method, Huber estimation method, minimum covariance determination, multivariate trimming, and proposed estimation method, as described in the Scout User's Guide (USEPA 2009). Only the minimum covariance determination method indicated that observations 11 and 12 were outliers; therefore, no outliers were determined and all 25 observations were used.

The data set was plotted using the Microsoft Excel 2007 software program (Figure 59). The coefficient of determination (R^2) of the linear regression was 0.277 with a formula for the line as follows:

$$y = -148.53x + 155137$$

Where y = gamma count rate (cps) and x = barometric pressure in mbar

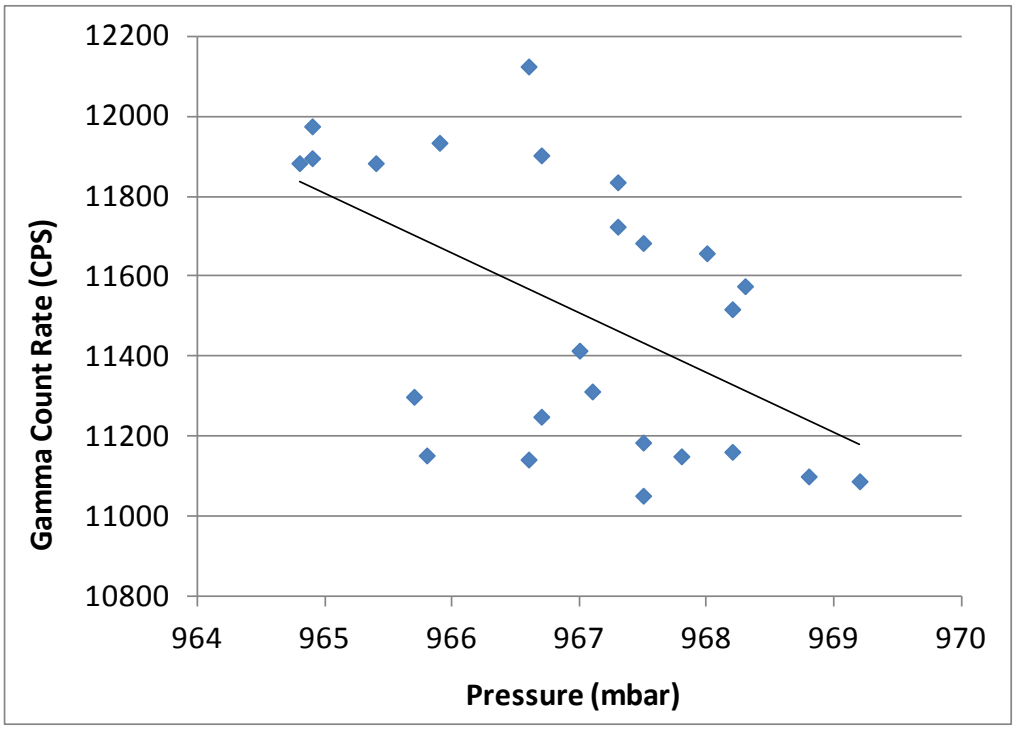

Figure 59
Total Gamma Count Rate versus Barometric Pressure

The correlation of the gamma count data indicates that a very slight negative trend exists with increasing barometric pressure. The low coefficient of determination indicates very low correlation between gamma radiation and barometric pressure. It should be noted that the count rate variability is generally greater than the count rate decrease observed throughout this study.

3.11 BOREHOLE DETECTOR RESPONSES TO THE GRAND JUNCTION BOREHOLE CALIBRATION MODEL U

The Ludlum models 44-2 and 44-62 scintillation detectors are essentially equivalent detectors, except for their size. The model 44-2 has a 1-inch diameter NaI crystal and the model 44-62 has a ½-inch diameter NaI crystal, hence their responses to gamma radiation will differ. Table 17 shows the data from both borehole detectors including gross and net counts and the ratio of net count rate data between the 0.5-inch and the 1 inch detectors. There is a subtle difference between the borehole detectors operation and the scanning detection equipment described earlier. In describing scanning results, a static or scanning count rate implies a dynamic rate

(for example, 2,127 cps collected over a specific time), which is mainly why multiple counts were collected and then mean or net mean count rate data was calculated. In the borehole data below, the count per minute data were collected as an integrated total number of counts per 1 minute period. Hence, no statistical means are calculated or presented. Gross data includes local ambient background of 761 and 2,156 counts per minute (cpm) for the 0.5-inch and 1 inch detectors, respectively. Net data is the count rate after subtraction of these same background values.

The data between 4 and 7 feet are highlighted, as this is the central contaminated zone of the calibration borehole which is calculated to contain 158 pCi/g. The contamination zone depth is described as 4.98 feet thick, beginning at 3 feet bgs and ending at 8 feet bgs. The detectors show significant increases in count rates at 3 feet depth, and similar decrease at 8 feet depth. This is due to the measurements taken at those locations are one-half in the contamination zone and one-half out of it. Hence, those measurements collected **entirely** within the contamination zone depth interval, from 4 feet to 7 feet, are selected to calculate the detector cpm per U-238 contamination.

The responses in detector cpm are seen more easily in Figure 60 which is a graph of the borehole detector count rate data with depth in the borehole. As expected, the 1-inch detector is approximately 2 to 2.5 times more sensitive than the 0.5 inch detector based on the tested sensitivity data of 1,199 and 503 cpm per pCi/g of U-238, respectively.

Table 17
Borehole Detector Response Data to the Grand Junction Borehole

Borehole Test Measurements (4.5 inch pipe diameter)					
Depth (feet)	**0.5 inch gross (cpm)**	**1 inch gross (cpm)**	**0.5 inch net (cpm)**	**1 inch net (cpm)**	**Ratio of 1/2:1**
0	1140	2654	379	498	0.761
1	1867	4890	1106	2734	0.404
2	3992	10454	3231	8298	0.389
3	*46334*	*86033*	*45573*	*83877*	*0.543*
4	79692	191818	78931	189662	0.416
5	81203	193982	80442	191826	0.419
6	81111	193217	80350	191061	0.421
7	79027	187336	78266	185180	0.423
8	*32885*	*93350*	*32124*	*91194*	*0.352*
9	3321	8288	2560	6132	0.417
10	1759	4279	998	2123	0.470
Mean of 4–7 ft	80528	191588	79497	189432	0.420
Test Sensitivity (cpm/pCi/g)			**503**	**1199**	

Notes:
The depths of the contaminated zone are highlighted in the zone and in italics at the boundaries of the zone.

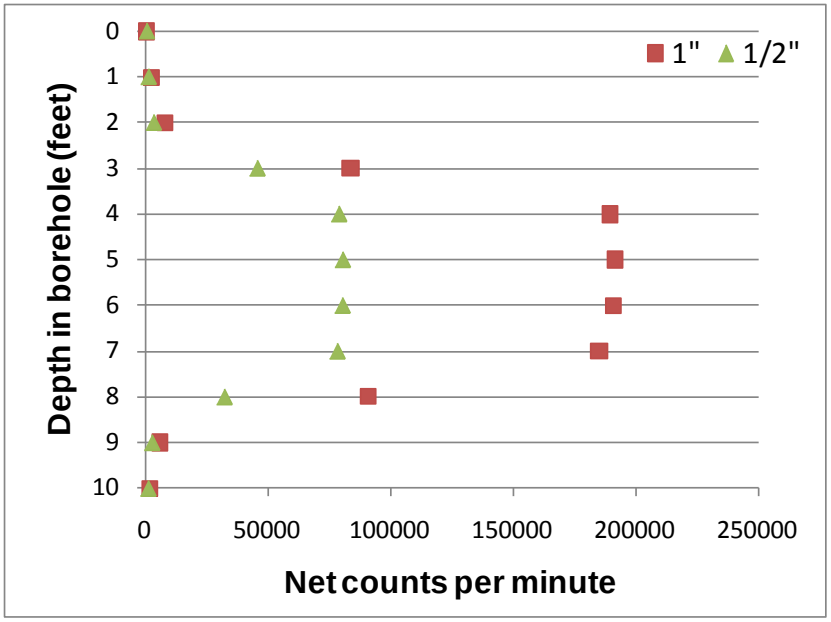

Figure 60
Borehole Detectors Net Counts per Minute versus Depth in the Borehole

The 1-inch borehole detector is 2.4 times more sensitive than the 0.5 inch detector. This is evident between 4 and 7 foot depth interval, which are in the zone of contamination.

4.0 CONCLUSIONS

These results address the sensitivities of several different types of gamma detection equipment. For the ERGS II, MMGS, TMGS, STGS, WMGS, and HHGS the FOV, scan height, and maximum scan velocities have been quantified and field minimum detectable concentrations have been estimated. The ERGS II is the most sensitive detection system for both small and large contaminant distributions. For small contaminant distribution areas, the TMGS, STGS and the WMGS are more sensitive than the MMGS. However, if the gamma emitting contaminant is distributed over a much larger area (e.g. as large as the MMGS FOV), then the MMGS is more sensitive than the WMGS and STGS and may, in some instances, be more sensitive than the TMGS. The HHGS is the least sensitive detection system but is useful in areas where no other detection system can be utilized.

The tested and operational parameters for the gamma scanning detection systems are summarized in Tables 7 and 8. For each detection system, an MDA and several MDC values were calculated for Cs-137 and Co-60 and are summarized in Table 11. Caution must be exercised in interpreting the calculated soil MDC values, due to both the extent and distribution of contamination in the field. Gamma transmission through soil is influenced by gamma energy, soil composition, and soil depth. Gamma emitters with energies below approximately 100 keV are far less likely to be detected than those with higher energies. Subsurface sensitivity tests verified estimated gamma transmission through soil was appropriate, affirming MDC calculations.

In general, detector efficiency, operating height, contaminant distribution, and physical parameters much more strongly influence gamma sensitivity than do environmental factors. However, there is a slight decrease in total gamma count rate with an increase in soil moisture and there is an even smaller decrease in total gamma count rate with increased barometric pressure. The total gamma attenuation attributable to soil moisture is less than 10 percent. The barometric pressure accounts for a smaller decrease of less than 5 percent over the range of pressures observed during the study period.

The ERGS II, MMGS, and WMGS responses to the Walker Field calibration pads were quite consistent, as indicated by response data for Th-232 and K-40 (Table 15). Measurements of each system collected at two different pads were within 20 percent relative percent difference for these isotopes. The results of two different pad measurements for U-238 were less consistent which likely reflects the fact that the U-238 concentrations of both pads have a much higher degree of uncertainty compared to their Th-232 and K-40 concentrations. The TMGS, STGS, and HHGS were designed, fabricated, and tested on the SSFL site specifically for the radiological study and were not transported to the Grand Junction facility for testing.

Borehole detector responses at the Grand Junction Calibration Facility were consistent and similar with the 1-inch diameter detector about 2.4 times more sensitive than the 0.5-inch detector.

5.0 REFERENCES

Aage, H.K., Korsbech, U., Bargholz, K., and Hovgaard, J., 2006. Carborne gamma-ray spectrometry: Calibration and applications. Applied Radiation and Isotopes, Vol. 64, 948–956.

American National Standards Institute National Committee on Radiation Instrumentation N42.43, 2006. American National Standard Performance Criteria for Mobile and Transportable Radiation Monitors Used for Homeland Security American National Standards Institute., IEEE New York, NY.

Bendix Field Engineering Corporation, 1981. EPA-02 Surface Gamma Scanner System. Prepared for the USEPA, Office of Radiation Programs – Las Vegas Facility, Las Vegas, NV. September.

Brodsky, A. and R. G. Gallaghar, 1991. Statistical Considerations in Practical Contamination Monitoring, Radiation Protection Management, Vol. 8(4), pp 64-78.

Currie, L.A., 1968. Limits for Qualitative Detection and Quantitative Determination: Application to Radiochemistry, Analytical Chemistry Vol. 40, 586-593.

Gollnick, Daniel A., 2006. Basic Radiation Protection Technology. Page 454. January.

HydroGeoLogic, Inc., and The Palladino Company, Inc., 2010a. Final Gamma Radiation Scanning Sampling and Analysis Plan, Area IV Radiological Study, Santa Susana Field Laboratory, Ventura County, California. February.

HydroGeoLogic, Inc., 2011. Normalization Report, Gamma Detection Systems, Area IV Radiological Study, Santa Susana Field Laboratory, Ventura County, California.

Institute of Electrical and Electronics Engineers, 1997, American National Standard for Radiation Protection Instrumentation Test and Calibration, Portable Survey Instruments, ANSI N323A-1997, New York, NY.

International Atomic Energy Agency, 2003. Guidelines for Radioelement Mapping Using Gamma Ray Spectrometry Data. Vienna, Austria.

Interstate Technology and Regulatory Council, 2006. Real-Time Measurement of Radionuclides in Soil: Technology and Case Studies. RAD-4. Interstate Technology & Regulatory Council, Real-Time Radionuclide Team. www.itrcweb.org. Washington, D.C.

Leino, R., George, D. C., Key, B. N., Knight, L., and W. D. Steele, 1994, Field Calibration Facilities for Environmental Measurement of Radium, Thorium, and Potassium, 3rd edition, Technical Measurements Center, Grand Junction, CO.

Multi-Agency Radiation Survey and Assessment of Materials and Equipment Manual, 2009. NUREG-1575, Supplement 1. U. S. Environmental Protection Agency, (Accessed online March 1, 2011), http://www.epa.gov/rpdweb00/marssim/marsame.html.

National Institute of Standards and Technology. 2010. X-Ray Mass Attenuation Coefficient, ordinary concrete. (Accessed online: November 1, 2010). http://physics.nist.gov/PhysRefData/XrayMassCoef/ComTab/concrete.html.

The Palladino Company, Inc., 2011. Technical Memorandum: Effect of Soil Moisture on Gamma Radiation Count Rate Measurements, Area IV Radiological Study, Santa Susana Field Laboratory, Ventura County, California. February.

United States Environmental Protection Agency, 2009, Scout 2008 Version 1.0 User Guide, EPA/600/R-08/038. Washington, D.C.

United States Nuclear Regulatory Commission, 1998, NUREG-1507, Minimum Detectable Concentrations with Typical Radiation Survey Instruments for Various Contaminants and Field Conditions, Washington, D.C.